Pavement thickness design charts derived from a rut depth finite element model

November 2010

Dr Greg Arnold, Pavespec Ltd

Dr Sabine Werkmeister, University of Canterbury

NZ Transport Agency research report 427

ISBN 978-0-478-37130-7 (print)
ISBN 978-0-478-37129-1 (electronic)
ISSN 1173 3756 (print)
ISSN 1173-3764 (electronic)

NZ Transport Agency
Private Bag 6995, Wellington 6141, New Zealand
Telephone 64 4 894 5400; facsimile 64 4 894 6100
research@nzta.govt.nz
www.nzta.govt.nz

Arnold, G[1] and S Werkemeister[2] (2010) Pavement thickness design charts derived from a rut depth finite element model. *NZ Transport Agency research report no.427*. 84pp.

[1] Pavespec Ltd, PO Box 570, Drury 2247, New Zealand (www.rltt.co.nz)

[2] Technische Universität Dresden, Mommsenstraße 13, 01069 Dresden, Germany

Keywords: aggregates, basecourse, deformation, pavement design, rut depth prediction, unbound granular, repeated load triaxial, rutting, specifications for aggregates.

An important note for the reader

The NZ Transport Agency is a Crown entity established under the Land Transport Management Act 2003. The objective of the Agency is to undertake its functions in a way that contributes to an affordable, integrated, safe, responsive and sustainable land transport system. Each year, the NZ Transport Agency funds innovative and relevant research that contributes to this objective.

The views expressed in research reports are the outcomes of the independent research, and should not be regarded as being the opinion or responsibility of the NZ Transport Agency. The material contained in the reports should not be construed in any way as policy adopted by the NZ Transport Agency or indeed any agency of the NZ Government. The reports may, however, be used by NZ Government agencies as a reference in the development of policy.

While research reports are believed to be correct at the time of their preparation, the NZ Transport Agency and agents involved in their preparation and publication do not accept any liability for use of the research. People using the research, whether directly or indirectly, should apply and rely on their own skill and judgement. They should not rely on the contents of the research reports in isolation from other sources of advice and information. If necessary, they should seek appropriate legal or other expert advice.

Acknowledgements

The authors would like to acknowledge the assistance provided by Stevenson Laboratory, Winstone Aggregates and CAPTIF staff in providing data.

Abbreviations and acronyms

AASHTO	American Association of State Highway and Transportation Officials
ASR	alkali-silica reaction
CalTrans	California Department of Transportation
CAPTIF	Canterbury accelerated pavement testing indoor facility
CBR	California bearing ratio
DOS	degree of saturation
ESA	equivalent standard axle pass
FE	finite element
HMA	hot mix asphalt
MDD	maximum dry density
MESA	millions of equivalent standard axles
NZTA	New Zealand Transport Agency
OMC	optimum moisture content
RLT	repeated load triaxial
Transit NZ	Transit New Zealand
UCS	unconfined compressive strength
VSD	vertical surface deformation (a measurement of rutting)

Contents

Executive summary

Repeated load triaxial (RLT) tests on subgrade, subbase and basecourse materials enabled relationships to be determined between permanent strain/rutting and stress (Arnold method) or elastic strain (Werkmeister method). Through these relationships it was possible to calculate the rutting within each pavement material, which was then summed to obtain a surface rut depth. The assumptions used to calculate the surface rut depths to ensure they were close to measured rut depths were validated and refined at the Canterbury accelerated pavement indoor testing facility (CAPTIF). The validated Arnold and Werkmeister rut depth prediction models were then used to calculate rutting for a range of pavement depths on subgrade soils with California bearing ratios (CBRs) of 2%, 8% and 10%. Results of this analysis were assessed by the number of equivalent standard axle passes (ESAs) to achieve a total surface rut depth defining the end of life. This information was used to develop pavement thickness design charts from the rut depth predictions and these were compared to the chart for granular pavements in the Austroads design guide (Austroads 2004, figure 8.1). For low traffic volumes the rut depth model required thinner pavements than the Austroads guide while for high traffic volumes the rut depth predictions showed significantly thicker pavements were required. In fact, the rut depth predictions showed that traffic loading limits for granular pavements were around 7 million ESAs for the subgrade CBR 2% and 11 million ESAs for the subgrade CBR 8%. A reason for this was the significant amount of rutting that occurred in the aggregate layers for the thicker pavement depths. As rutting occurred within the granular layers, adding more granular material did not decrease the amount of rutting nor increase pavement life.

Rut depth predictions were repeated with different quality aggregates in terms of resistance to rutting found from the RLT test at optimum moisture content in drained conditions. The effect of using very good unbound aggregates increased the maximum pavement life from 11 million ESAs for average quality to 14 million ESAs for a subgrade with CBR 8%. However, when using poor quality aggregates the maximum life decreased to 3 million ESAs.

Finally, a combined Austroads and rut depth prediction pavement thickness design chart was produced by using the largest pavement thickness from the two methods. It is recommended that this replace the Austroads design chart (Austroads 2004, figure 8.4).

Abstract

Repeated load triaxial (RLT) tests were conducted on the granular and subgrade materials used at CAPTIF (NZ Transport Agency's test track). Permanent strain relationships found from RLT testing were later used in finite element models to predict rutting behaviour and magnitude for the pavements tested at the CAPTIF test track. Predicted rutting behaviour and magnitude were close to actual rut depth measurements made during full-scale pavement tests to validate the methods used. This method of assessing rutting in granular materials was used to predict the life or number of axle passes to achieve a rut depth defining the end of life for a range of pavement thicknesses, and the subgrade types to produce new pavement thickness design charts. The results of these rut depth predictions showed the Austroads guide required thicker pavements for low traffic volumes, while the rut depth predictions showed significantly thicker pavements were required for high traffic volumes. In fact the rut depth predictions indicated the traffic loading limits for granular pavements were around 7 million equivalent standard axle passes (ESAs) for the subgrade California bearing ratio (CBR) 2% and 11 million ESAs for the subgrade CBR 8%.

1 Introduction

1.1 Background – current pavement design method

The Austroads pavement design guide (Austroads 2004) is currently used in New Zealand for pavement design. A pavement thickness design chart (Austroads 2004, figure 8.4) is used to design unbound thin-surfaced granular pavements (figure 1.1). This shows that for a known design traffic volume and subgrade California bearing ratio (CBR), the granular pavement thickness can be determined.

Figure 1.1 Pavement thickness design chart (Austroads 2004, figure 8.4)

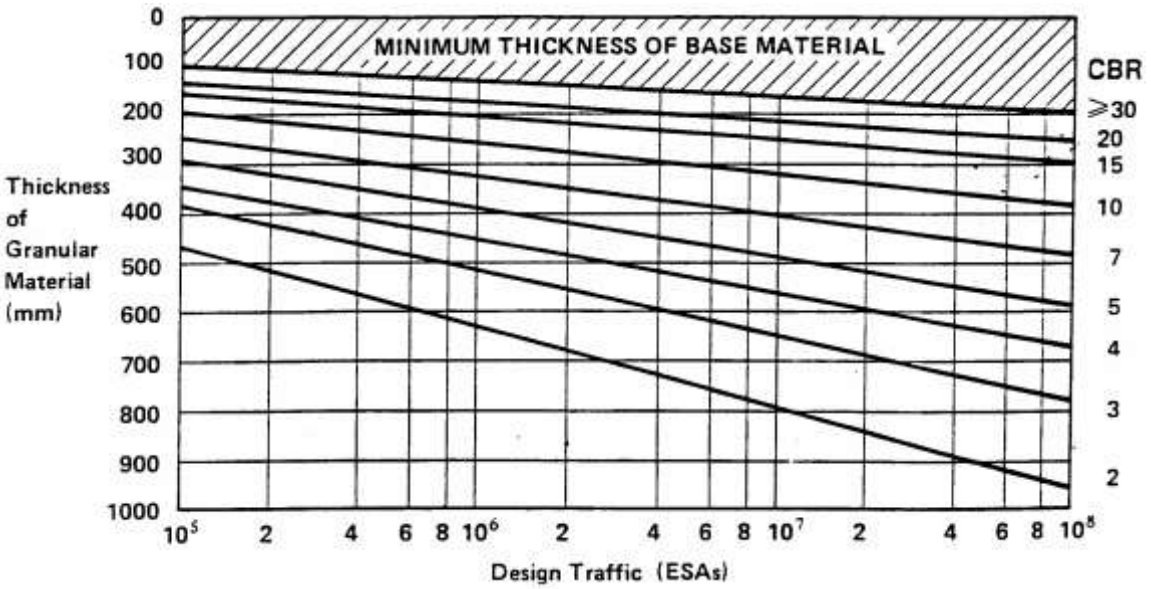

Porter's development of the (laboratory) CBR test (Porter 1938) can be taken as the starting point for the derivation of the pavement thickness design chart (figure 1.1). Using this test to characterise subgrades, the California State Highway Department, in reviewing the performance of its roads over the period 1929–1938, found that soil with a certain CBR always required the same thickness of flexible macadam (granular material) construction on top of it in order to prevent plastic deformation of the soil (Davis 1949). The curve relating the required thickness of flexible macadam to subgrade CBR for a '7000lb wheel load (light traffic)' was produced first. The curve for the wheel load of 12,000lb was added later as the result of further experience in California of heavier traffic conditions subsequent to 1938. The curve for the wheel load of 9000lb was obtained by interpolation between the curves for the wheel loads of 7000lb and 12,000lb. It is an implied assumption of these curves that all kinds of flexible construction of the macadam type spread the load to approximately the same extent.

George and Gittoes (1959) included in their report to the 1959 PIARC Congress a thickness design chart in a format very similar to the one currently in the Austroads (2004) guide (figure 1.1) – except that design traffic was expressed as repetitions of a 5000lb wheel load, as shown in figure 1.2.

Figure 1.2 Early Victoria, Australia thickness design chart (Source: George and Gittoes 1959)

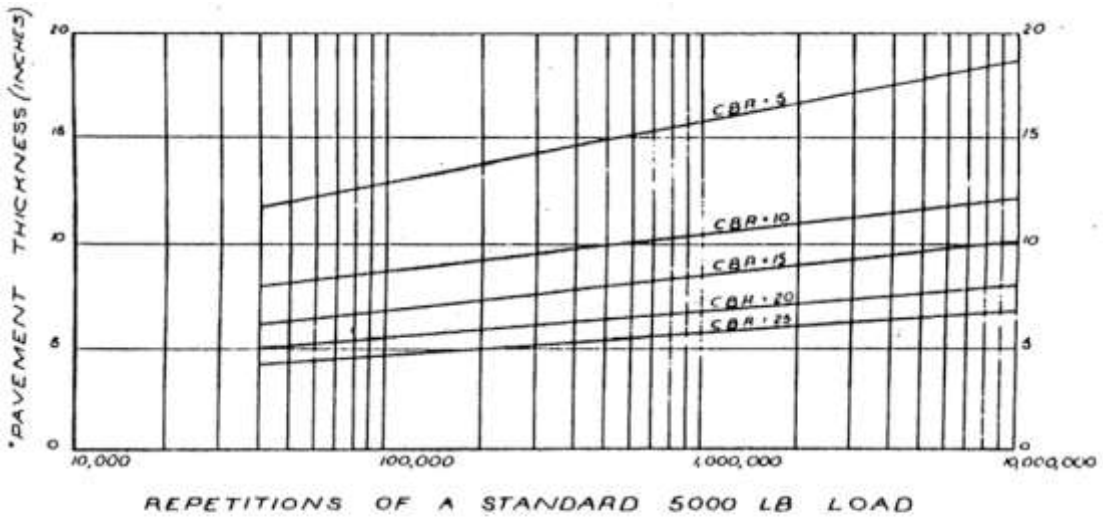

RELATIONSHIP BETWEEN PAVEMENT THICKNESS AND REPETITIONS OF A STANDARD WHEEL LOAD FOR VARYING SUBGRADE CALIFORNIA BEARING RATIOS. (C.B.R.)

During the development of the pavement thickness design chart, essentially the only finding from the American Association of State Highway Officials (AASHO 1962) road test which was 'picked up' was the adoption of the equivalent standard axle (ESA) as a basis for quantification of traffic loading.

The document investigating the basis for the current Austroads (2004) pavement design guide found that there was a lack of performance data (except at the macroscopic level) that could be used to justify the pavement thickness design chart.

Rodway (1997), in an overview of mechanistic pavement design, makes the following statements in relation to the pavement thickness design chart:

- The CBR design method is based on a failure mode that involves loss of shape of the pavement surface caused by overstressing the subgrade.
- The empirical CBR method implies that loss of surface shape is primarily caused by overstressing the subgrade. Deformation within the pavement layers is not directly addressed by this method.
- The CBR design procedure involves increasing pavement life by increasing pavement thickness to further protect the subgrade, not by improving the pavement materials.

Implicit in the pavement thickness design chart is a terminal condition. However, there is no evidence of what this terminal condition is except that the committee developing the Austroads pavement design guide agreed that it was probably a rut depth of 20mm and/or when the roughness was three times the initial roughness (Austroads 2008).

A further development to the pavement thickness design chart was mechanistic analysis using CIRCLY (Wardle 1980). CIRCLY uses linear elastic theory to calculate the stresses and strains in a pavement caused by the application of a dual-tyred ESA. The highest strain calculated on top of the subgrade is used to determine the pavement life as in the subgrade strain criterion (equation 1.1).

$$N_f = \left(\frac{9\ 300}{\mu\varepsilon} \right)^7 \qquad \text{(Equation 1.1)}$$

where:

N_f	[-]	number of standard axle repetitions (SAR) to failure
$\mu\varepsilon$	[10^{-6} m/m]	compressive elastic strain at the top of the subgrade produced by the load (Austroads 2004).

The subgrade strain criterion was developed by computing the vertical compressive strain (using CIRCLY and standard assumptions) on top of the subgrade for a range of subgrade CBRs and thicknesses and plotting this with life (number of ESAs) from the pavement thickness design chart (figure 1.1). Hence, whether CIRCLY or the design chart (figure 1.1) is used, the same life will be determined.

In summary, the current design procedure started with a CBR thickness design chart in California which at best was developed from experience at the time of what seemed to work, rather than a specific scientific experiment. The AASHTO road test only made a minor improvement by developing a method for combining all traffic types into one ESA. Further, the introduction of mechanistic pavement design with the use of CIRCLY has not improved the design procedure as it is aimed to achieve the same answer as the design chart.

Implicit in the current pavement design procedure is that pavement life can increase exponentially by simply increasing the depth of granular cover to the subgrade. This may be the case for roads with traffic volumes most likely up to 2 million ESAs, which is the limit of observed pavement performance by roading designers. This observation has been extrapolated to 10 and 100 million ESAs but never validated with experiments. There is some anecdotal evidence in New Zealand from the Canterbury accelerated pavement testing indoor facility (CAPTIF) and recent roads constructed on high traffic roads (eg Alpurt) that granular pavements require rehabilitation before 10 million ESAs regardless of the granular pavement thickness. A reason for this is that rutting occurs in the sub-base and basecourse materials and this has not been considered in the current design procedure.

Research at CAPTIF has shown that at least 50% of rutting can occur in the unbound granular material layers (Arnold et al 2001). Further, different aggregates complying to the same specification have clearly shown differences in the amount of rutting occurring within the layer. Average results from 51 trenches in the AASHTO road test were described as follows: 'a rut on the surface of the pavement was attributed to changes in thickness of 32 percent, 14 percent, and 45 percent, respectively, in surfacing, base and subbase, and to a rut in the embankment soil equal to 9 percent of the total' (Benkelman 1962). Thus the quality/rut resistant properties of the granular pavement layers can influence the pavement design. The use of rut depth modelling in this research project was intended to determine the differences in pavement life with different quality aggregates.

1.2 Observations at the Canterbury accelerated pavement testing indoor facility (CAPTIF)

Tests at CAPTIF studying the effects of changes in mass limits, used two different pavement depths and three aggregate types on the same subgrade type (CBR=10). The two basecourse depths used were 200mm and 275mm and from figure 8.4 in the Austroads pavement design guide (1992 and 2004) this represents pavement lives of 0.1 and 2 million ESAs respectively. However, the results from the CAPTIF tests (Arnold et al 2005) predicted only minor differences in pavement life due to changes in pavement

depth (table 1.1). This questions the applicability of the current Austroads pavement thickness design chart and associated Austroads subgrade strain criterion (equation 1.1) currently used in design.

Table 1.1 Pavement life predicted for each segment in CAPTIF mass limits test (Arnold et al 2005)

Segment	Material	Depth (mm)	Number ESAs[a] for 20mm rut depth (Predicted from linear extrapolation of data)	Life predicted by Austroads
A	Australian AP20	275	3.5 million	2 million
B	Australian AP20	200	4.2 million	0.1 million
C	TNZ M4 (AP40)	200	3.6 million	0.1 million
D	TNZ M4 (AP40)	275	4.2 million	2 million

[a] ESA is equal to 8.2 tonnes on a dual-tyred single axle or 80kN.

1.3 Models to predict pavement rutting

The CAPTIF pavements detailed in table 1.1 were modelled as part of Arnold's PhD at the University of Nottingham, England (Arnold 2004). This model utilised a relationship with stress and deformation derived from repeated load triaxial tests (RLT) on the aggregates and subgrade used at CAPTIF. A finite element model was used to compute stresses, which were inputted into the RLT deformation model to calculate the surface rut depth. Predicted rut depths were close to those that actually occurred at CAPTIF (table 1.1).

Werkmeister also developed a pavement model using relationships between resilient strain and permanent strain found from RLT tests to predict rutting at CAPTIF and found a good match between measured and predicted rutting (Werkmeister et al 2005).

Rut depth models (Arnold 2004; Werkmeister 2007) were used to derive pavement thickness design charts for granular pavements. After validating the rut depth model against recent CAPTIF tests, a range of pavements with different thicknesses and subgrade types was modelled to predict life (number of ESA passes until a 10, 15, 20 and 25mm rut depth). Results of this analysis were amalgamated to produce a granular pavement thickness design chart relating subgrade CBR, life (ESAs) and granular pavement thickness in the same format as the Austroads design chart (figure 1.1). Production of the design chart was repeated for poor, average and very good quality granular material as determined from the RLT test. It should be noted that the poor, average and very good aggregates all comply with the relevant NZ Transport Agency specifications and are only differentiated by the RLT test.

1.4 Other models to predict rutting

Over the years many researchers have begun to develop models for the prediction of permanent strain/rutting in unbound materials. Many of these relationships have been derived from permanent strain RLT tests. The aim of the models is to predict the magnitude of permanent strain from known loads and stress conditions. There are many different relationships reviewed in this section with quite different

trends in permanent strain development. The differences in relationships are likely to be a result of the limited number of load cycles and different stress conditions tested in the RLT apparatus. It is likely that more than one relationship is needed to fully describe the permanent strain behaviour of granular material.

For convenience and comparison, the relationships proposed for permanent strain prediction have been group in table 1.2 (after Lekarp 1997 except for those relationships from Theyse 2002). Details of the Werkmeister and Arnold methods for predicting rutting are described in the next section.

Table 1.2 Models proposed to predict permanent strain (after Lekarp 1997 except relationships from Theyse 2002)

Expression	Eqn.	Reference		Parameters
$\varepsilon_{1,p} = a\varepsilon_r N^b$	1.1	Veverka (1979)	$\varepsilon_{1,p}$	= accumulated permanent strain after N load repetitions
$K_p(N) = \frac{p}{\varepsilon_{v,p}(N)}$, $G_p(N) = \frac{q}{3\varepsilon_{s,p}(N)}$	1.2	Jouve et al (1987)	$\varepsilon^*_{1,p}$	
			$\varepsilon_{1,p}(N_{ref})$	= additional permanent axial strain after first 100 cycles
$G_p = \frac{A_2\sqrt{N}}{\sqrt{N}+D_2}$, $\frac{G_p}{K_p} = \frac{A_3\sqrt{N}}{\sqrt{N}+D_3}$	1.3		$\varepsilon_{v,p}$	= accumulated permanent axial strain after a given number of cycles N_{ref}, N_{ref} > 100
			$\varepsilon_{s,p}$	
$\frac{\varepsilon_{1,p}}{N} = A_1 N^{-b}$	1.4	Khedr (1985)	ε_N	= permanent volumetric strain for N > 100
			ε_i	
$\varepsilon_{1,p} = a + b\log(N)$	1.5	Barksdale (1972)	ε_r	= permanent shear strain for N > 100
			K_p	= permanent strain for load cycle N
$\varepsilon_{1,p} = aN^b$	1.6	Sweere (1990)	G_p	= permanent strain for the first load cycle
$\varepsilon_{1,p} = a(N + a(1 - e^{-bN}))$	1.7	Wolff and Visser (1994)	q	= resilient strain
$\varepsilon^*_{1,p} = \frac{A_4\sqrt{N}}{\sqrt{N}+D_4}$	1.8	Paute et al (1988)	p	= bulk modulus with respect to permanent deformation
			q^0	
$\varepsilon^*_{1,p} = A\left(1 - \left(\frac{N}{100}\right)^{-B}\right)$	1.9	Paute et al (1996)	p^0	= shear modulus with respect to permanent deformation
			p^*	
$\varepsilon_{1,p} = \sum \varepsilon_N = \sum \frac{1}{N^h}\varepsilon_i$	1.10	Bonaquist and Witczak (1997)	p_0	= deviator stress
			L	= mean normal stress

Expression	Eqn.	Reference		Parameters
$\varepsilon_{1,p} = \dfrac{q/a\sigma_3^b}{1-\left[\dfrac{R_f q/2(C\cos\phi+\sigma_3\sin\phi)}{1-\sin\phi}\right]}$	1.2	Barksdale (1972)	σ_3 N S $\varepsilon_{0.95S}$	= modified deviator stress= $\sqrt{2/3}\cdot q$ = modified mean normal stress= $\sqrt{3}\cdot p$ = stress parameter defined by intersection of the static failure line and the p-axis = reference stress = stress path length = confining pressure = number of load applications = static strength = static strain at 95% of static strength
$\varepsilon_{1,p} = \varepsilon_{0.95S}\ln\left(1-\dfrac{q}{S}\right)^{-0.15} + \left\{\dfrac{a(q/S)}{1-b(q/S)}\right\}\ln N$	1.3	Lentz and Baladi (1981)	C ϕ fn$N$ R_f h A_1 *A2-A4, D2-D4* M *a, b, c, d* *A, B, t, u* *PD* σ_1^a *SR*	= apparent cohesion = angle of internal friction = shape factor = ratio of measured strength to ultimate hyperbolic strength = repeated load hardening parameter, a function of stress to strength ratio = a material and stress-strain parameter given (function of stress ratio and resilient modulus) = parameters which are functions of stress ratio q/p = slope of the static failure line = regression parameters (*A* is also the limit value for maximum permanent axial strain) = permanent deformation (mm) = applied major principal stress = shear stress ratio (a theoretical maximum value of 1 indicates the applied stress is at the limit of materials shear strength defined by *C* and ϕ)
$\varepsilon_{1,p} = 0.9\dfrac{q}{\sigma_3}$	1.4	Lashine et al (1971)		
$\varepsilon_{s,p} = \ln N \left(\dfrac{q^0}{p^0}\right)^{2.8}_{\max}$	1.5	Pappin (1979)		
$A = \dfrac{\dfrac{q}{\phi+p^*}}{b\left(m-\dfrac{q}{\phi+p^*}\right)}$	1.6	Paute et al (1996)		
$\dfrac{\varepsilon_{1,p} N_{ref}}{1/p_0} = a\left(\dfrac{q}{p}\right)^b_{\max}$	1.7	Lekarp and Dawson (1998)		
$\varepsilon_p N = A\left(1-\left(\dfrac{N}{100}\right)^{-B}\right)\times\left(\dfrac{1}{p_a}\right)^r\times\left(\dfrac{q}{p}\right)^s$	1.8	Akou et al (1999)		

Expression	Eqn.	Reference		Parameters
$PD = dN + \frac{cN}{\left[1+\left(\frac{cN}{a}\right)^{b}\right]^{1/b}}$	1.9	Theyse (2002)	*RD* *St* *PS*	= relative density (%) in relation to solid density = degree of saturation (%) = plastic strain (%)
$PD = dN + a\left(1-e^{-bN}\right)$	1.10			
$PD = te^{aN} - ue^{-bN} - t + u$	1.11			
$\log N = -13.43 + 0.29RD - 0.07St + 0.07PS - 0.02SR$	1.12			
$SR = \frac{\sigma_1^a - \sigma_3}{\sigma_3\left(\tan^2\left(45^0+\frac{\phi}{2}\right)-1\right)+2C\tan\left(45^0+\frac{\phi}{2}\right)}$	1.13			

1.5 Repeated load triaxial tests to obtain parameters for rut depth models

The RLT apparatus (figure 1.3) applies repetitive loading on cylindrical materials for a range of specified stress conditions, the output is deformation (shortening of the cylindrical sample) versus number of load cycles (usually 50,000) for a particular set of stress conditions. Multi-stage RLT tests are used to obtain deformation curves for a range of stress conditions to develop models for predicting rutting (figure 1.4). The method developed by Arnold (2004) for interpreting the RLT results involves relating stress to permanent deformation found from the test. Similarly Werkmeister (2007) developed a model that relates resilient strain to permanent deformation found from the RLT test.

Figure 1.3 Repeated load triaxial apparatus

Figure 1.4 Typical results from multi-stage permanent strain RLT test (note: A, B, C, D, E and F represent different loading stresses for both cell pressure and vertical load)

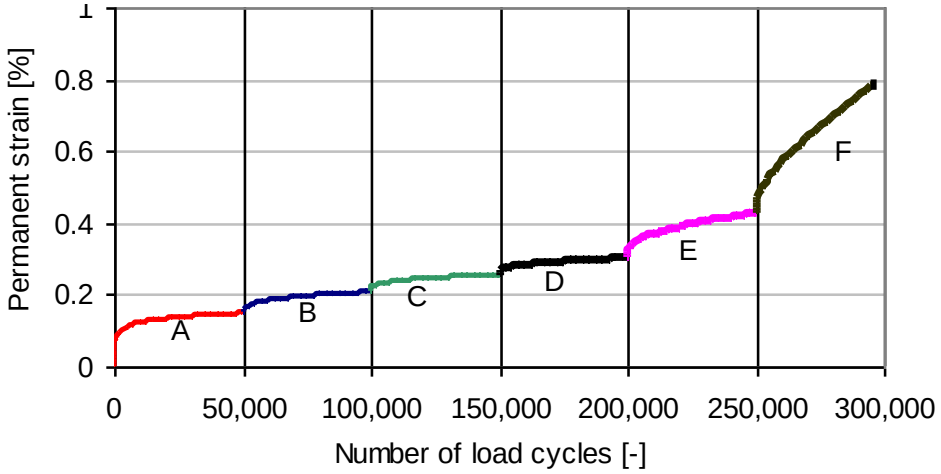

A standard test for granular materials has been developed and detailed in NZTA T/15 *Specification for repeated load triaxial testing (RLT) of unbound and modified road base aggregates* which gives stresses suitable for testing granular materials. However, these stresses are not suitable for testing subgrade soils

which will fail by shear after the first load is applied. Arnold (2004) conducted RLT tests on the subgrade at CAPTIF using stresses that were less than the shear strength of the soil. Another method for determining appropriate stresses to test soils is to allow the first test to be sacrificial and then to conduct a 30-stage test of 1000 cycles for each test. Each stage results in an increase in loading and the stage when the soil fails represents the highest loading that can be applied. Ideally at least six full stages are completed to provide enough data for the rut depth models. In this research project, many RLT tests were conducted on subgrade soils of CBR 2, 8 and 10 as used at CAPTIF to determine the necessary parameters for the rut depth model.

2 Rut depth prediction methods

2.1 Arnold (2004) rut depth prediction method

2.1.1 Introduction

The first step in predicting rutting is to undertake multi-stage permanent strain RLT tests on the materials in the pavement including the subgrade, subbase and basecourse. This allows relationships between stress and permanent deformation to be determined for each material in the pavement. From the RLT tests, a relationship between stress and resilient modulus is also determined for use in a finite element programme to determine stresses and strains in the pavement at incremental depths. These stresses and strains are imported into a spreadsheet where the rut depth is calculated at each depth increment using the relationships to predict rutting found from RLT testing.

2.1.2 RLT tests

Using the RLT apparatus, Arnold (2004) studied the effect of different combinations of cyclic vertical and horizontal stress levels on a range of granular materials. The granular materials chosen were those used in full-scale pavement tests in Northern Ireland, UK and at CAPTIF. The subgrade silty clay soil used at CAPTIF was also tested in the RLT apparatus.

The aim of the RLT tests was to determine the effect of stress condition on permanent strain. RLT permanent strain tests are time consuming and many tests are needed to cover the full spectrum of stresses expected within the pavement. To cover the full spectrum of these stresses Jouve and Guezouli (1993) conducted a series of permanent strain tests at different combinations of cell pressure and cyclic vertical load. Most of the stresses calculated by Jouve and Guezouli (1993) showed the mean principal stress ($p = (\sigma_1 + 2\sigma_3)/3$) varied from 50kPa to 300kPa and the deviatoric stress ($q = (\sigma_1 - \sigma_3)$) from 50kPa to 700kPa. These ranges of stresses were confirmed by the authors through pavement analysis using the CIRCLY linear elastic program (Wardle 1980). Although at the base of the granular layers negative values of p were calculated, as a granular material has limited tensile strength, negative values of mean principal stress were discounted. The results of the static shear failure tests conducted on the materials plotted in p–q stress space were used as an approximate upper limit for testing stresses.

It is common to use a new specimen for each stress level. However, to reduce testing time, multi-stage tests were devised and conducted. These tests involved applying a range of stress conditions on one sample. After the application of 50,000 load cycles (if the sample had not failed) new stress conditions were applied for another 50,000 cycles. These new stress conditions were always slightly more severe (ie closer to the yield line) than the previous stress conditions.

Test stresses were chosen by keeping the maximum value of p constant while increasing q for each new increasing stress level closer and occasionally above the static yield line. Three samples for each material were tested at three different values of maximum mean principal stress p (75kPa, 150kPa and 250kPa). This covered the full spectrum of stresses in p–q stress space so as to allow later interpolation of permanent strain behaviour in relation to stress level. A typical output and stress paths from a multi-stage RLT test is shown in figure 2.1.

Figure 2.1 Typical RLT permanent strain test result for NI Good UGM

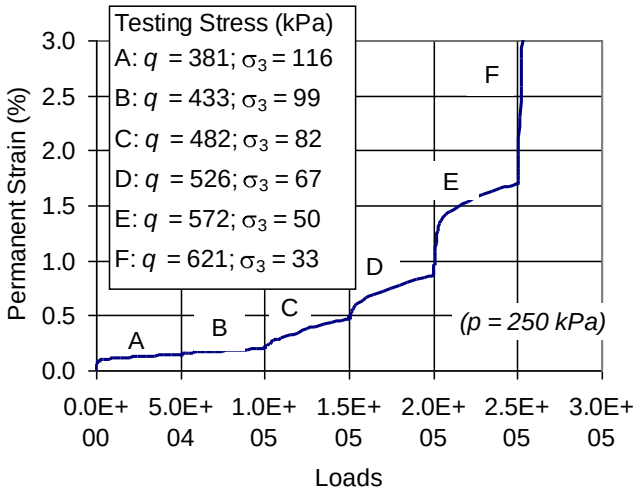

2.1.3 Modelling permanent strain

Results from RLT tests showed a high dependence on stress level. Plots of maximum deviator stress, *q* versus permanent strain rate for each multi-stage test analysed separately with mean principal stress, *p* constant, resulted in exponential relationships that fitted well to the measured data (figure 2.1). This prompted an investigation of an exponential model that could determine the secant permanent strain rate from the two maximum values of *q, p* stress.

Utilising the rate of deformation seemed more appropriate for RLT multi-stage tests than using the accumulated sum of the permanent strain for each part of the multi-stage test. Adding the sum of the permanent strains of all the previous stages would likely over-estimate the amount of deformation, for example by increasing the number of test stages conducted prior to that of the present stress level in question, and would lead to a higher magnitude of permanent strain. Also on reviewing the RLT permanent strain results during the first 20,000 load cycles, there was a 'bedding in' phase until a more stable/equilibrium type state was achieved. It had been argued that this equilibrium state was unaffected by differences in sample preparation and previous tests in the multi-stage tests. Therefore, relationships considering permanent strain rate were explored.

The scatter in results was reduced by using the secant rate of permanent strain between 25,000 and 50,000 load cycles in place of permanent strain magnitude when plotted against stress ratio (q/p). This rate of permanent strain was calculated in percent per 1 million load cycles. These units have some practical interpretation, as a value of 5% per million load cycles can be approximately related to 5mm of deformation occurring for a 100mm layer after 1 million load applications.

Figure 2.2 Example plot showing how exponential functions fit measured data for individual multi-stage tests

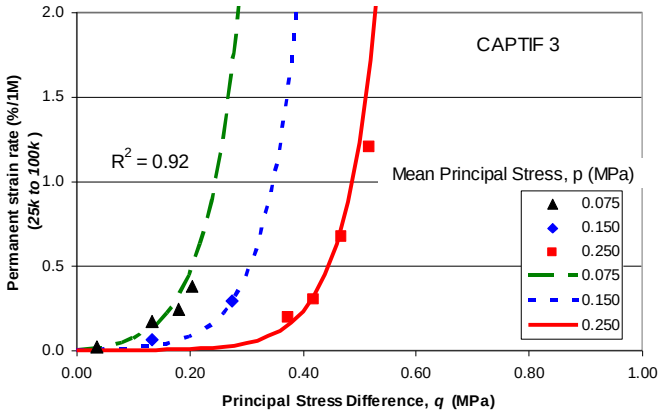

Regression analysis was undertaken on the RLT test data with stress invariants *p* and *q* against the associated natural logarithm of the strain rate. Permanent strain rate is thus defined by equation 2.1:

$$\varepsilon_{p(\text{rate or magn})} = e^{(a)}\, e^{(bp)}\, e^{(cq)} - e^{(a)}\, e^{(bp)} \qquad \text{(Equation 2.1)}$$

$$= e^{(a)}\, e^{(bp)}\, (e^{(cq)} - 1)$$

where:

e = 2.718282

$\varepsilon_{p(\text{rate or magn})}$ = secant permanent strain rate or can be just permanent strain magnitude

a, b & c = constants obtained by regression analysis fitted to the measured RLT data

p = mean principal stress (MPa)

q = mean principal stress difference (MPa).

To determine the total permanent strain for any given number of load cycles and stress condition, the permanent strain data in four zones was observed. In the New Zealand accelerated pavement tests (Arnold 2004) the permanent strain rates changed during the life of the pavements, different values being associated with the early, mid-, late- and long-term periods of trafficking. Similarly RLT permanent strain tests showed changing permanent strain rates during their loading. After studying RLT and accelerated pavement test results, a power law equation of the form, $y = ax^c$ was fitted to each 50,000 RLT load cycle stage (figure 2.3) to extend the permanent strain data to 500k or 1 million load cycles (note the analysis for determining pavement life uses both methods for comparison). To limit the number of times equation 2.1 was used to fit the RLT data, it was decided to break the RLT permanent strain data into the following four zones of different behaviour for use in calculating permanent strain at any given number of load applications (*N*) (figure 2.3):

1 Early behaviour (compaction important): 0–25,000 load applications. The magnitude of permanent strain at 25,000 load applications, being the incremental amount $\varepsilon_p(25{,}000)$, was used for the reasons outlined above. Keeping the magnitude of permanent strain separate at 25,000 was useful when predicting rut depth in terms of identifying where the errors occurred.

2 Mid-term behaviour: 25,000–50,000 load applications. The secant permanent strain rate between 25,000 and 50,000 load applications was used.

3 Mid-term behaviour: 50,000–100,000 load applications. The secant permanent strain rate between 50,000 and 100,000 load applications was used.

4 Late behaviour: 100,000–500,000 load applications. The secant permanent strain rate between 100,000 and 500,000 load applications was used. This is extended to represent the long-term behaviour as a conservative approach to predicting the rut depth.

This assumed that the permanent strain rate remained constant after 1 million load applications. The approach was appropriate as the aim was to calculate rut depth for pavements with thin surfacings where at CAPTIF Arnold (2004) found the rate of rutting was linear. Further, assuming the permanent strain rate did not decrease after 1 million load applications was a conservative estimate compared with the assumption of permanent strain rate continually decreasing with increasing load cycles (ie a power model, $y = ax^b$).

Hence, four versions (four sets of constants) of equation 2.1 were determined and used for describing the permanent strain behaviour at any given number of loadings.

Figure 2.3 Methods of extrapolation of RLT data and rut depth prediction

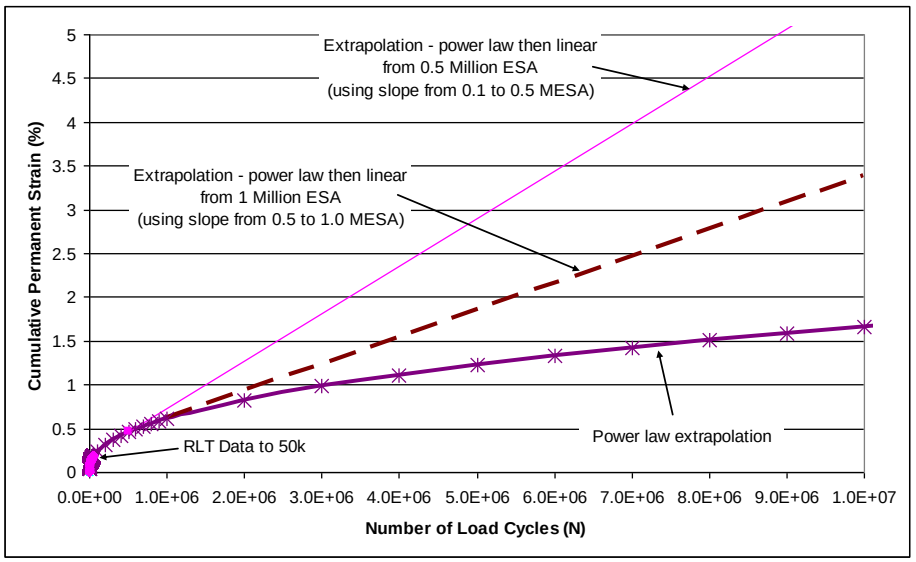

The RLT multi-stage permanent strain test results for six granular and one subgrade material were analysed by relating the permanent strain rate with the stress level for each stage. Microsoft Excel© Solver was used to determine the equation constants *a* and *b* by minimising the mean error which was the difference in measured and calculated strain rates. For the CAPTIF 3 granular material, the model fitted the data well with a R^2 value of 0.92 (figure 2.2). A similar good fit to the model (equation 2.1) was found for the other five granular and one subgrade materials tested. Mean errors were less than 1%/1 million which, when applied to rut prediction, gave an equivalent error of 1mm per 100mm thickness for every 1 million wheel passes. Overall the model (equation 2.1) showed the correct trends in material behaviour as there was an increasing permanent strain rate with increasing deviatoric stress (q) while a higher load could be sustained with higher confining stress.

2.1.4 Calculating pavement rut depth

To predict the surface rut depth of a granular pavement from equation 2.1 required a series of steps. There were assumptions required in each step which significantly affected the magnitude of calculated rut depth. Steps and associated errors and assumptions are summarised below. The first five steps related to the interpretation of RLT permanent strain tests as already described in section 2.1.3 above. The final three steps involved pavement stress analysis, calculations and validation required to predict the surface rut depth of a pavement.

2.1.4.1 Pavement stress analysis

Equation 2.1 is a model where for any number of load applications and stress conditions the permanent strain can be calculated. Stress is therefore computed within the pavement under a wheel load for use in equation 2.1 to calculate permanent strain. It is recognised from literature and RLT tests that the stiffness of granular and subgrade materials are highly non-linear. A non-linear finite element (FE) model, DEFPAV (Snaith et al 1980) was originally used to compute stresses within the pavement (Arnold 2004). Rubicon is now used as a more versatile finite element program to calculate stresses and strains in the pavement using non-linear relationships between stress and resilient modulus for each material. Further, the small residual confining stresses considered to occur during compaction of the pavement layers were assumed to be nil in the analysis.

From the pavement stress analysis, the mean principal stress (p) and deviatoric stress (q) under the centre of the load were calculated for input into a spreadsheet along with depth for the calculation of rut depth. The calculated stresses had a direct influence on the magnitude of permanent strain calculated and resulting rut depth. Thus any errors in the calculation of stress would result in errors in the prediction of rut depth. Some errors in the calculation of stress from Rubicon and DEFPAV were a result of not considering the tensile stress limits of granular materials and the assumption of a single circular load of uniform stress approximating dual tyres, which did not have a uniform contact stress (de Beer et al 2002).

2.1.4.2 Surface rut depth calculation

The relationships derived from the RLT permanent strain tests were applied to the computed stresses in the FE analysis. Permanent strain calculated at each point under the centre of the load was multiplied by the associated depth increment and summed to obtain the surface rut depth.

2.1.4.3 Validation

The calculated surface rut depth with the number of wheel load applications was compared with actual rut depth measurements from accelerated pavement tests in New Zealand (CAPTIF) and the Northern Ireland (NI) field trial. This comparison determined the amount of rut depth adjustment required at 25,000 cycles while the long-term rate of rut depth progression and, in part, the initial rut depth at 25,000 cycles was governed by the magnitude of horizontal residual stress added. An iterative process was required to determine the initial rut depth adjustment and the amount of horizontal residual stress to add, in order that the calculated surface rut depth matched the measured values.

The result of this validation process was detailed fully in Arnold (2004). Overall the predictions of rut depth were good, particularly the trends in rut depth progression with increasing loading cycles (ie this relationship was sensibly the same for actual and predicted measurements in 11 out of 17 analyses). Adjustment of up to a few millimetres to the predicted rut depth at 25,000 cycles was generally all that was needed to obtain an accurate prediction of rut depth. For the six tests with poor predictions, three of these could be accurately predicted by applying a small residual stress of 17kPa to the stresses calculated

in the pavement analysis. The other three poor results were due to an asphalt layer of 100mm and a moisture sensitive aggregate where the RLT test was at a higher moisture content than what actually occurred in the test pavement. The predictions were as expected in terms of accurately predicting the rate or rutting but inaccurately predicting the initial rutting due to secondary consolidation. This is because the actual magnitude for the first 25,000 load applications from the RLT test was difficult to estimate, as it was unknown whether the value was the cumulative or incremental value of permanent strain from the multi-stage RLT test (figure 2.1 1). The method adopted was to take the incremental value of permanent strain at 25,000 cycles, which was considered to be a low estimate. This was the case for pavement test sections 3, 3a and 3b which all used the CAPTIF 3 granular material and for test sections 4, 5 and 6 where an additional amount of rutting was added to coincide with the measured values in the pavement test. The opposite occurred for the test sections 1, 1a and 1b which all used the CAPTIF 1 material where the predicted rutting was higher than the measured rutting.

Further validation of the Arnold method was undertaken when analysing recent CAPTIF tests that used a different subgrade material. These are described in chapter 4 of this report.

2.2 Description of Werkmeister model

This section presents an approach to predict the plastic deformation of the basecourse/subgrade in pavements using the elastic strains. The investigation was based on RLT and CAPTIF test results and used the axial elastic strain to predict the axial plastic strain rate per load cycle. The relationship developed using laboratory and field results was applied to the axial elastic strains calculated and integrated over the depth of the basecourse layer and the number of load cycles in the CAPTIF tests to determine the plastic deformation (rut depth) occurring in the basecourse. The advantage of this simplified method to predict the rut depth of the basecourse was that only elastic FE calculation results (elastic strain distribution in the wheel path) were required. The elastic FE calculation process was less complicated and time consuming than plastic FE calculations.

A similar approach was suggested by Theyse (2004) for the pavement subgrade from heavy vehicle simulator (HVS) results. However, the plastic subgrade deformation was not taken into account in this investigation.

2.2.1 Modelling the steady state phase using RLT test results

The raw RLT test data was obtained from Arnold (2004) and analysed in terms of elastic axial strain (ε_{el}) and the plastic strain rate ($\dot{\varepsilon}_p$ /N). Because the initial part of the plastic deformation curve is often influenced by the technique used in preparing the sample, it was decided to extrapolate the plastic deformation curve and focus on the steady state response of the sample (load cycles 100,000 to 500,000, see figure 2.4).

Figure 2.4 Determination of plastic strain rate value

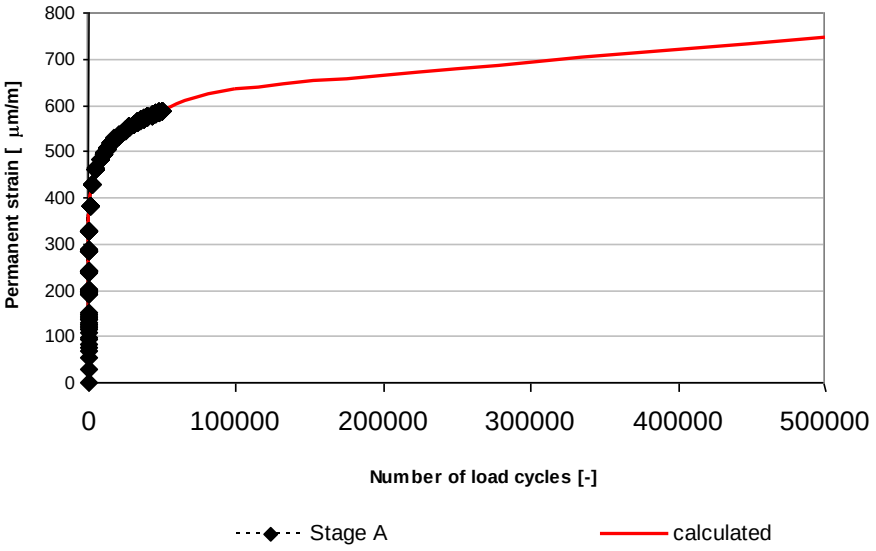

The elastic strain value (ε_{el}) was averaged over the same interval (load cycles 100,000 to 500,000) to give an average value of ε_{el}.

Using the RLT test results, the following relationship (equation 2.2) between the elastic strain (ε_{el}) and plastic strain rate ($\dot{\varepsilon}_p$) can be determined as long as the shear stresses within the basecourse are sufficiently small and the material behaviour corresponds to either a continually reducing plastic strain rate with increasing load cycles or a constant plastic strain rate. Excluded from the fit were the tests that failed prior to 50,000 load cycles, which was usually the highest stress level in each multi-stage (MS) test. Results where failure occurs do not follow the same trend as the other results due to significantly larger deformations/shear failure (range C behaviour) and this mechanism of accumulation of plastic strain is different from the other test results.

$$\dot{\varepsilon}_p = E \cdot \varepsilon_{el}^{\ F} \qquad \text{(Equation 2.2)}$$

where:

$\dot{\varepsilon}_p$	[10^{-3}/cycle]	major principal plastic strain rate
ε_{el}	[10^{-3}]	major principal elastic strain
E, F	[-]	material parameter.

The parameters E and F are mainly dependent on the material, moisture content and degree of compaction and were determined for the CAPTIF 1, Todd clay and Waikari clay materials. Figures 2.5, 2.6 and 2.7 show the relationship between axial elastic strain and axial plastic strain rate per load cycle on a (ε_{el}) vs ($\dot{\varepsilon}_p$) plot.

Figure 2.5 Axial elastic strain versus plastic strain rate for CAPTIF 1 material, RLT test results

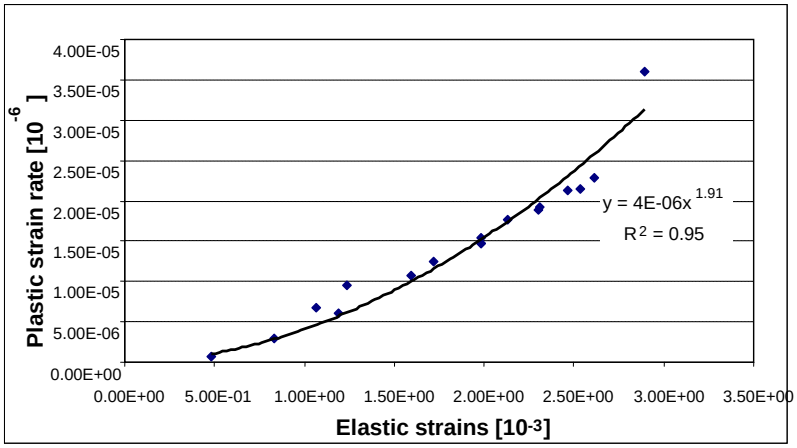

Figure 2.6 Axial elastic strain versus plastic strain rate for Todd Clay material, RLT test results

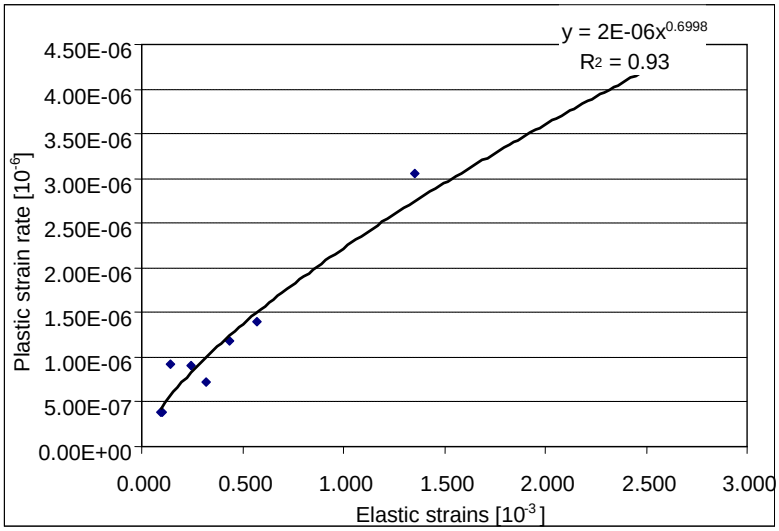

Figure 2.7 Axial elastic strain versus plastic strain rate for Waikari Clay material, RLT test results

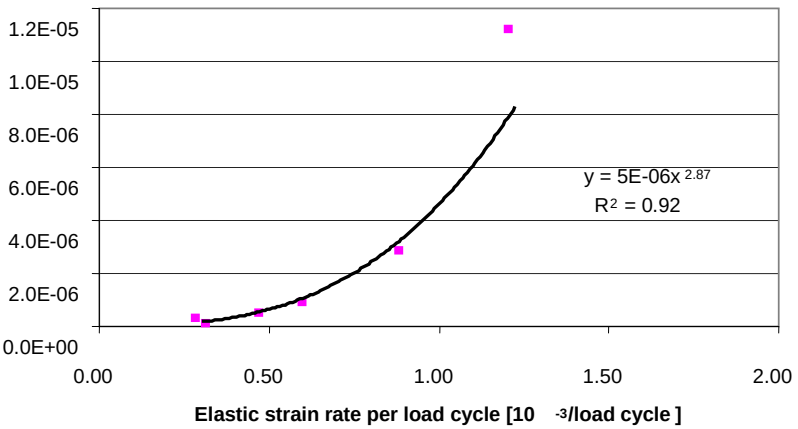

In most cases, CAPTIF elastic data consists of direct measurements of the elastic strains between the two wheels using εmu strain coils. The program ReFEM (Oeser 2004) was used to determine the distribution of axial elastic strains directly underneath the wheels for the load applied in the CAPTIF tests. The averages of these axial elastic basecourse strain values were taken for the determination of the CAPTIF elastic strain values (field results).

The CAPTIF test results showed a similar dependency between the elastic strain and the plastic strain rate to the results of laboratory tests. By comparing the elastic/plastic relationship from laboratory tests and the elastic/plastic relationship from field tests, a good correlation was observed. In addition, the results proved that the RLT test was a suitable testing method to investigate the stress-strain behaviour of basecourse materials used in pavements.

The model developed (equation 2.2) was linear and therefore suited only to cases where plastic strain was expected to be a shakedown range B response. Although, for low-stress levels the model would calculate a low value of plastic strain and therefore it might suffice for expected range A responses also.

Figure 2.8 illustrates the elastic strain distribution in the basecourse layer under a 40kN and 50kN wheel load using the FE calculation results. The plastic strain values during the steady state phase were determined for the basecourse using equation 2.2 (PR3-0404 test, CAPTIF 1 material). The analysis shows that the most critical (maximum) vertical elastic and plastic strains occurred at the first third of the basecourse layer for the pavements investigated.

In addition, the calculated plastic strain values using equation 2.2 were compared with the measured plastic strain values at CAPTIF. The calculated plastic strain values ($\dot{\varepsilon}_p$) at different depths of the basecourse were calculated to give an average value of ($\dot{\varepsilon}_p$). A good agreement between the calculated plastic strain rates and the measured plastic basecourse strain rate values at CAPTIF could be observed. For most of the pavements, range B behaviour was measured. However, one station of the PR3-0610 test showed range A behaviour.

Figure 2.8 Measured plastic strain rate versus calculated plastic strain rate, PR3-0610 test, inner and outer wheel path

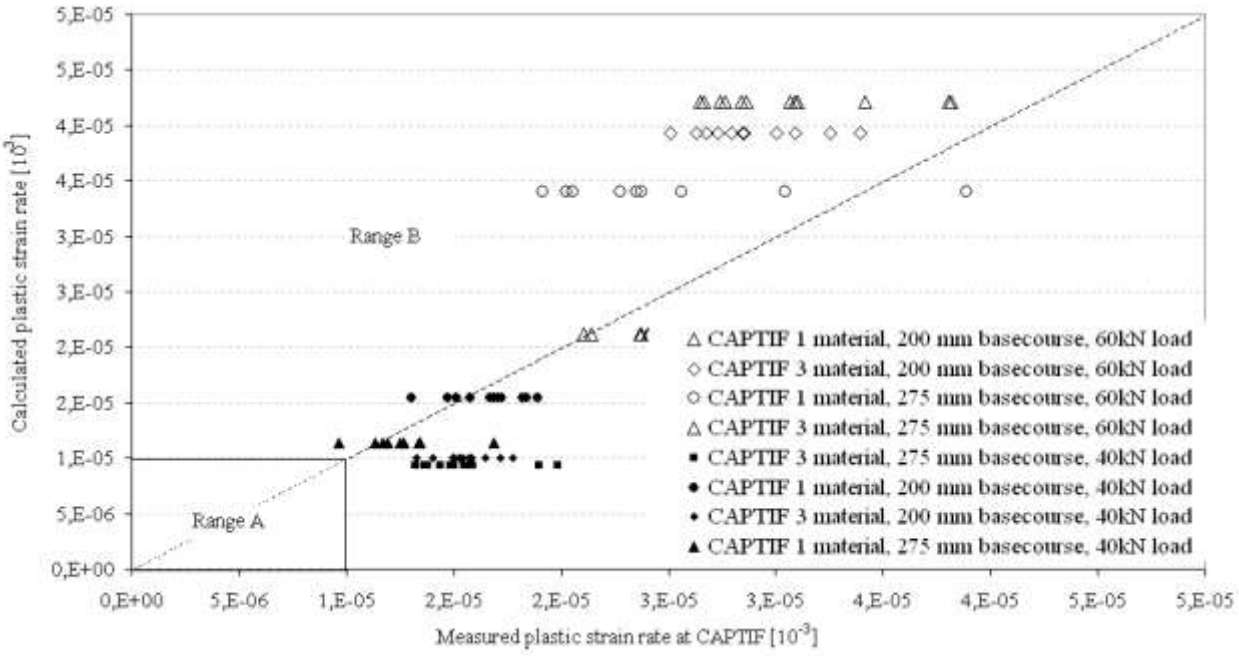

2.2.2 Modelling of post-construction compaction using CAPTIF test results

CAPTIF test data was used to investigate the post-construction compaction and to determine a relationship between the axial plastic strain rate during post-construction compaction and during the steady state phase.

CAPTIF test results showed that the number of load cycles until completion of post-construction compaction was dependent on the elastic strains. Using CAPTIF test results (PR3-0404 and PR3-0610 tests) a relationship between the axial elastic strains (ε_{el}) and the number of load cycles (*Npc*) for the completion of post-construction compaction could be determined (equation 2.3 and figure 2.9).

$$N_{pc} = 211.71 \cdot \varepsilon_{el}^{0.8232} \qquad \text{(Equation 2.3)}$$

where:

N_{pc} [-] = number of load cycles for completion of post-construction compaction.

ε_{el} [10^{-6}] = axial elastic strain.

Figure 2.9 Axial elastic strain versus number of load cycles until post-construction compaction is completed

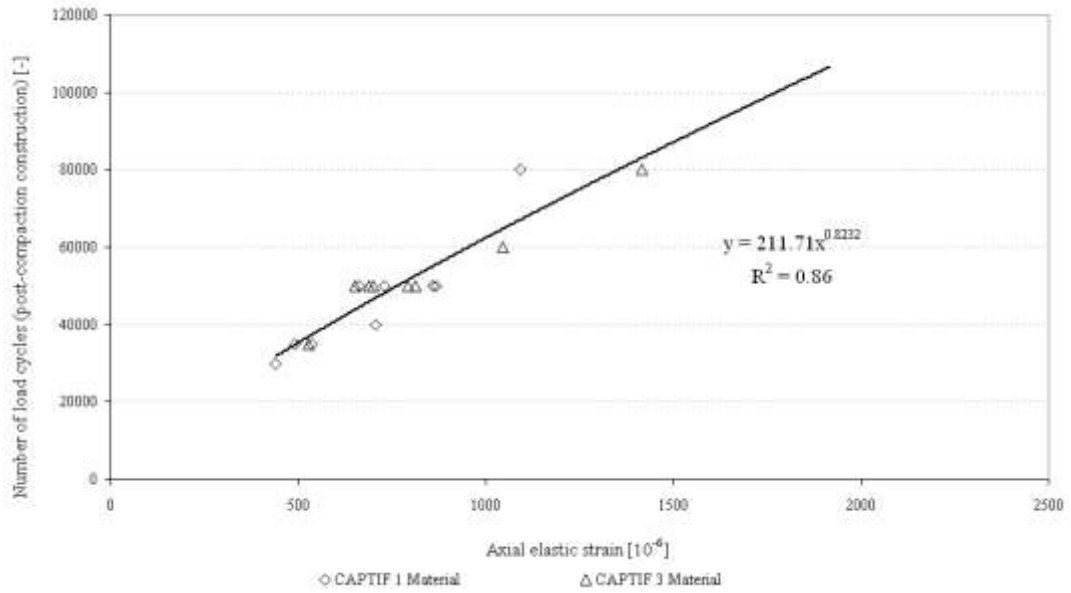

The following exponential relationship (equation 2.4) between the plastic strain rate during the steady state phase ($\dot{\varepsilon}_p$) and the plastic strain rate during post-construction compaction ($\dot{\varepsilon}_{p\,pc}$) was found using CAPTIF test results (PR3-0404 and PR3-0610 test).

$$R = 0.0042 \cdot \dot{\varepsilon}_p^{-0.6869} \qquad \text{(Equation 2.4)}$$

where:

$\dot{\varepsilon}_p$ [10^{-3}/cycle] = plastic strain rate per load cycle during steady state phase

R [-] = ratio between plastic strain rate (post-construction compaction) and plastic strain rate (steady state).

Equations 2.3 and 2.4 are valid for CAPTIF 1 material. The equations were adopted for the subgrade solids as well. Figure 2.10 shows the relationship between plastic strain rate per load cycle during the steady state phase and axial plastic strain rate per load cycle during the post-construction compaction (CAPTIF test results) on a ($\dot{\varepsilon}_p$) vs. (R) plot.

Figure 2.10 Axial plastic strain rate (steady state) versus the ratio of axial plastic strain rate (post-construction compaction) and axial plastic strain rate (steady state)

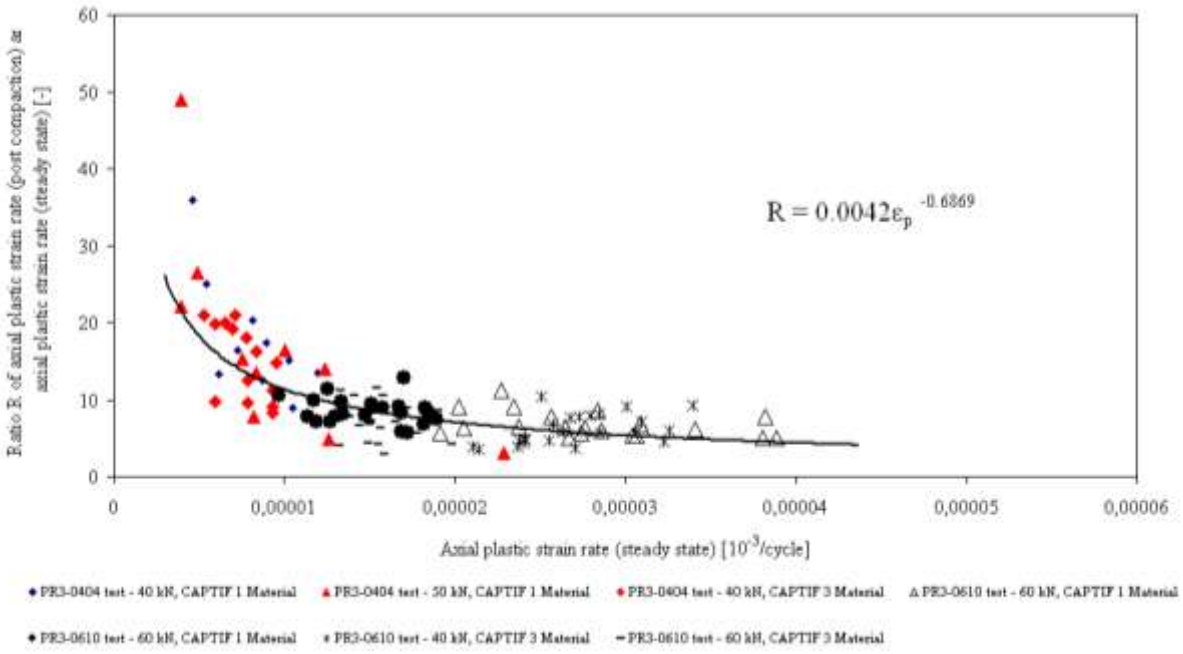

2.2.3 Model validation comparing laboratory results with CAPTIF test results

As discussed, the development of plastic defomation at CAPTIF can be divided into the initial post-construction compaction and the steady state phase. The initial post-construction compaction at CAPTIF is usually completed within the first 25,000 to 100,000 load cycles (see equation 2.3). The amount of plastic deformation that occurred from the start of the test to the completion of post-construction compaction and the plastic deformation that occurred from completion of post-construction compaction to the end of the test were calculated.

The axial elastic strain profile of the pavement was determined for the load applied in the CAPTIF tests under the wheels (beneath the centre of one tyre) using 3D-FE caluation results. The basecourse layer was divided into a number of sublayers and the axial elastic strain values at the mid-points of the layers were used to determine the value of ($\dot{\varepsilon}_p$) for each layer. Finally, the plastic deformation of the basecourse was determined by multiplying each ($\dot{\varepsilon}_p$) value by the sublayer thickness and the number of load cycles. The total amount of plastic deformation of the basecourse layer was calculated by summing the contributions of each sublayer. Table 2.1 shows an example of the calculation process for section D, inner wheelpath, PR3-0404 test.

Table 2.1 Plastic deformation calculation for section D, PR3-0610 test (275mm BC, 40 kN load, subgrade stiffness 50 MPa, CAPTIF 1 material)

Depth to midheight of the sublayer	Sublayer thickness	Elastic strains	Plastic strain rate steady state	Plastic deformation steady state	Load cycles post-construction compaction	Plastic strain rate post-construction compaction	Plastic deformation post-construction compaction
[mm]	[mm]	[10-3]	[10-3/cycle]	[mm]	[-]	[10-3/cycle]	[mm]
25	34	1.364	1.35E-05	0.43	80,597	1.26E-04	0.35
94	69	1.575	1.97E-05	1.23	90,728	1.41E-04	0.88
163	69	1.221	1.01E-05	0.64	73,574	1.15E-04	0.58
231	69	0.981	5.71E-06	0.37	61,445	9.58E-05	0.40
325	34	0.971	5.56E-06	0.18	60,928	9.50E-05	0.20
Plastic basecourse deformation [mm]				2.85		2.41	

In addition, the plastic basecourse deformation at CAPTIF was determined using the measured vertical surface deformation/rutting (VSD) values. VSD values of both tyres were averaged to eliminate any imbalance in plastic deformation between the two paths. Based on the results of the trench profiles the plastic surface deformation values obtained were reduced to remove the plastic deformation that occurred in the subgrade. The plastic deformation values for the different test sections are given in table 2.2. It can be seen that the plastic deformation values for the post-construction compaction are relatively high compared with the plastic deformation values during the steady state period.

Table 2.2 Comparison between calculated and measured plastic deformations beneath the tyre

				Total		Basecourse	
CAPTIF Test	Basecourse	Basecourse	Loading	Measured	Calculated	Measured	Calculated
Section	Material	[mm]	[kN]	[mm]	[mm]	[mm]	[mm]
PR3-0805 E	CAPTIF 1	300	40	5.0	6.81	3.7	4.55
PR3-0805 E	CAPTIF 1	300	50	7.6	9.46	5.7	6.7
PR3-0610 C	CAPTIF 1	200	40	6.5	6.16	4.9	4.2
PR3-0610 C	CAPTIF 1	200	60	11.1	14.87	8.3	10.6
PR3-0404 A	CAPTIF 1	275	40	6.0	6.44	3.6	4.4
PR3-0404 A	CAPTIF 1	275	50	11.4	9.62	7.4	6.5

Figure 2.11 shows the number of load cycles versus the axial plastic deformation (in the wheel path) using equations 2.2, 2.3 and 2.4.

Figure 2.11 Axial plastic basecourse deformation versus N (data and model), PR3-0404 test, CAPTIF 1 material

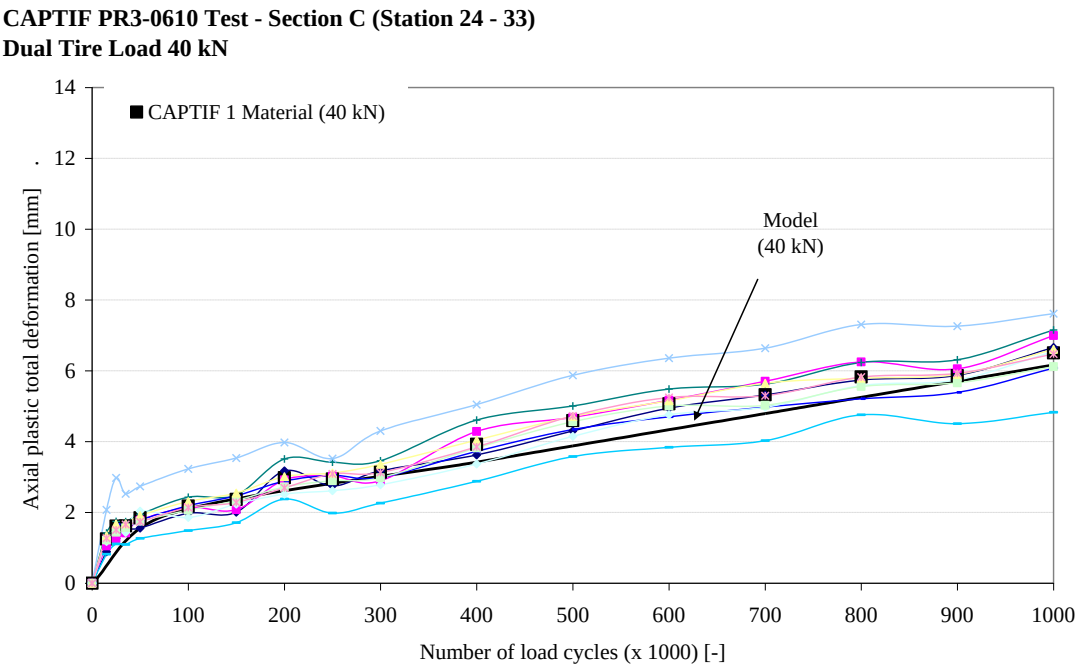

2.2.4 Discussion

The results of the investigations showed a good agreement between the measured and calculated results. However, an exact agreement between the real performance and the modelling results can never be achieved because so many factors influence the deformation performance of the pavements. This is clearly shown by the relatively high variation of the rut depth values measured at CAPTIF for the same pavement structure within one section.

Furthermore the real pavement contact pressure distribution was not taken into account in the calculation process. The accuracy of the models depends on the accurate portrayal of tyre/road contact stress distributions. In a research project funded by the NZTA (Douglas 2009), an apparatus to measure tyre/road surface contact stress distributions in all three coordinate directions was fabricated and calibrated. A wide range of full-scale trafficking tests was carried out on the apparatus at CAPTIF and the contact stress distributions were measured. The distributions were then input to numerical models of pavement behaviour and the results compared to those models' predictions where the loading was a uniformly distributed vertical pressure only, within the contact patch.

The research showed that due to the different tyre contact pressure modelling there were differences in response, but they were often not large. Vertical stresses on top of the subgrade were 3% to 8% greater when the non-uniform contact stresses were used. For dual tyres, the differences were greater at 12% to 27%, but the larger differences may well have been due to the unequal loading of the two tyres in the dual set. These differences in response, though not particularly great, especially if some credit is given to the unequal tyre loads in the dual tyre configurations, were enough however to affect the long-term pavement performance significantly. The rut depths predicted using the non-uniform contact stresses were a little over a quarter greater than those predicted using the conventional uniform pressure. However, it is felt that there was enough evidence in the experimental results to conclude that there were small though measurable differences in pavement response when modelled using non-uniform contact stresses, and

that these differences in pavement response gave rise to substantial differences in predicted pavement performance (Douglas 2009).

3 Repeated load triaxial testing

3.1 Introduction

This section provides a summary of the results of RLT testing of subgrade soils used at CAPTIF. RLT tests apply repetitive loading to cylindrical soil or aggregate specimens at user-defined vertical and confining stresses. The aim is to replicate in some way the loadings expected to occur on the material when used in a pavement. Information from the tests, such as rate of permanent deformation at a range of different stress conditions, can be used in pavement models to calculate the amount of rutting expected to occur. Rutting in all the pavement layers and subgrade soils are added together to compute the rut depth at the surface and determine the number of wheel loads required to reach a defined end of life rut depth (eg 15mm or 25mm). Two different approaches of pavement modelling and rut depth prediction were used in this research project: one was stress based (the Arnold 2004 method) and the other a strain-based approach (the Werkmeister method). After validation of the assumptions and criteria used in each model against CAPTIF results, the models were used to predict rutting for a range of pavement cross sections.

3.2 RLT test results for basecourse and sub-base aggregates

The first year of this research project involved getting the necessary laboratory data required for pavement modelling and validation with CAPTIF data. RLT data is required for all the materials that make up the different layers of the pavement: basecourse, sub-base and subgrade. RLT data from basecourses are readily available from the many tests already conducted commercially and for research. Sub-base aggregates are being tested in a related NZTA research project, 'Development of a basecourse/subbase design criterion' which is being carried out by the authors of this report. Out of the database of RLT tests a poor, average and very good basecourse and sub-base were selected for rut depth modelling in this project. All aggregates selected complied with NZTA specifications and they were only classified as poor, average and very good depending on their performance in the RLT test (ie lower permanent deformation was considered the best performance). In selecting aggregates, outliers were not considered (ie those aggregates that behaved significantly different from the norm). Figure 3.1 shows the results of rut depth prediction of RLT tests on a large number of basecourse aggregates from the NZTA research project, 'Development of a basecourse/subbase design criterion'. The poor basecourse confirmed to the lower boundary in figure 3.1, while the average was the medium boundary and the 'very good' was the upper boundary.

Figure 3.1 Results of basecourse RLT tests

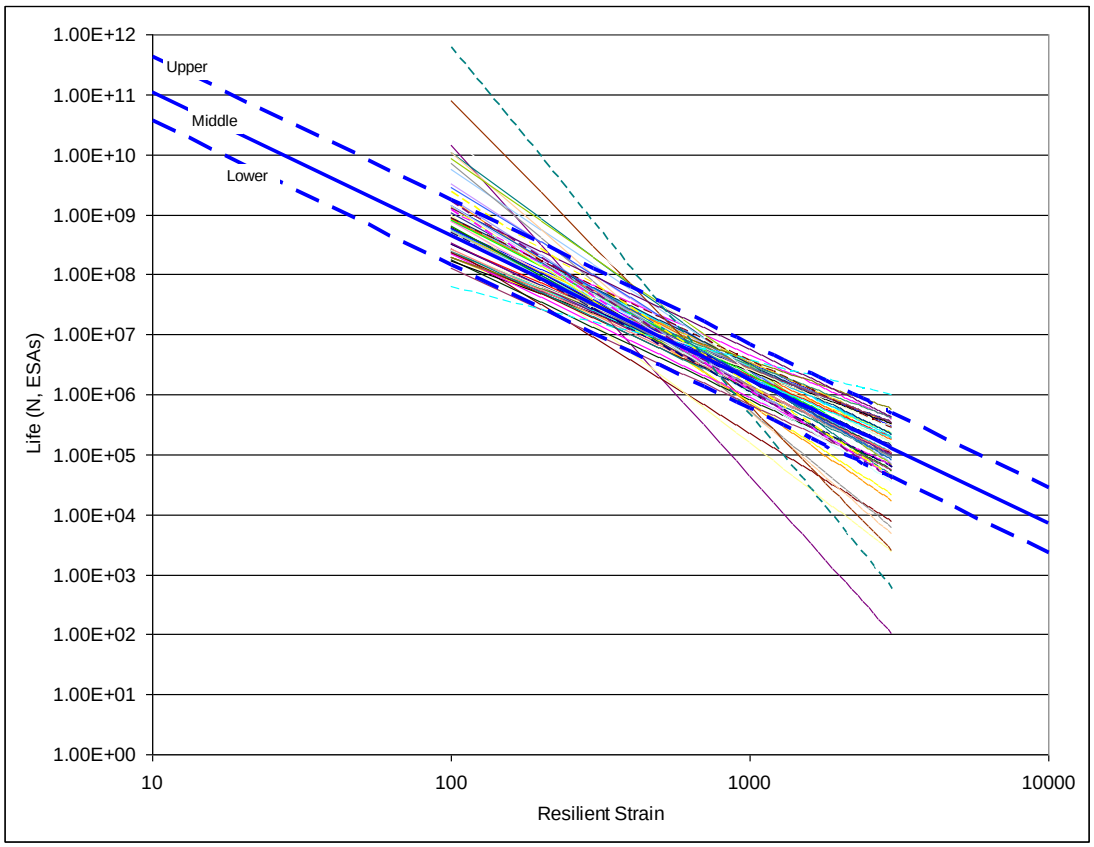

A similar method to selecting sub-base aggregates was also used; however, on a significantly smaller subset of RLT tests as found in the related NZTA research project, 'Development of a basecourse/subbase design criterion'.

3.3 RLT test results for subgrade soils

The initial subgrade soils chosen for testing were the Waikari Silty Clay and the Todd Clay as used in the CAPTIF pavement tests. Different moisture contents and densities were tested both in the RLT test and laboratory CBR.

RLT testing on subgrade soils was found to be problematic because for each type of soil, moisture content and density causes large variation in strength. The strength of the soil governs the stress levels at which each of the 50,000 load stages are set. The aim is to choose at least six stress stages (as this takes 24 hours to test) where the sample survives sufficiently to provide the Werkmeister and Arnold models with enough data to relate deformation to stress and strain.

Initial RLT testing proved worthless for its data use but useful in helping to establish a suitable RLT test for two reasons:

1 The six stress levels guessed were either too high or too low.

2 In the testing regime for each of the stress stages, the change in confining stress caused a slow response of the soil to expand or contract in all directions.

Changing the confining stress for a RLT soil test had a negative effect on vertical deformation as, in some cases, the sample expanded with increasing number of load cycles as a result of the new reduced confining stress.

All RLT tests on soils were repeated and now the standard process is to conduct three RLT tests per soil type, density and moisture. Each of the three RLT tests is a 6- to 8-stage test at one particular confining stress and between each stage only the vertical load changes. To determine the most appropriate vertical stresses in each stage, a 24-stage test was conducted first at 1000 load cycles, which was completed in two hours. Results of this preliminary test determined the maximum vertical load that the soil could support, which in turn became the upper limit for setting the stress levels for the 50,000 6- to 8-stage test. This extensive testing yields at least 18 data points relating permanent strain rate to either stress or strain.

A summary of RLT tests conducted on subgrades is detailed in table 3.1 with full results in appendix A.

Table 3.1 RLT tests on subgrade soils conducted

RLT # PS0026 #	Soil	MC	DD	Lab CBR	Comments
1, 2, 3	Waikari Silty Clay	11.9	1.72	25	Not used - confining pressure changes caused expansion and too strong
7	Todd Clay	19.4	1.60	17	
8	Todd Clay	24.2	1.58	8	
10, 11, 12, 13	Todd Clay	30.0	1.43	2.0	Used
21, 22, 33	Fine Pumice	11.7	1.06	25	May use for comparison
40,41	Drury Quarry Subgrade	50.5	1.09	6	May use for comparison
50, 51, 52	Todd Clay	21.2	1.51	?	Too dry and thus too strong cf in situ at CAPTIF - not used
53, 54, 55	Todd Clay	23.7	1.56	8	Used
56, 57, 58	Todd Clay	26.5	1.49	5	Not used as not the same as at CAPTIF
73, 74, 75	Waikari Silty Clay	12.0	1.85	10	Used

4 Rut depth prediction – CAPTIF pavements – validation – Arnold method

The main dataset used to validate the rut depth prediction models was from the NZTA research project using CAPTIF entitled, 'Fatigue design criteria for low noise surfaces on New Zealand roads' (Alabaster and Fussell 2006). This project used the Todd Clay at two different moisture contents (ie 2% and 8% CBR) in unbound granular pavements with OGPA surfacings. Both the basecourse aggregate and subgrade soils were tested in the RLT apparatus to obtain the parameters required, first for the Rubicon non-linear finite element model and then for the model relating stress to permanent deformation to calculate the rutting. Two predictions of rutting were undertaken, the first assuming a linear increase in rutting 1 million ESAs and the second a linear relationship assumed from 0.5 million ESAs. Results of these rutting predictions are shown in figures 4.1 and 4.2 where both methods result in rut depths very close to those actually measured. The linear extrapolation from 0.5 million ESAs results is shown, however, to be more appropriate (figure 4.2) and is therefore the method used to determine rutting for other pavements. No initial adjustments to the rutting predictions were needed to predict the rutting for the Todd CBR 8% sections. However, as discussed below, a minor reduction of 2mm in the predicted rutting was required to predict rutting in the Todd Clay CBR 2% sections.

Figure 4.1 Rut depth prediction assuming linear extrapolation from 1 MESA for the CAPTIF section using Todd Clay with CBR 8%

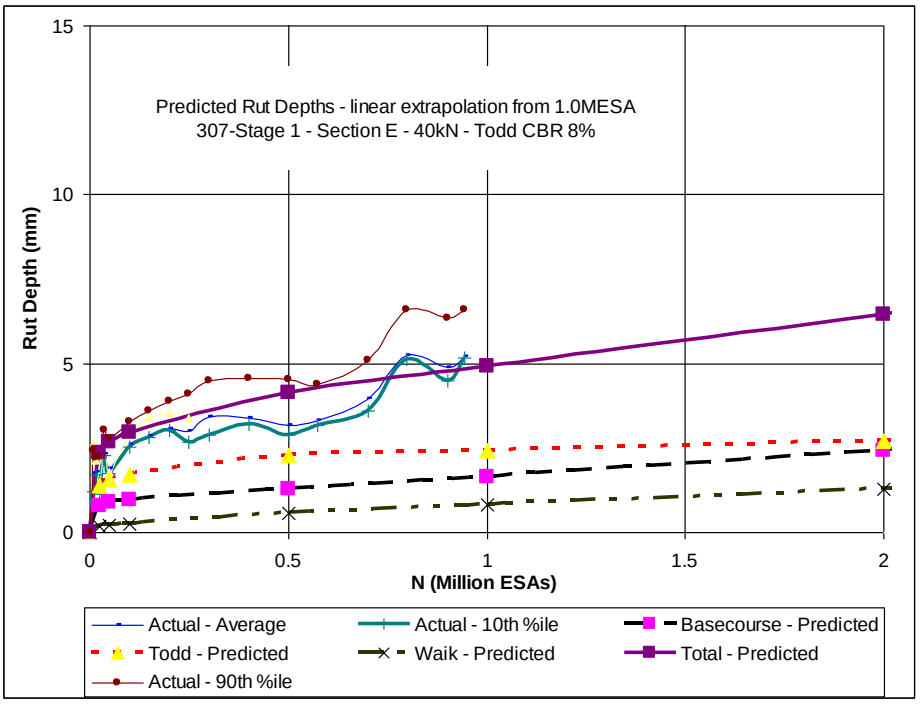

Figure 4.2 Rut depth prediction assuming linear extrapolation from 0.5 MESA for the CAPTIF section using Todd Clay with CBR 8%

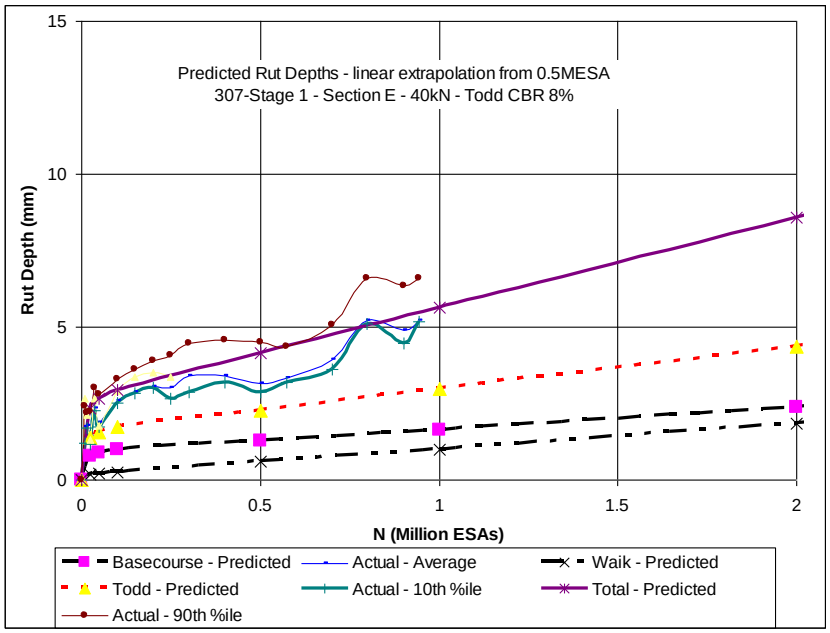

As discussed, predicting the rutting for the CAPTIF Todd Clay CBR 2% section required a subtraction of 2mm to the predictions (figures 4.3 and 4.4). This 2mm subtraction is considered minor and at least it shows the predictions of rutting were not underestimating the rut depth. Therefore, to predict rutting for other pavements with a CBR of 2% it was decided not to subtract 2mm from the predicted rut depths. This is because the aim of this project was to develop new pavement thickness design charts for adoption by the NZTA and hence the need to take a conservative approach. Should the need arise in the future, the 2mm could be deducted from the predicted rut depths.

Figure 4.3 Rut depth prediction assuming linear extrapolation from 0.5 MESA for the CAPTIF section using Todd Clay with CBR 2% with no adjustment

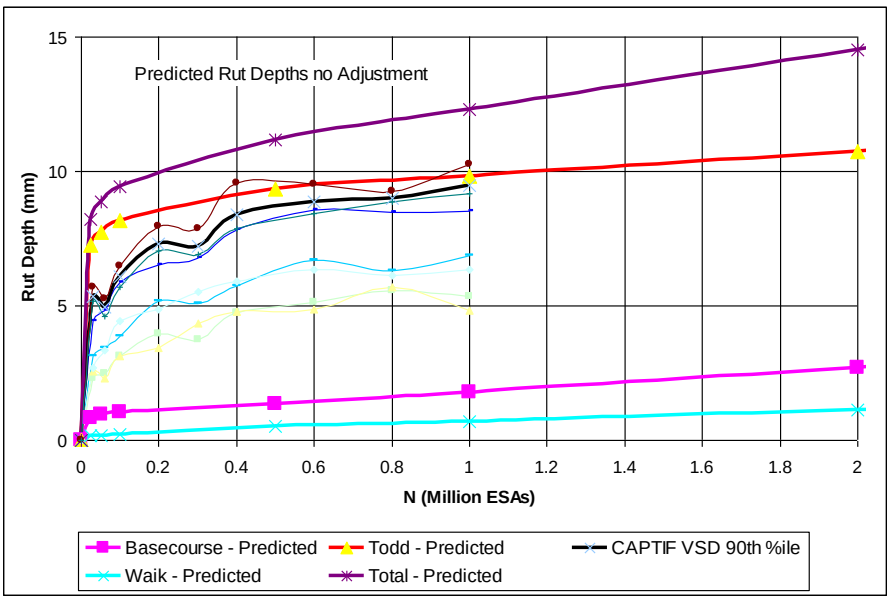

Results from the rut depth predictions of the CAPTIF pavements validated the rut depth prediction model used by Arnold. The model was then used to calculate rutting for many other pavement depths in order to develop pavement design charts for granular pavements and compare predictions of life with figure 8.4 in the Austroads (2004) pavement design guide.

Figure 4.4 Rut depth prediction assuming linear extrapolation from 0.5 MESA for the CAPTIF section using Todd Clay with CBR 2% with 2mm subtracted from predicted rut depths

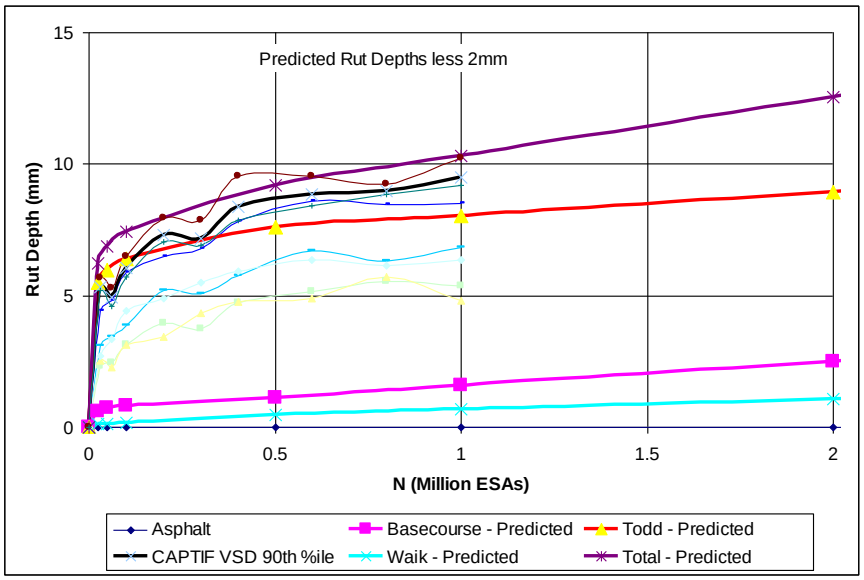

5 Rut depth prediction – other pavements – Arnold method

Rutting was predicted using the validated Arnold method for a range of granular pavement depths using the triaxial data for the CAPTIF subgrades (Todd Clay CBR 2 and 8% and Waikari Clay CBR=10%) and selected triaxial data for the granular layers. Predictions were made for each pavement depth and subgrade type with three different performing (in terms of rutting) granular base and subbase materials representing poor, average and very good rut resistance. Figure 5.1 details the pavement depths modelled for each subgrade type where the depth of basecourse and sub-base were the same as that required by the Austroads (2004, figure 8.4) pavement design guide for the total pavement depth.

Figure 5.1 Pavement depths where rut depths were predicted

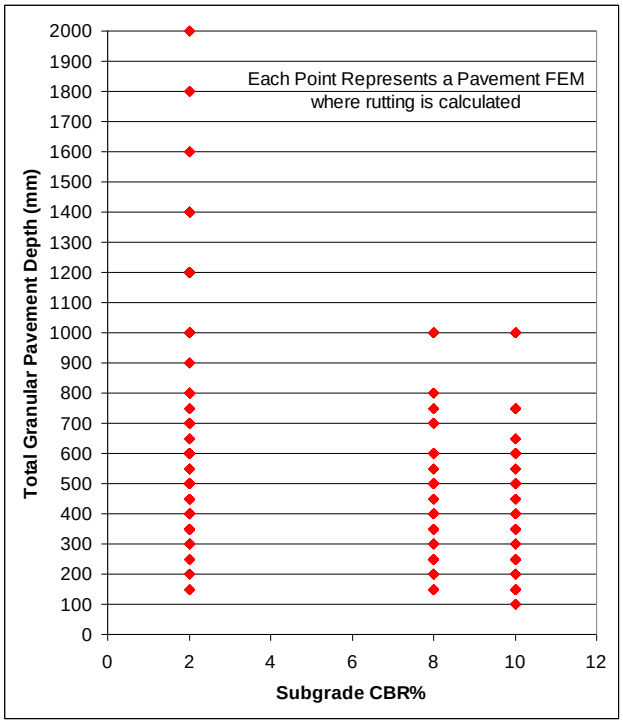

Results of the analysis to predict rutting were plotted on pavement thickness design charts for comparison with Austroads (2004, figure 8.4). Figures 5.2, 5.3 and 5.4 show pavement lives predicted to achieve a certain rut depth of 10mm, 15mm and 20mm for all three subgrade types for average quality aggregates. All the predictions of rutting show that after around 4 MESAs, more pavement depth is needed than that required by Austroads. In addition, results show that no matter how deep the pavement is the life is limited to around 15 MESAs. This is because all the rutting occurs in the granular layers, as discussed and shown later.

Figure 5.2 Pavement lives predicted for average quality granular materials over a subgrade CBR of 10%

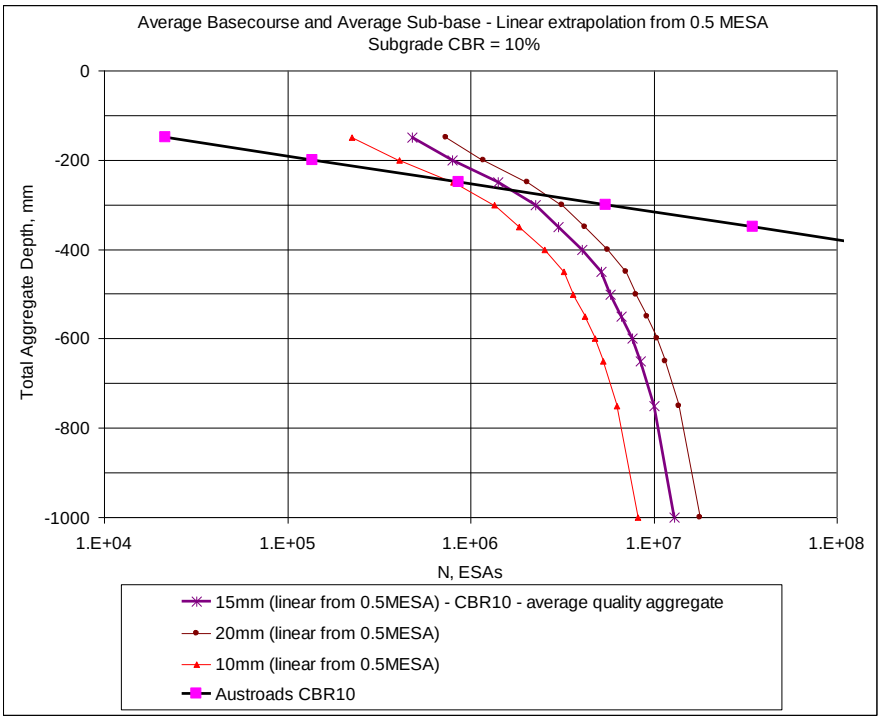

Figure 5.3 Pavement lives predicted for average quality granular materials over a subgrade CBR of 8%

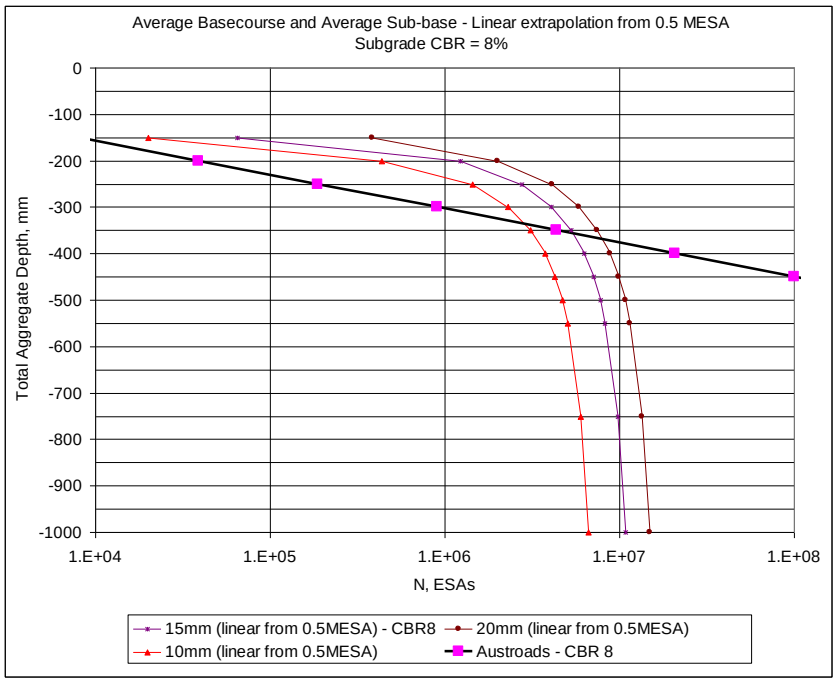

Figure 5.4 Pavement lives predicted for average quality granular materials over a subgrade CBR of 2%

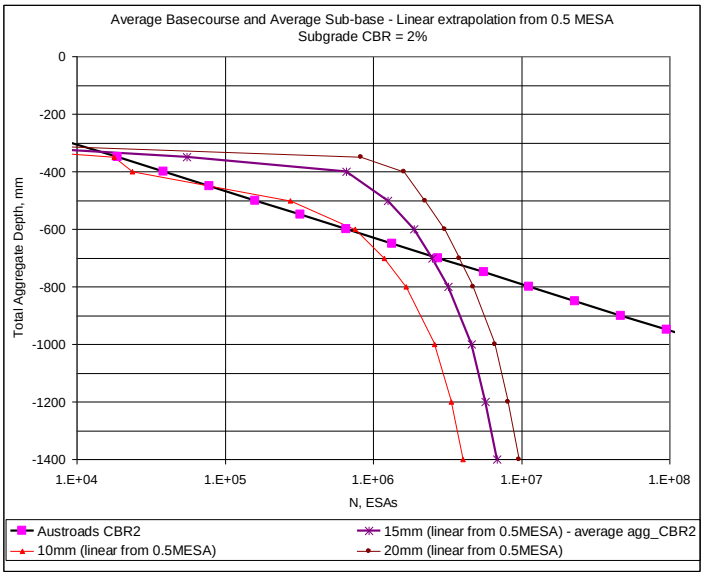

To assess the effect of the different quality of aggregates on pavement life, it will be assumed that the end of life is when a 15mm rut depth is achieved. As the rut depth models are validated from CAPTIF trials, the end of life at a 15mm rut depth is considered appropriate as this value was agreed in the CAPTIF mass limits project (Arnold et al 2005). It was found from CAPTIF tests that, in sections of the pavement where 15mm rutting occurred, the rutting then increased rapidly to failure. Another reason why 15mm is considered appropriate is that the rut depth prediction process does not full take account of chip embedment and some initial further compaction which will cause about 5mm of rutting, taking the predicted rut depth to 20mm (15mm + 5mm). As mentioned in the literature review, it was thought that the development of the Austroads (2004, figure 8.4) pavement thickness design chart was based on a rut depth of 20mm.

Figure 5.5 – Pavement lives predicted for poor, average and very good quality granular materials over a subgrade CBR of 10%

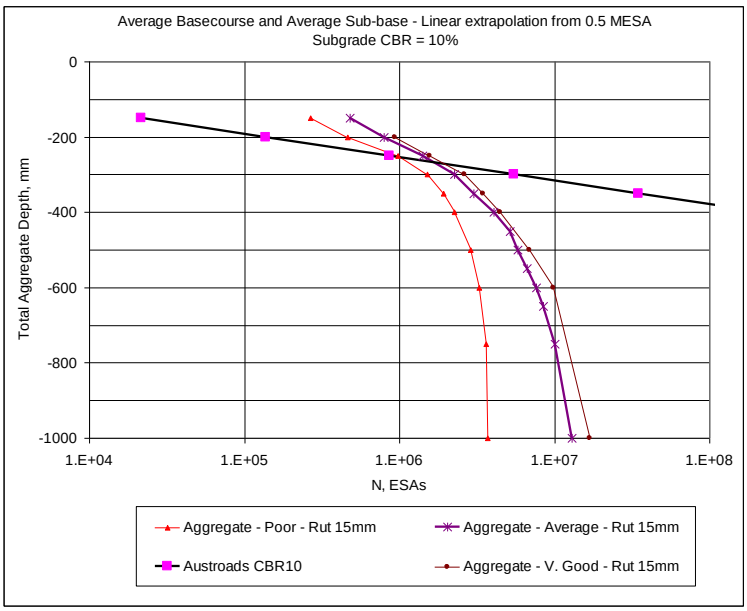

Figure 5.6 Pavement lives predicted for poor, average and very good quality granular materials over a subgrade CBR of 8%

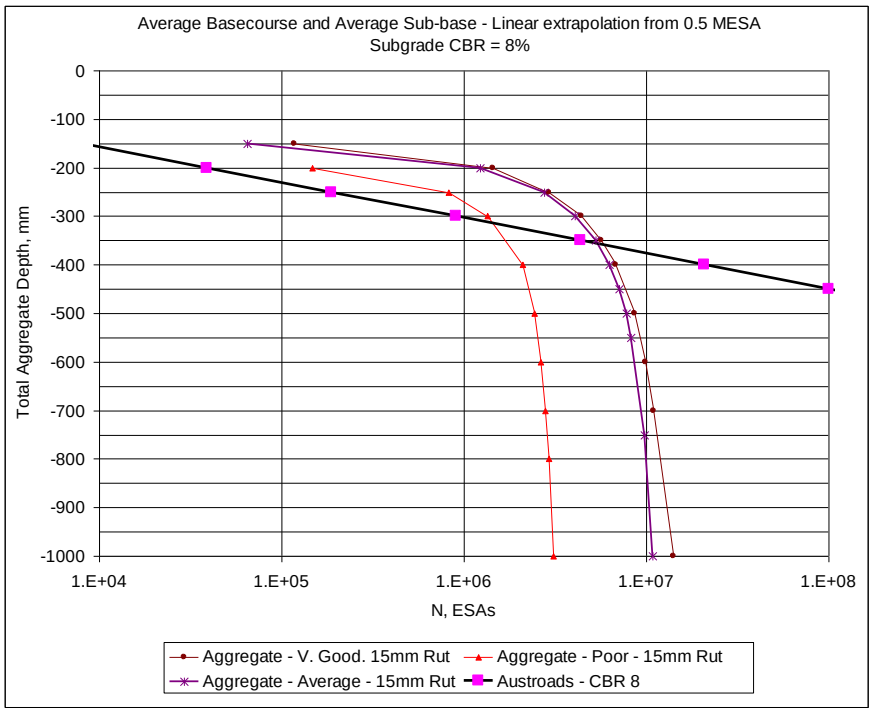

Figure 5.7 Pavement lives predicted for poor, average and very good quality granular materials over a subgrade CBR of 8%

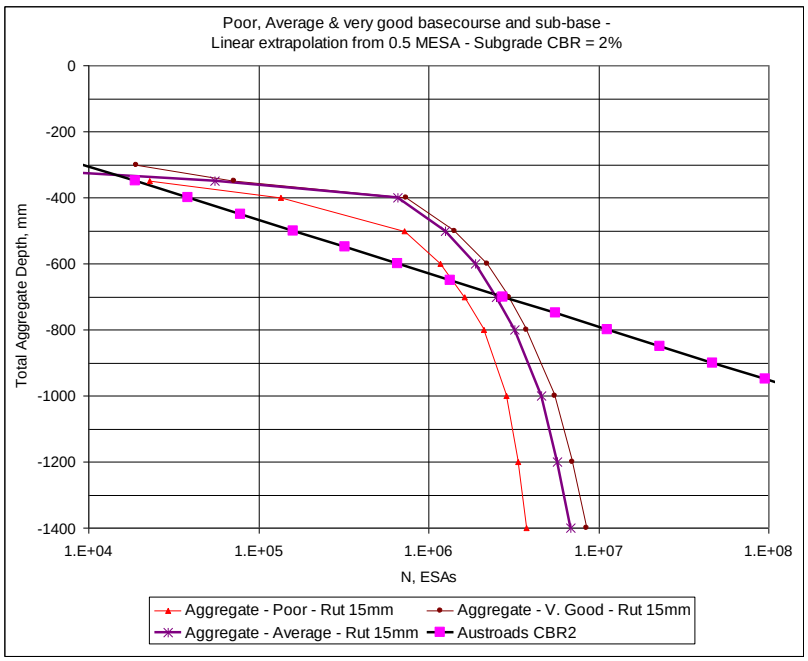

Other interesting data obtained from the rut depth models was the amount of rutting that occurred in the granular and subgrade layers. As would be expected, as the pavement thickness increased then more rutting occurred in the granular layers (figure 5.8). Figure 5.9 shows a higher proportion of rutting in the

aggregate layers when poor quality aggregates are used. The effect on pavement life by using poor quality aggregates is significant as shown in figure 5.10.

Figure 5.8 Proportion of total 15mm rut depth in each pavement layer with a CBR 8% subgrade and average quality basecourse and subbase aggregates

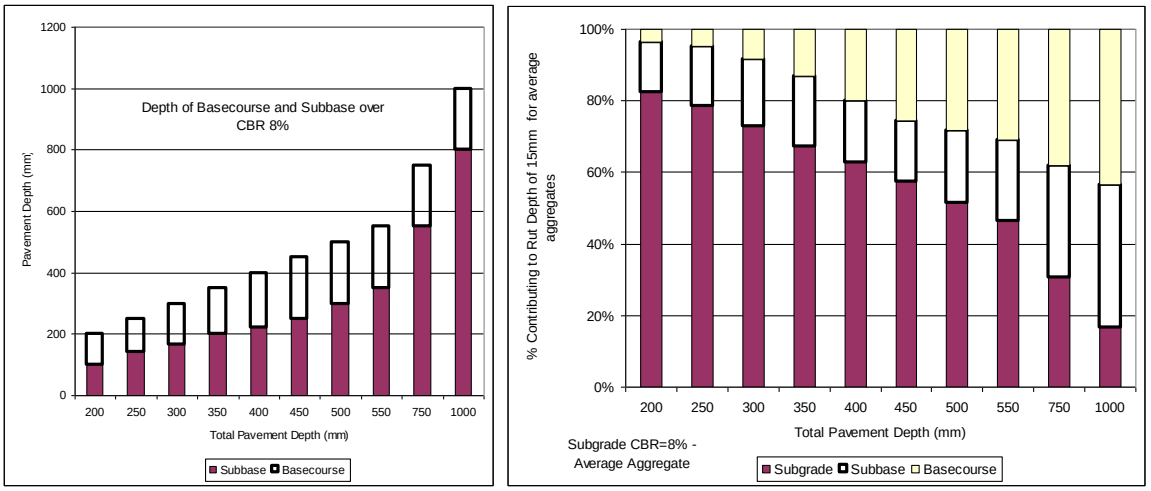

Figure 5.9 Proportion of total 15mm rut depth in each pavement layer with a CBR 8% subgrade and poor quality basecourse and subbase aggregates

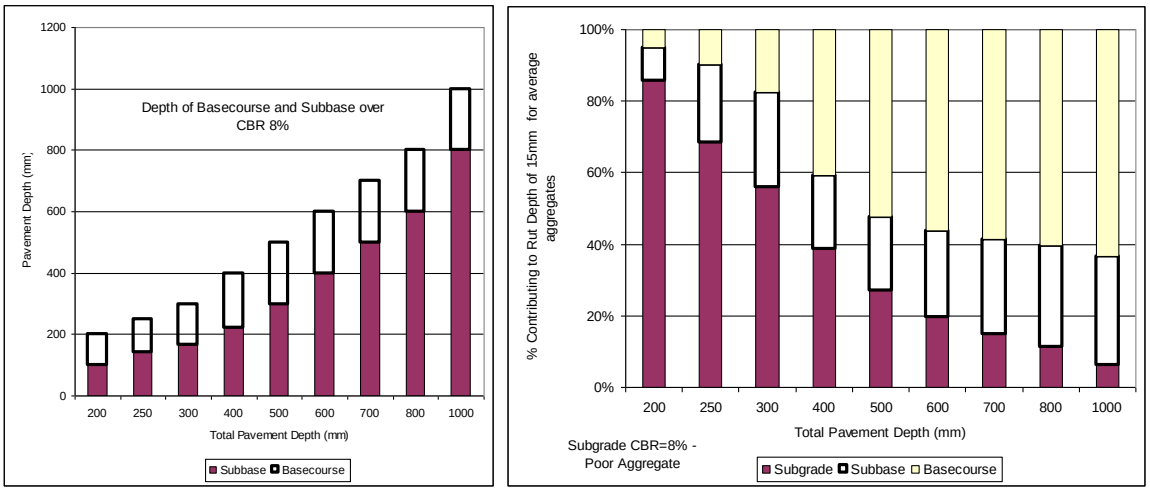

Figure 5.10 Proportion of total 15mm rut depth in each pavement layer with a CBR 8% subgrade and very good quality basecourse and subbase aggregates

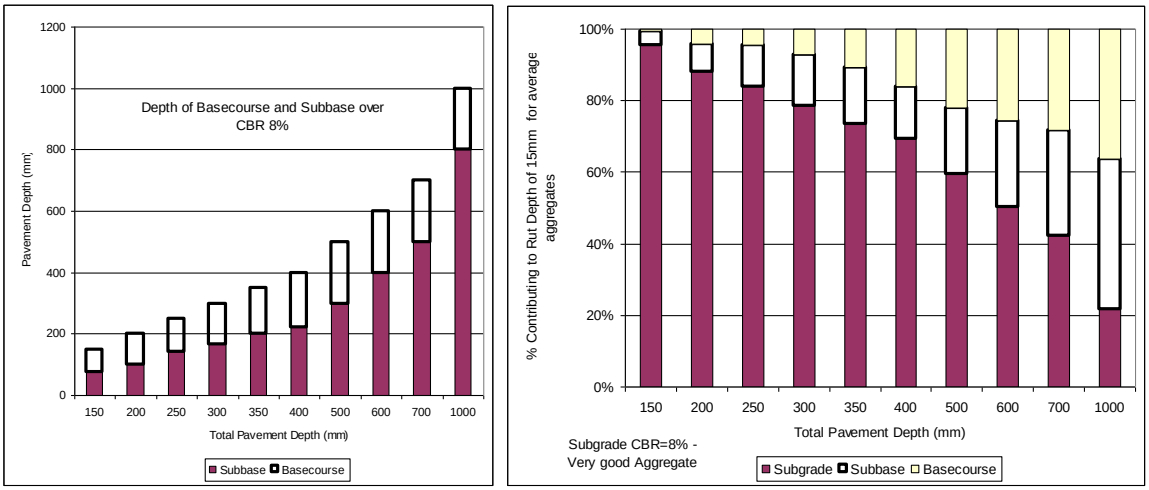

Figure 5.11 Effect on pavement life with different quality aggregates

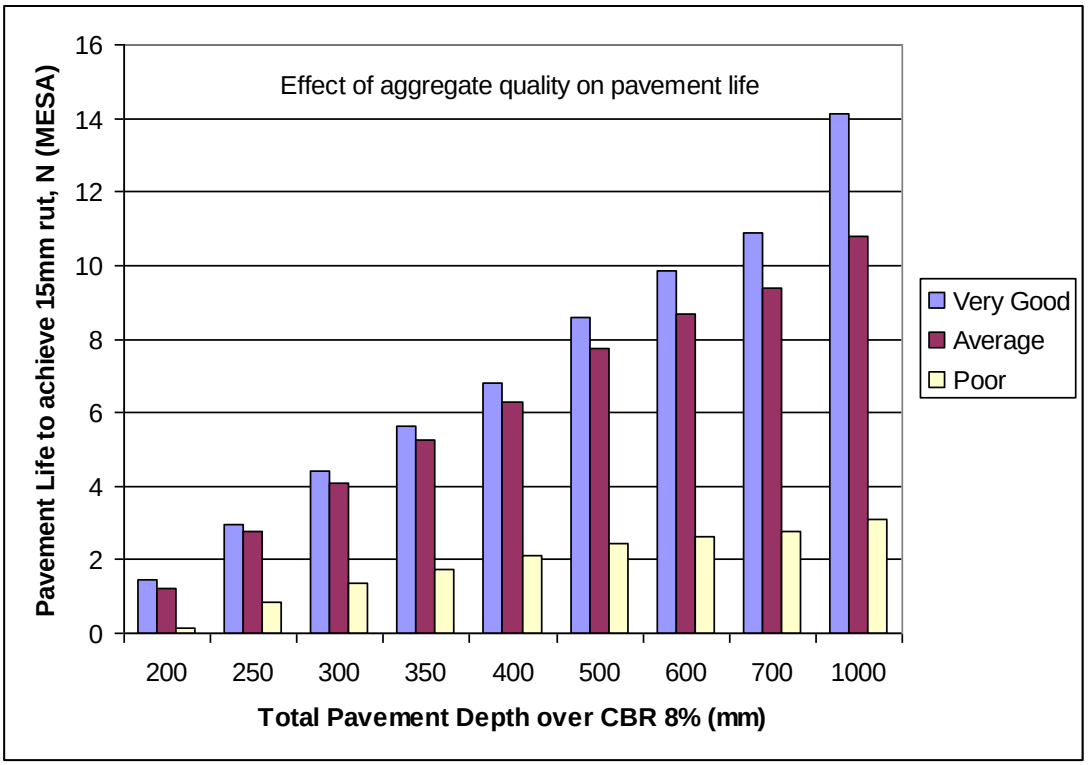

6 Granular pavement design charts based on rut depth prediction – Arnold method

Only limited data in terms of subgrade strengths are available in the database of pavement lives found by rut depth models. Therefore, to determine pavement lives for other subgrade types, some interpretation between the CBR 10%, 8% and 2% is required (figures 6.1 and 6.2). It is assumed that the model to interpret the lives for other subgrade types follows the same trend as the granular pavement design chart in Austroads (2004, figure 8.4). The same ratio of pavement depths between each subgrade CBR values found from the design chart in the Austroads guide was used to determine pavement thickness design charts for other subgrade CBR values not tested in the triaxial apparatus. A design chart from rut depth modelling for the full range of subgrade strengths is shown in figure 6.1 plotted using a linear scale. Figure 6.2 uses a log scale which is more difficult to interpolate.

Figure 6.1 Pavement thickness design chart from rut depth modelling plotted on a linear scale

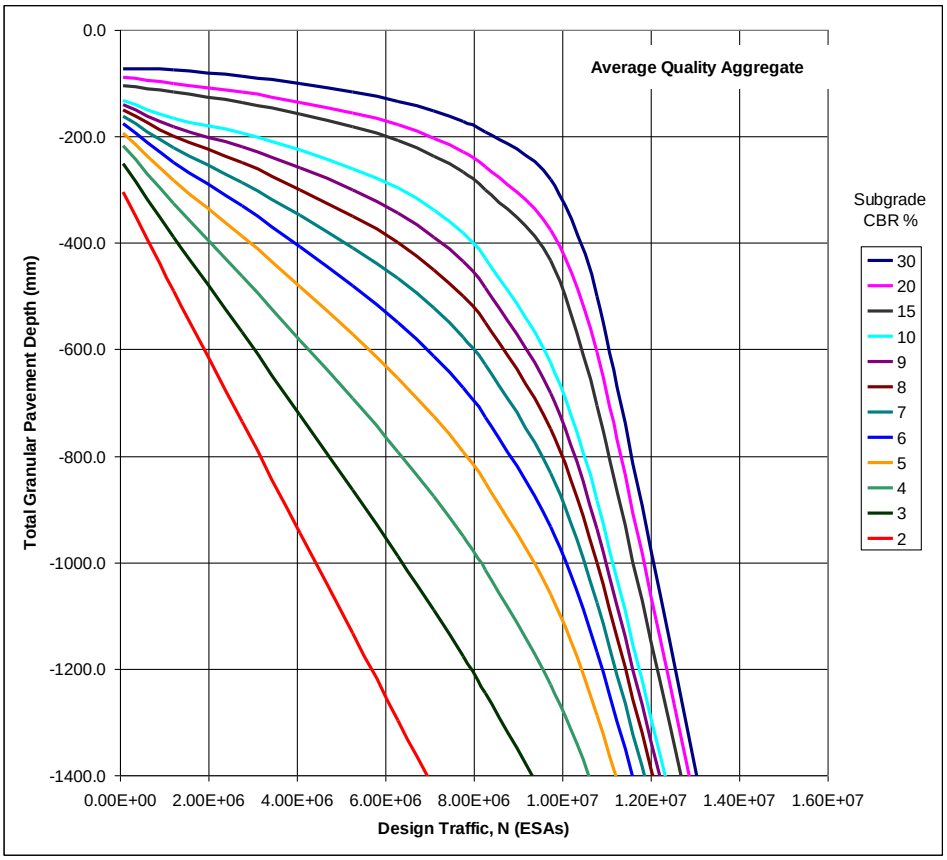

Figure 6.2 Pavement thickness design chart from rut depth modelling plotted on a log scale

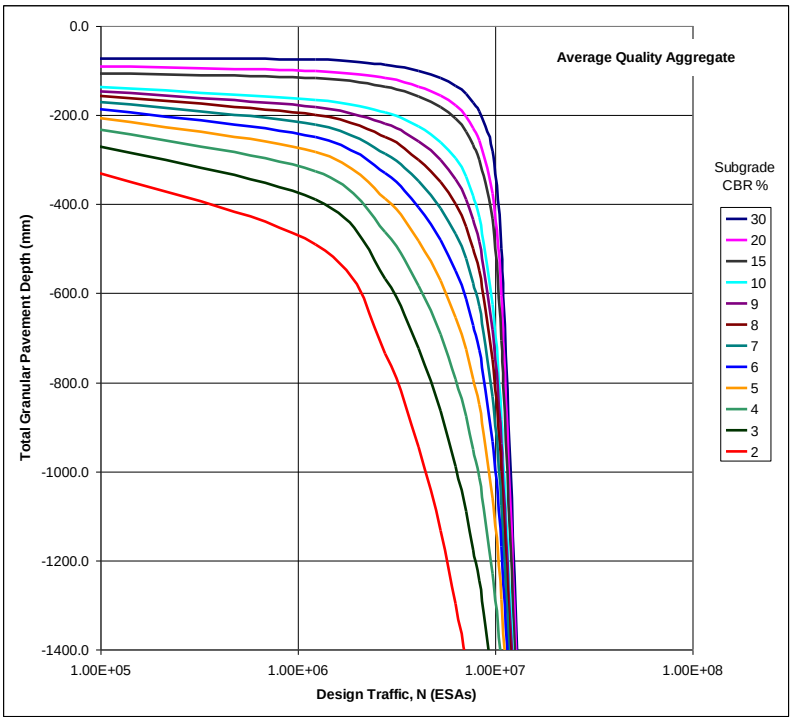

A recommended conservative approach to these new design charts is to use the pavement thickness that is the largest out of the Austroads (2004 figure 8.4) guide and the chart derived from rut depth predictions. Combining the Austroads design chart and the rut depth predictions results in the design chart shown in figures 6.3 and 6.4.

Figure 6.3 Pavement thickness design chart for average quality aggregate derived from Austroads (2004) design guide and from rut depth modelling plotted on a linear scale

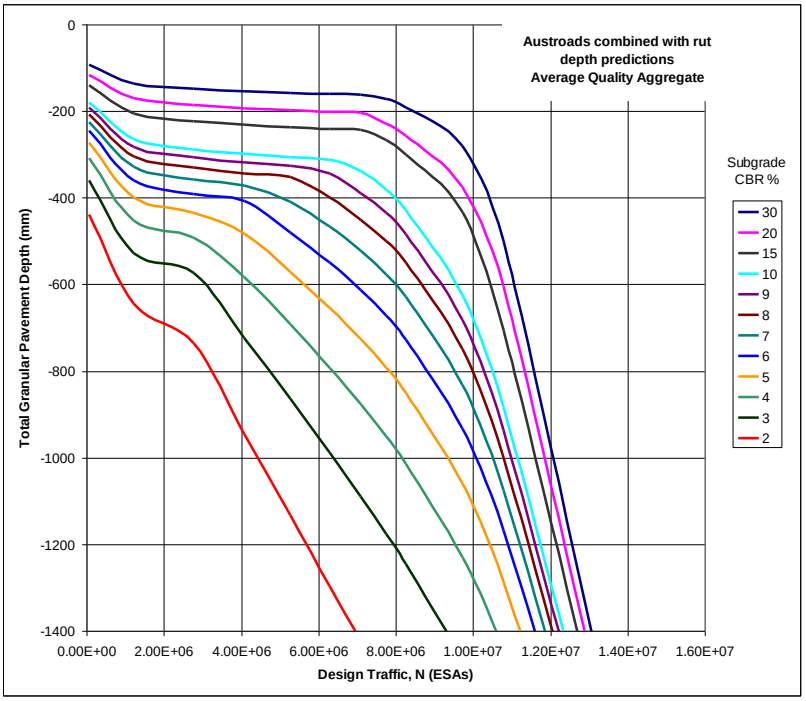

Figure 6.4 Pavement thickness design chart for average quality derived from Austroads (2004) design guide and from rut depth modelling plotted on a log scale

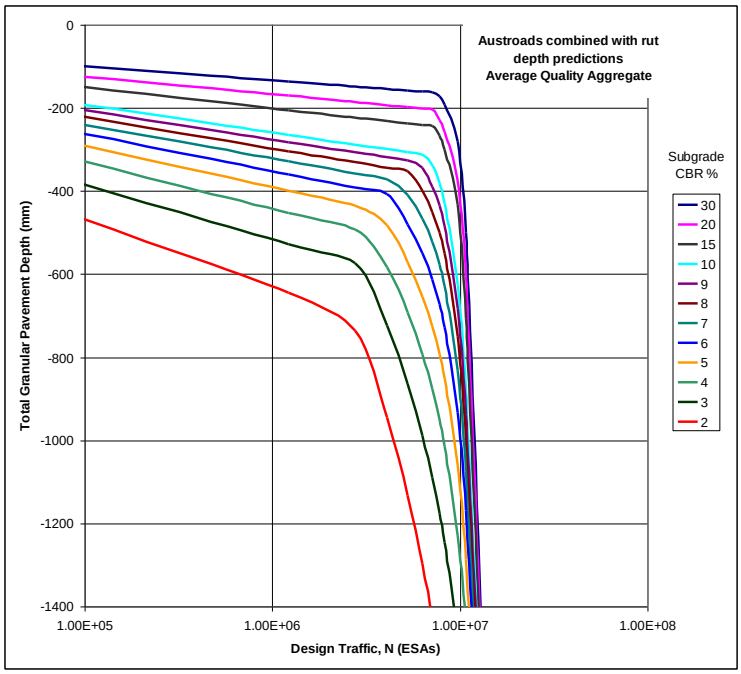

Design charts combined with the Austroads design chart were also produced for different quality aggregates being the poor and the very good aggregates. These charts are shown in figures 6.5, 6.6, 6.7 and 6.8. Using poor quality aggregates has a significant effect on pavement life where the maximum life achievable is around 3 million ESAs. For very good quality aggregates, the life achieved can extend to 15 million ESAs for subgrade CBRs of greater than 6%.

Figure 6.5 Pavement thickness design chart for very good quality aggregate derived from Austroads (2004) design guide and from rut depth modelling plotted on a linear scale

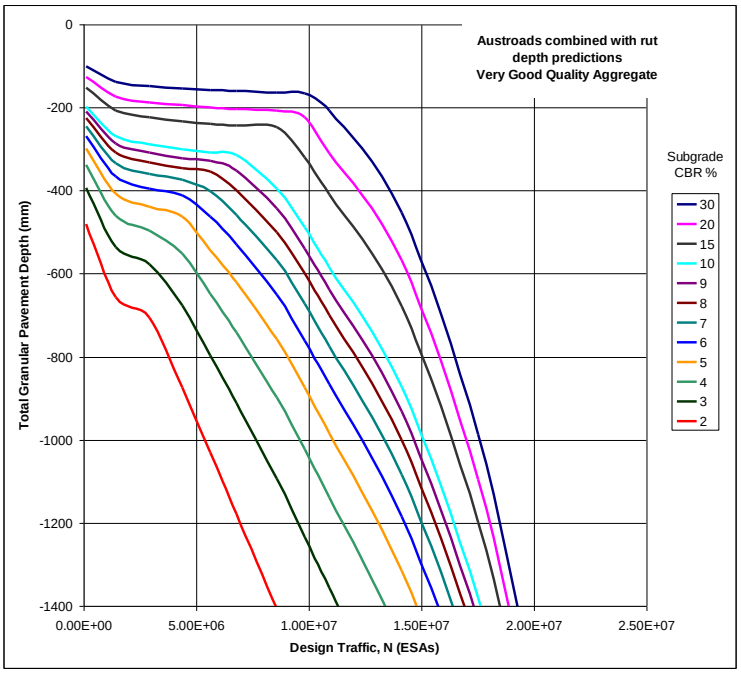

Figure 6.6 Pavement thickness design chart for very good quality aggregate derived from Austroads (2004) design guide and from rut depth modelling plotted on a log scale

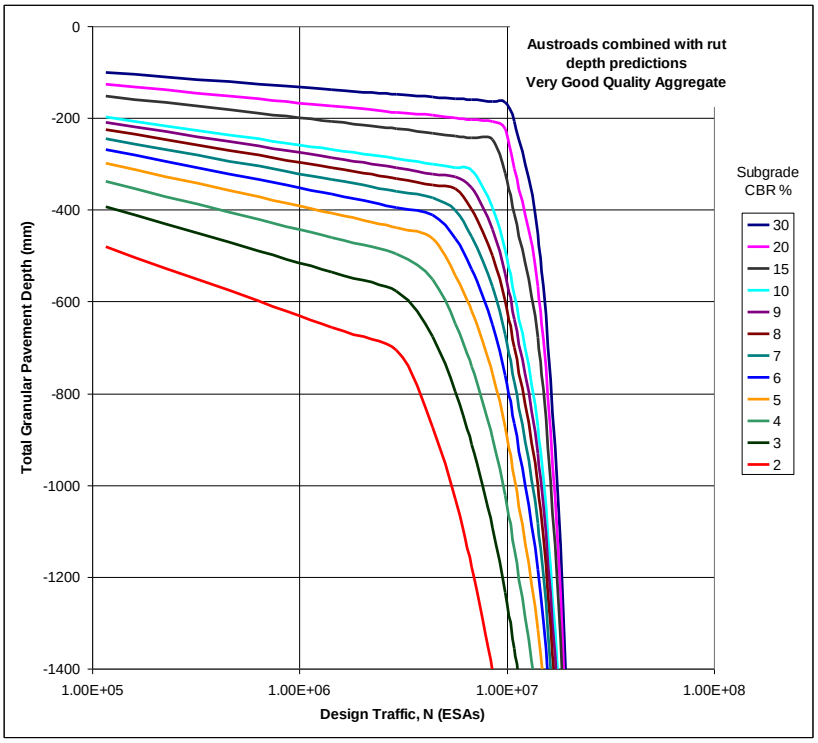

Figure 6.7 Pavement thickness design chart for poor quality aggregate derived from Austroads (2004) design guide and from rut depth modelling plotted on a linear scale

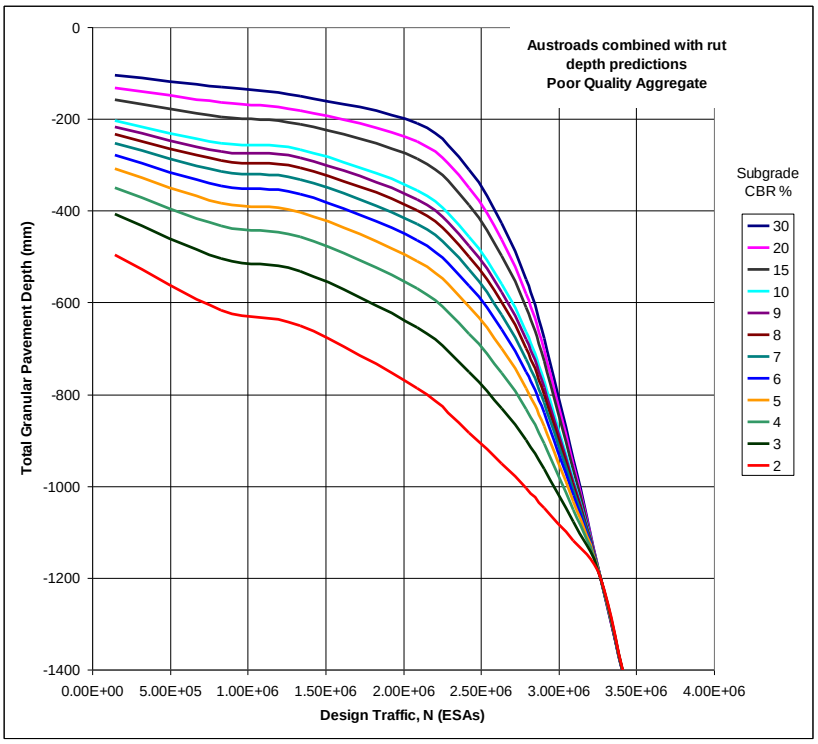

Figure 6.8 Pavement thickness design chart for poor quality aggregate derived from Austroads (2004) design guide and from rut depth modelling plotted on a log scale

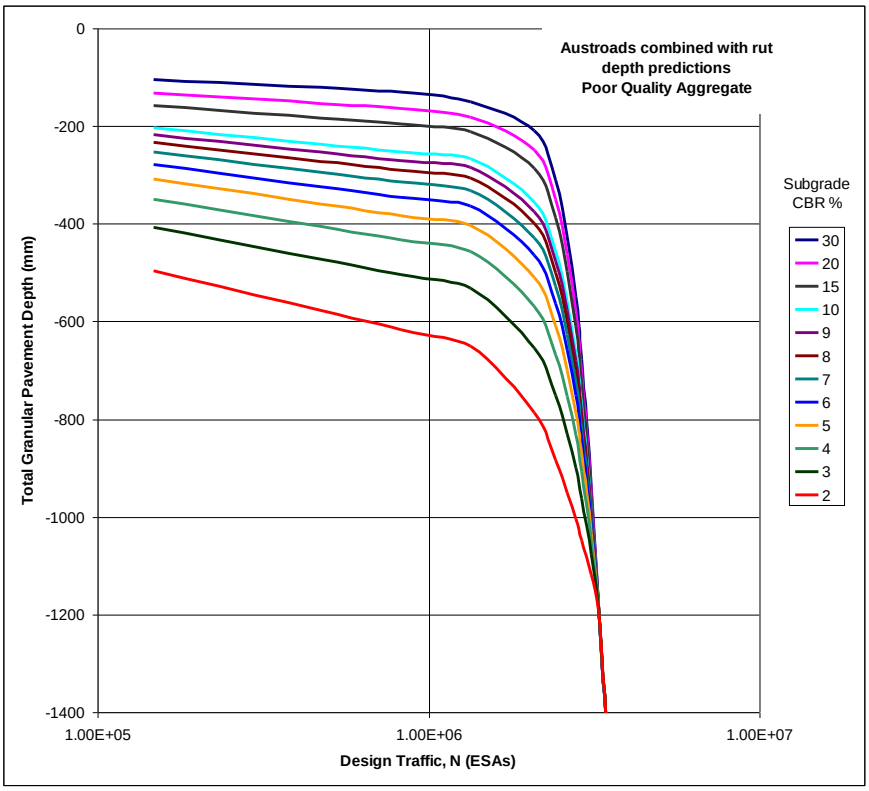

7 Granular pavement design charts based on rut depth prediction – Werkmeister method

Rutting was predicted using the validated Werkmeister method for a range of granular pavements on CBR 2%, 8% and 10% subgrade soils. The range of granular pavements was smaller than that used with the Arnold method due to greater complexity and time required using the Werkmeister method. Nevertheless, there were sufficient data points to interpolate with and develop a full pavement thickness design chart as shown in figure 7.1 for a end of pavement life of 15mm rut depth. The analysis was repeated for a 25mm end of life rut depth as shown in figure 7.2.

Figure 7.1 Pavement thickness design chart for a rut depth of 15mm using the Werkmeister model

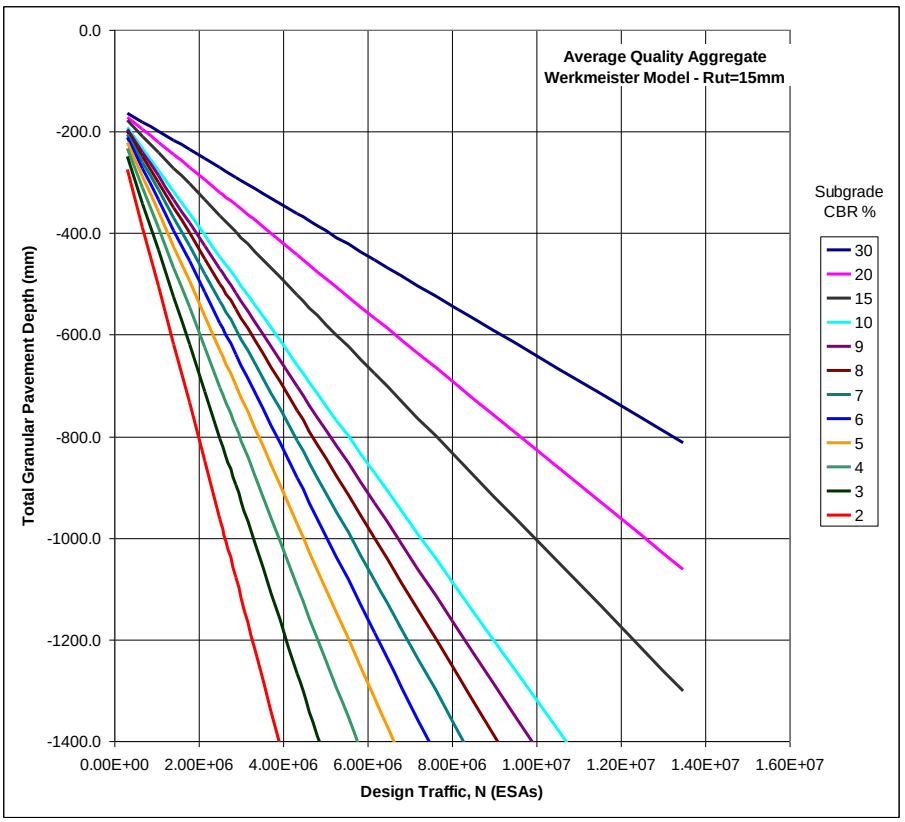

Figure 7.2 Pavement thickness design chart for a rut depth of 25mm using the Werkmeister model for average quality aggregate

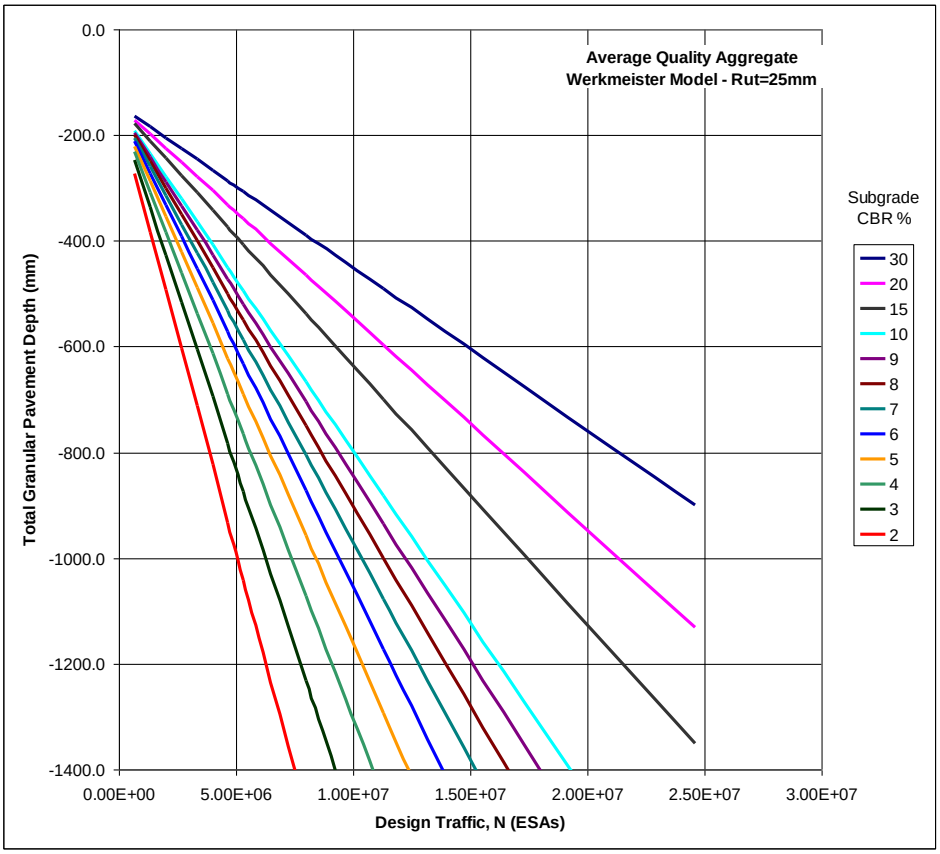

8 Comparing the Arnold and Werkmeister methods for determining pavement thickness design charts

The life predicted by the Werkmeister method is shorter than the life predicted by the Arnold model because of different extrapolation methods of the RLT data (figure 8.1). This difference between the two models is also shown in figure 8.2 for a portion of the design chart with CBRs 2% and 8%. It was found that if the end of pavement life was set to a rut depth of 25mm, then the Werkmeister model was a closer fit to the Arnold model with a 15mm rut limit (figure 8.3).

Figure 8.1 Predictions of rutting using the Werkmeister method for subgrade CBR 2% and average quality aggregate (note the linear progression of rut depth from 100k)

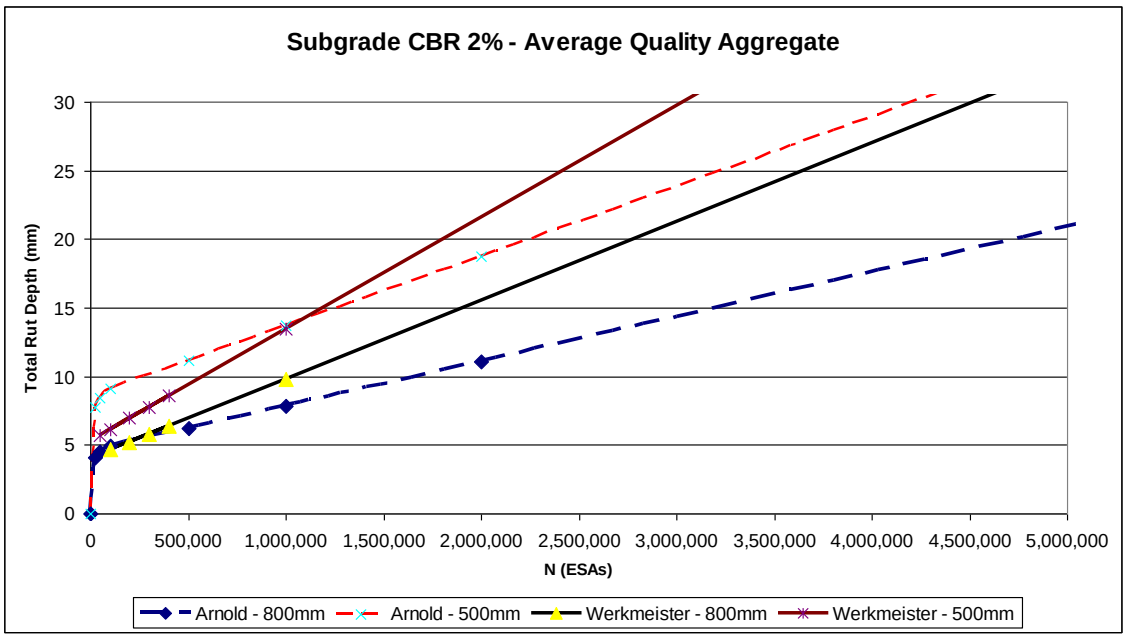

Figure 8.2 Pavement thickness design chart comparison between the Arnold and Werkmeister models for a rut depth of 15mm

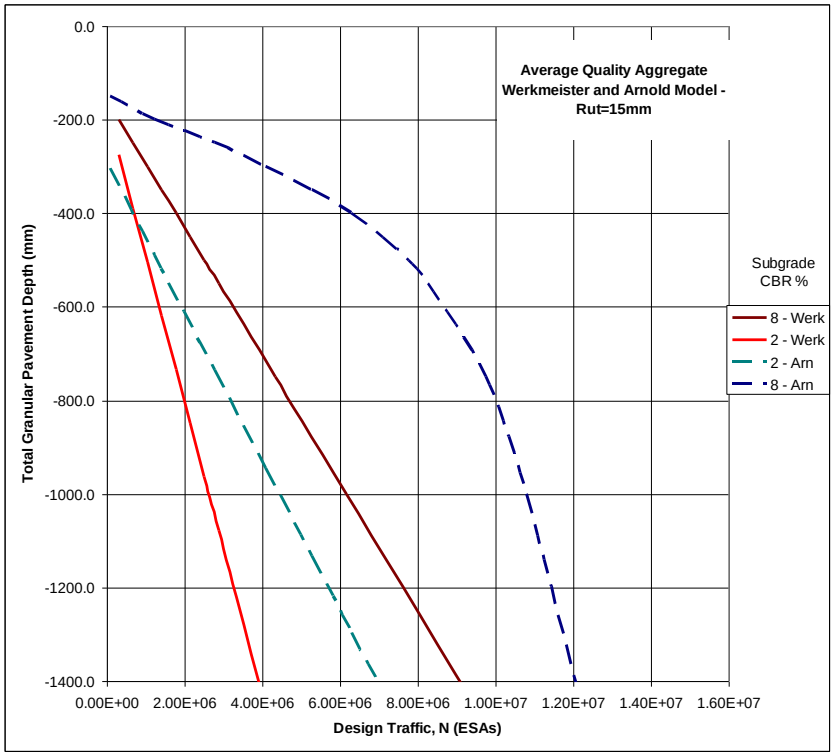

Figure 8.3 Pavement thickness design chart comparison between the Arnold (rut=15mm) and Werkmeister (rut=25mm)

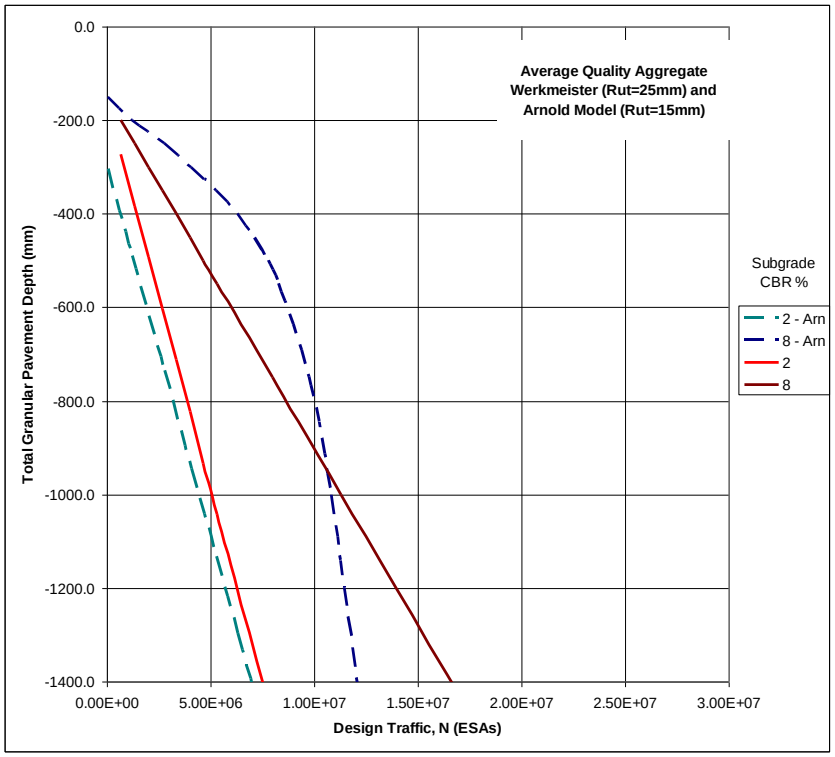

On reviewing the Werkmeister rut depth predictions, it can be seen that they are linear with the same slope after approximately 10,000 load cycles (figure 7.1). This is because the Werkmeister method uses one relationship between permanent strain rate and elastic strain from one portion of the permanent strain curve found from RLT testing. This one relationship has the effect of a linear increase in rutting and is likely to predict a higher rut depth than would be expected to occur. In contrast, the Arnold method uses five different relationships between stress and permanent strain rate for different portions of the permanent strain curve found from RLT testing, being: 0–25,000; 25,000–50,000; 50,000–100,000; 100,000–500,000; 500,000 onwards linear using same slope as 100,000 to 500,000. This has the effect of flattening the rutting curve with less rutting being calculated using the Arnold method (figure 8.1). It would be possible to use the Werkmeister model also for different stages of the RLT curve as per the Arnold method and thus for similar predictions in rut depth.

A current shortcoming of the Werkmeister method is the absence of a suitable model for the subgrade soils. For all of the pavement cross-sections analysed, the Werkmeister model found most of the surface rutting was in the granular layers regardless of the pavement depth even for a 200mm pavement on a subgrade CBR of 2%. The Arnold method used a more suitable model for the subgrade and thus showed that surface rutting was dominated by subgrade rutting for shallow pavement depths.

9 Conclusions

The design charts are produced from a range of assumptions that result in similar rut depth predictions to those that actually occurred at the CAPTIF test track. Number of wheel passes at the test track are relatively short (< 1.5 MESA) compared with design lives of state highways (approximately 10 MESA). Therefore, aggregate shakedown which may occur in the field where after many applications load there is no further rutting is not considered in the rut depth model validated with CAPTIF data. If shakedown or partial shakedown was assumed, then the rutting model would follow a log or power function, that continually decreases the rate of rutting with increasing load cycles. This would increase life significantly and the maximum life obtainable for average quality granular pavements would likely be around 50 MESA. The current assumption assumes a conservative linear rutting relationship after 0.5 MESA to follow the trend of the CAPTIF data.

Despite possible errors in the rut depth predictions, the exercise was useful in demonstrating the relative effect on pavement life for different qualities of aggregates and and showing that increasing the depth of the aggregates did not always increase the pavement life. The results showed that after 6 MESA one or more modified or bound pavement layers were required to limit rutting in the granular pavement layers.

RLT tests on subgrade, subbase and basecourse materials have enabled relationships to be determined between permanent strain/rutting and stress (Arnold method) or elastic strain (Werkmeister method). These relationships permit the calculation of rutting within each pavement material which is summed to obtain a surface rut depth. CAPTIF pavements were used to validate and refine the assumptions used to calculate the surface rut depths to ensure they were close to measured rut depths. The validated Arnold and Werkmeister rut depth prediction models were then used to calculate rutting for a range of pavement depths on CAPTIF subgrade soils with CBRs of 2%, 8% and 10%. Results of this analysis were assessed by the number of ESAs to achieve a total surface rut depth defining the end of life. This information was used to develop pavement thickness design charts from the rut depth predictions and compared to the chart for granular pavements in Austroads (2004, figure 9.1). For low traffic volumes, the Austroads guide requires thicker pavements, while for high traffic volumes the rut depth predictions show significantly thicker pavements are required. In fact the rut depth predictions show there are traffic loading limits for granular pavements at around 7 million ESA for the subgrade CBR 2% and 11 million ESAs for the subgrade CBR 8% (figure 9.1). A reason for this is the significant amount of rutting that occurs in the aggregate layers for the thicker pavement depths as shown in figure 9.2. Because rutting occurs within the granular layers, adding more granular material does not decrease the amount of rutting and increase pavement life.

Figure 9.1 Rut depth predictions in comparison with Austroads

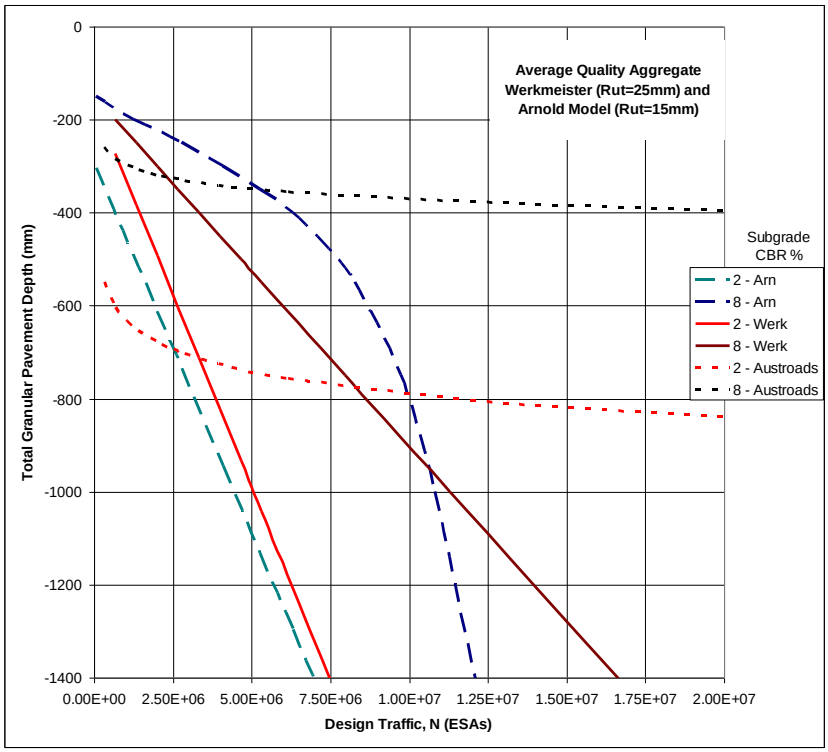

Figure 9.2 Proportion of total 15mm rut depth in each pavement layer with a CBR 8% subgrade and average quality basecourse and subbase aggregates

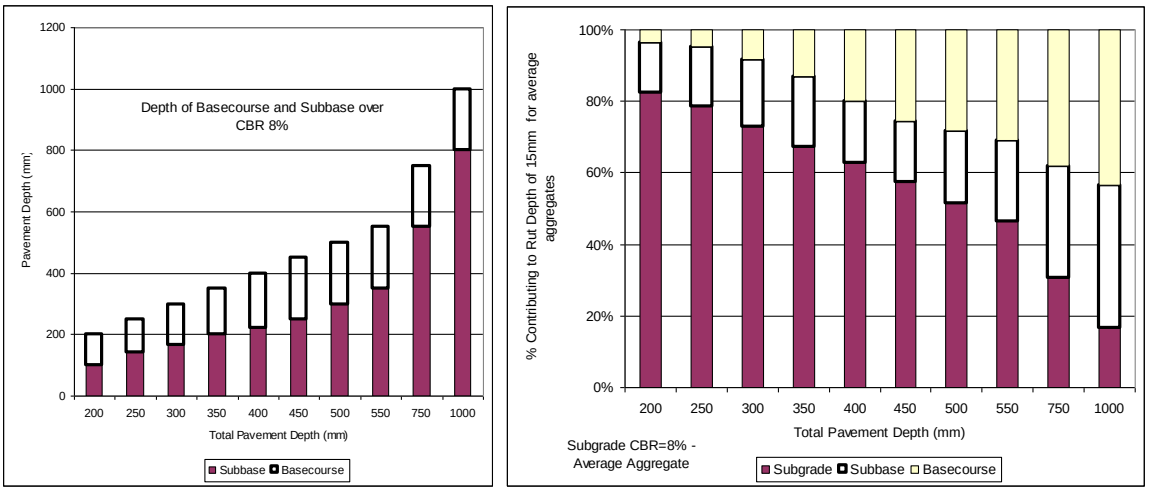

Rut depth predictions were repeated with different quality aggregates in terms of resistance to rutting found from the RLT test. The effect of using very good unbound aggregates increased the maximum pavement life from 11 million ESAs for average quality to 14 million ESAs for a subgrade with CBR 8% (figure 9.3). However, when using poor quality aggregates the maximum life decreased to 3 million ESAs (figure 9.3).

Figure 9.3 Effect on pavement life with different quality aggregates

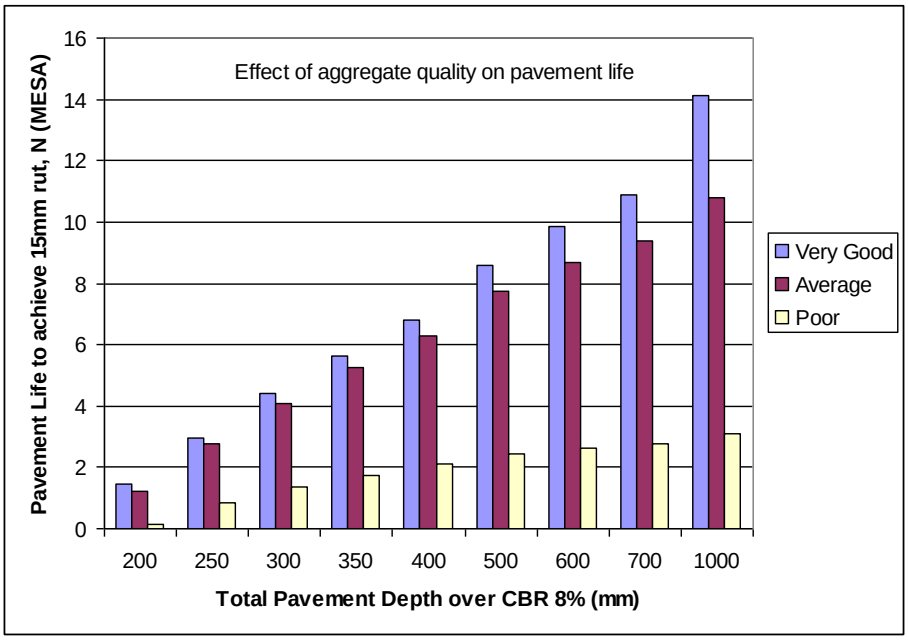

Finally, a combined Austroads and rut depth prediction pavement thickness design chart was produced by using the largest pavement thickness from the two methods as shown in figures 9.4 and 9.5. It is recommended that this replace the Austroads (2004) figure 8.4.

Figure 9.4 Combining Austroads and rut depth predictions for subgrade CBR 8%

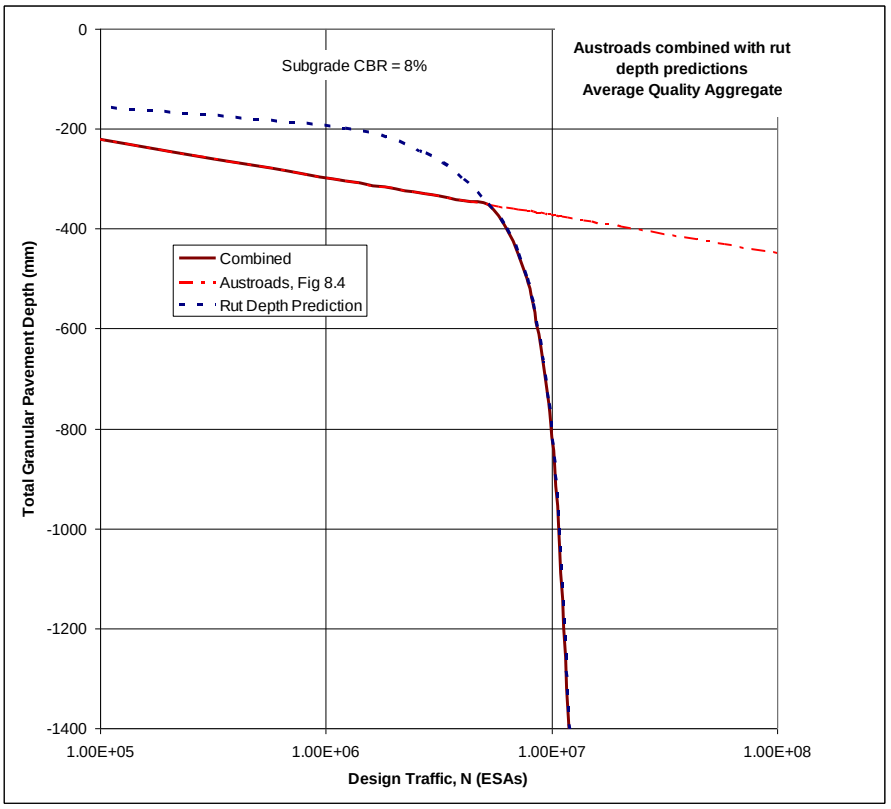

Figure 9.5 Recommended pavement thickness design chart for average quality aggregate combining Austroads and rut depth prediction

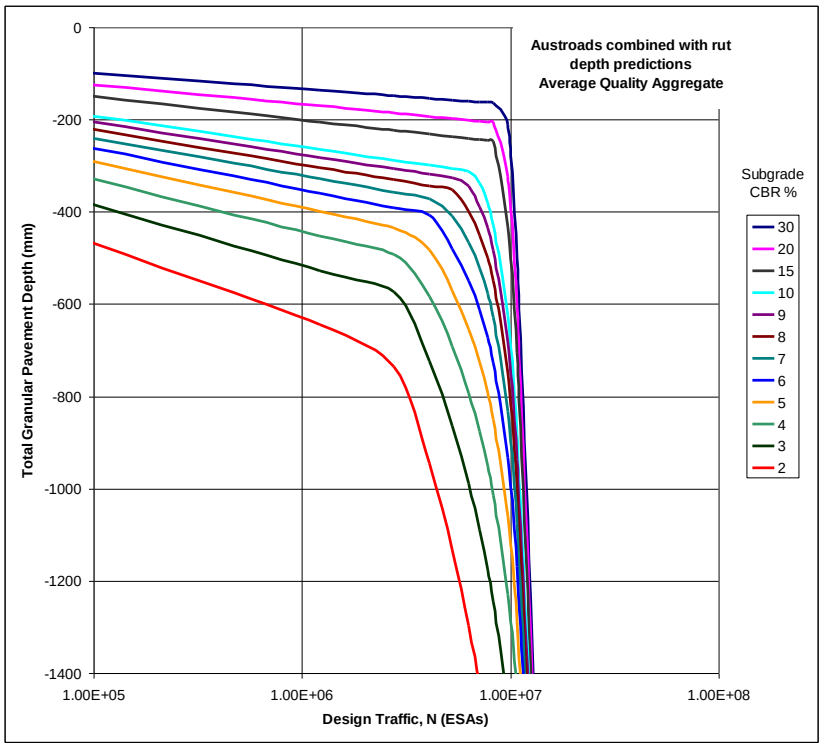

10 Recommendations

It is recommended that the findings of this research project (see figure 9.4) be implemented in the *New Zealand supplement to the Austroads pavement design guide* (NZTA 2007) as shown in appendix C. Appendix C also details the design method using a basecourse and sub-base strain criterion as developed in a parallel project by Arnold and Werkmeister on the development of a basecourse/sub-base design criterion. The aim of this parallel project was to develop basecourse and sub-base strain criteria for use with CIRCLY pavement design that would obtain the same life as shown in the pavement thickness design chart from rut depth modelling (figure 9.4). Use of basecourse and sub-base strain criteria is more versatile as it allows options such as increasing asphalt cover and/or stabilising a pavement layer to be investigated as alternative design options that will meet the design life. Initial use of these criteria should be optional for a time period of two years to gather feedback on their use so the method can be further validated and refined.

11 References

AASHO (1962) The AASHO road test. *Conference Proceedings: Special Report 73. Highway Research Board, National Academy of Sciences – National Research Council*. Washington DC, USA.

Alabaster, D and A Fussell (2006) Fatigue design criteria for low noise surfaces on New Zealand roads. *Transfund NZ research report no.307*.

Arnold, G (2004) Rutting of granular pavements. PhD thesis. University of Nottingham, Nottingham, UK.

Arnold, G, D Alabaster and B Steven (2001) Prediction of pavement performance from repeat load triaxial tests on granular materials. *Transfund NZ research report no.214.* 120pp.

Arnold, G, D Alabaster and B Steven (2005) Effect on pavement wear of an increase in mass limits for heavy vehicles. *Land Transport NZ research report no.281*.

Arnold, G, S Werkemeister and D Alabaster (2008) Performance tests for road aggregates and alternative materials. *Land Transport NZ research report no.335*.

Austroads (2004) *Pavement design. A guide to the structural design of road pavements.* Sydney: Austroads.

Austroads (2008) Technical basis of Austroads guide to pavement technology part 2: pavement structural design. *Austroads no. AP–T98/08.*

Benkelman, AC (1962) Structural deterioration of test pavements: flexible. The AASHO road test. *Highway Research Board Special Report 73*.

Chan, FWK (1990) Permanent deformation resistance of granular layers in pavements, PhD thesis, University of Nottingham, Nottingham, UK.

Davis, EH (1949) The California bearing ratio method for the design of flexible roads and runways, *Géotechnique 14*: 249–63.

de Beer, M, C Fisher and FJ Jooste (2002) Evaluation of non-uniform tyre contact stresses on thin asphalt pavements. *Ninth International Conference on Asphalt Pavements,* August 17–22, 2002, Copenhagen, Denmark.

Douglas, R (2009) Tyre/road contact stresses measured and modelled in three coordinate directions. *NZ Transport Agency research report 384.* 54pp and appendix.

George, HP and CA Gittoes (1959) *Report to Permanent International Association of Road Congresses (PIARC)*, Section 2, Question VI, Part A. Rio de Janeiro.

Jouve, P and S Guezouli (1993) Comparison and harmonized development of some finite element programs. Flexible Pavements. Edited by A. Gomes Correia, Technical University of Lisbon. Proceedings *of the European Symposium Euroflex 1993*, Lisbon, Portugal 20–22 September 1993.

Korkiala-Tanttu, L, R Laaksonen and J Törnqvist (2003) Effect of the spring and overload to the rutting of a low-volume road. HVS-Nordic-research. Helsinki 2003. Finnish Road Administration. *Finnra Reports 22/2003.* 39pp and appendix.

Lekarp, F (1997) Permanent deformation behaviour of unbound granular materials; Licentiate Thesis, Kungl Tekniska Högskolan, Sweden.

Little, PH (1993) The design of unsurfaced roads using geosynthetics, PhD thesis, Dept. of Civil Engineering, University of Nottingham.

NZ Transport Agency (NZTA) NZ supplement to the Austroads pavement design guide. Accessed September 2010*. www.nzta.govt.nz/resources/nz-supplement-2004-austroads-pavement-design/docs/supplement.pdf*

Oeser, M (2004) Numerische Simulation des nichtlinearen Verhaltens flexibler mehrschichtiger Verkehrswegebefestigungen, PhD thesis, University of Technology, Dresden, Germany.

Pidwerbesky, B (1996) Fundamental behaviour of unbound granular pavements subjected to various loading conditions and accelerated trafficking. PhD thesis, University of Canterbury, Christchurch, New Zealand.

Porter, OJ (1938) The preparation of subgrades, *18th Highway Research Board Meeting*, Washington DC, United States, pp324–31.

Rodway, B (1997) Going round in Circlies, *Geomechanics Society Pavements Symposium,* Sydney.

Semmelink, CJ, FJ Jooste and M de Beer (1997) Use of the K-mould in determination of the elastic and shear properties of road materials for flexible pavements. *8th Int. Conf. on Asphalt Pavements*, August, Seattle, Washington, USA.

Snaith, MS, D McMullen, RJ Freer-Hewish and A Shein (1980) Flexible pavement analysis. Contracted report to sponsors, European Research Office of the US Army.

Standards Australia (1995) *AS 1289.6.8.1: Methods of testing soils for engineering purposes. Soil strength and consolidation tests – determination of the resilient modulus and permanent deformation of granular unbound pavement materials*. Sydney: Standards Australia.

Theyse, HL (2002) *Stiffness, strength, and performance of unbound aggregate material: application of South African HVS and laboratory results to California flexible pavements*. University of California Pavement Research Center.

Theyse, HL (2004) Mechanistic empirical design models for pavement subgrades. In *Unbound aggregates in roads. Proceedings of the 6th International Symposium UNBAR6*: 229–238. Nottingham.

Thom, N and S Brown (1989) The mechanical properties of unbound aggregates from various sources. *Proceedings of the Third International Symposium on Unbound Aggregates in Roads*, *UNBAR3,* Nottingham, 11–13 April 1989.

Transit NZ (2005) *TNZ B/02 Specification for construction of unbound granular pavement layers.* Wellington: Transit NZ.

Transit NZ (2006) *TNZ M/4 Specification for basecourse aggregate*. Wellington: Transit NZ.

Transit NZ (2007) *TNZ T/15 specification for repeated load triaxial (RLT) testing of unbound and modified road base aggregates*. Wellington: Transit NZ.

Vuong, BT and R Brimble (2000) Austroads repeated load triaxial test method – determination of permanent deformation and resilient modulus characteristics of unbound granular materials under drained conditions. *APRG 00/33* (MA) June.

Vuong, BT (2001) Improved performance-based material specifications and performance prediction models for granular pavements. PhD thesis. Department of Civil and Geological Engineering, Faculty of Engineering, RMIT University: Melbourne, Australia.

Wardle LJ (1980) *Program CIRCLY, a computer program for the analysis of multiple complex loads on layered anisotropic media*.

Werkmeister S (2007) *Prediction of pavement response using accelerated test results of New Zealand's CAPTIF facility.* Dresden, Germany: TU.

Appendix A: Repeated load triaxial test summary for subgrade soils

RLT subgrade soil tests

RLT PS0026 #	Subgrade Soil	MC	DD	Lab CBR	RLT Test Date
1	Waikari Silty Clay	14.2	1.74	17	12/11/2007
est 1_Waik_ 14_11_07v1.xls					
NA	Waikari Silty Clay	7.8	1.68	50	8/11/2007
1a & 1b	Waikari Silty Clay	11.9	1.72	25	31/01/2008
2	Waikari Silty Clay	11.9	1.72	25	4/02/2008
3	Waikari Silty Clay	11.9	1.72	25	7/02/2008

Single test	σ3 [kPa]	σ1 [kPa]	q [kPa]	p [kPa]	E-Modulus [MPa]	resilient strain [mm/m]	permanet strain rate [Slope 25k to 50k %/1M]
A	68	85	17	74	78	89	0.050
B	234	277	43	249	127	259	0.107
C	218	310	92	249	163	503	0.312
D	201	340	139	248	149	863	1.118
E	119	210	91	149	107	755	0.379
F	60	102	42	74	81	394	-0.038
G	102	241	139	149	104	1242	1.984
H	185	371	186	247	155	1143	0.838
I	169	401	232	246	137	1619	2.666
J	152	429	277	245	138	1927	3.491

RLT Test Not Conducted as Too strong - CBR = 50%

A	50	150	100	84	80	1190	2.313
B	50	170	120	90	79	1458	2.395
C	50	190	140	97	82	1655	2.514
D	50	210	160	103	84	1838	2.627
E	50	230	180	110	87	2011	2.900
F	50	250	200	117	90	2176	2.871

A	100	350	250	183	121	2021	2.348
B	100	400	300	200	128	2301	3.206
C	100	450	350	217	130	2651	3.977
D	100	500	400	233	136	2903	4.208
E	100	550	450	250	141	3158	4.645

A	200	350	150	250	135	1077	1.249
B	200	400	200	267	135	1447	1.972
C	200	450	250	283	141	1738	2.401
D	200	500	300	300	149	1979	2.684
E	200	550	350	317	158	2188	2.901
F	200	600	400	333	168	2346	3.201
G	200	650	450	350	178	2491	2.971

RLT PS0026 #	Subgrade Soil	MC	DD	Lab CBR	RLT Test Date	Single test	σ3 [kPa]	σ1 [kPa]	q [kPa]	p [kPa]	E-Modulus [MPa]	resilient strain [mm/m]	permanet strain rate [Slope 25k to 50k %/1M]
13A	Todd Clay	30 28.3	1.425 1.5	2.5 approx. (CBR 13/2/08)	21/01/2008	**A**	200	210	10	203	125	39	0.945
						B	200	215	15	205	122	82	0.845
						C	200	220	20	207	110	136	1.382
						D	200	230	30	210	64	391	1.444
						E	200	240	40	213	42	1107	2.093
						F	200	250	50	217	17	2678	12.071
12	Todd Clay	30 28.3	1.425 1.5	2.5 approx. (CBR 13/2/08)	17/01/2008	**A**	100	110	10	103	97	51	1.056
						B	100	115	15	105	91	109	1.034
						C	100	120	20	107	74	201	1.027
						D	100	130	30	110	34	729	1.340
						E	100	140	40	113	18	1982	2.593
						F	100	150	50	117	15	3032	153.233
7	Todd Clay	19.4	1.6	17	8/11/2007	**A**	68	85	17	74	181	38	0.081
						B	234	277	43	249	172	191	0.148
						C	218	310	92	249	127	647	0.429
						D	201	340	139	248	88	1457	0.816
						E	119	210	91	149	107	758	0.211
						F	60	102	42	74	185	173	-0.069
						G	102	241	139	149	85	1510	0.404
						H	185	371	186	247	60	2959	3.445
8	Todd Clay	24.2	1.58	8	23/11/2007	**A**	68	85	17	74	154	45	0.168
						B	234	277	43	249	165	200	3.159
						C	218	310	92	249	127	816	2.830
11	Todd Clay	30 28.3	1.425 1.5	2.5 approx. (CBR 13/2/08)	16/01/2008	**A**	50	60	10	54	77	64	0.742
						B	50	65	15	55	64	155	0.813
						C	50	70	20	57	46	328	0.880
						D	50	80	30	60	21	1205	1.656
						E	50	90	40	63	14	2510	45.715
10a	Todd Clay	30 28.3	1.425 1.5	2.5 approx. (CBR 13/2/08)	14/12/2008	**A**	243	265	22	250	61	277	0.279

21	Very Fine Pumice Test Pit # 6 @ 2	11.7	1.06	25	9/05/2008

A	50	60	10	53	52	95	0.057
B	50	100	50	67	55	814	0.555
C	50	150	100	83	71	1333	1.457
D	50	200	150	100	84	1722	1.702
E	50	250	200	117	95	2055	2.124
F	50	300	250	133	105	2340	2.883
G	50	350	300	150	113	2615	3.229
H	50	400	350	167	119	2900	5.152

22	Very Fine Pumice Test Pit # 6 @ 2	11.7	1.06	25	9/05/2008

A	100	200	100	133	101	937	0.658
B	100	300	200	167	106	1847	2.370
C	100	350	250	183	111	2214	2.930
D	100	400	300	200	116	2532	4.186
E	100	450	350	217	120	2872	7.750
F	100	500	400	233	124	3181	11.011

70	Waikari Silty Clay - CBR 12%?

A	50	200	150	100	84	1736	3.793
B	50	250	200	117	90	2177	4.492
C	50	300	250	133	96	2541	5.074
D	50	350	300	150	103	2869	6.058
E	50	400	350	167	110	3142	17.761
F	50	449	399	183	118	3348	0.000

52	Todd Clay CBR = 5%

A	200	225	25	208	205	97	-0.015
B	200	250	50	217	175	257	0.181
C	200	300	100	233	74	1278	0.861
D	200	325	125	242	48	2489	2.241
E	200	350	150	250	48	2997	0.000
F	200	400	200	267	37	5241	

51	Todd Clay CBR = 5%

A	100	150	50	117	171	264	0.407
B	100	200	100	133	83	1145	1.092
C	100	250	150	150	65	2220	0.000
D	100	300	200	167	43	4474	0.000
E	100	350	250	183	15		0.000

50 Todd Clay CBR = 5%

A	50	100	50	67	114	393	0.730
B	50	150	100	83	53	1783	2.048
C	50	200	150	100	44	3273	0.000

41 Drury Test Pit # 1 CBR + 6%

A	100	150	50	117	150	300	0.567
B	100	200	100	133	128	742	0.943
C	100	250	150	150	98	1488	0.000
D	100	299	199	166	44	4383	0.000
E	100	349	249	183	0	0	0.000

40 Drury Test Pit # 1 CBR = 6%

A	50	100	50	67	145	310	0.461
B	50	150	100	83	123	775	0.906
C	50	250	200	117	41	4705	0.000
D	50	299	249	133	37	2201	0.000

33 Pumice CBR=25%

A	200	300	100	233	140	677	0.480
B	200	400	200	267	137	1425	1.639
C	200	450	250	283	139	1766	2.114
D	200	500	300	300	144	2055	2.646
E	200	550	350	317	148	2331	3.531
F	200	600	400	333	151	2608	5.035

56 Todd Clay 26.5% MC - cell =50kPa

57 Todd Clay 25.5% MC - cell = 100kPa

58 Todd Clay 25.5% MC - cell = 200kPa

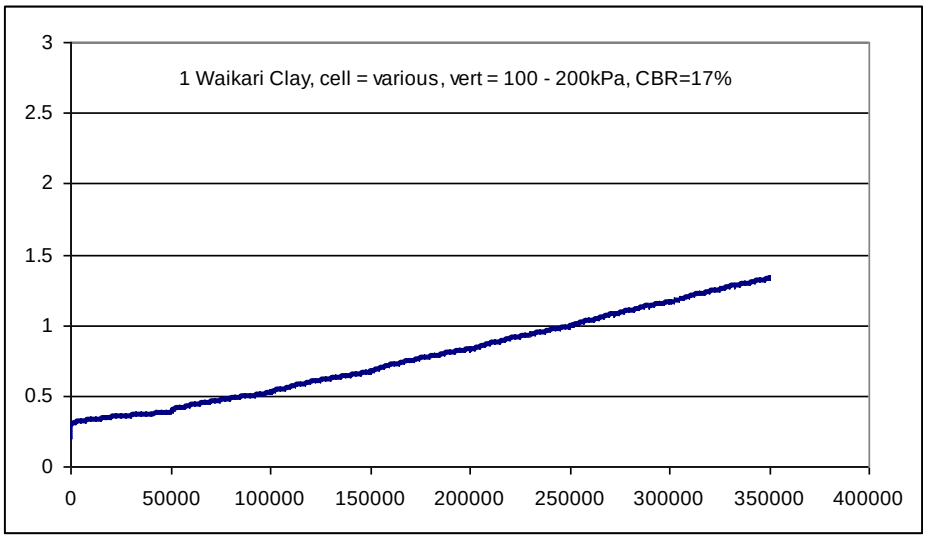
1 Waikari Clay, cell = various, vert = 100 - 200kPa, CBR=17%
3
2.5
2
1.5
1
0.5
0
0
50000
100000
150000
200000
250000
300000
350000
400000

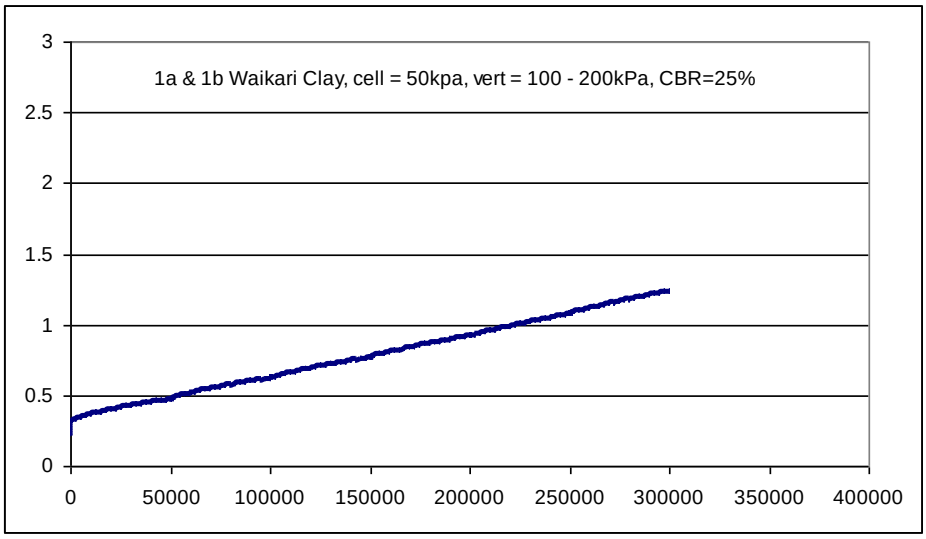
1a & 1b Waikari Clay, cell = 50kpa, vert = 100 - 200kPa, CBR=25%
3
2.5
2
1.5
1
0.5
0
0
50000
100000
150000
200000
250000
300000
350000
400000

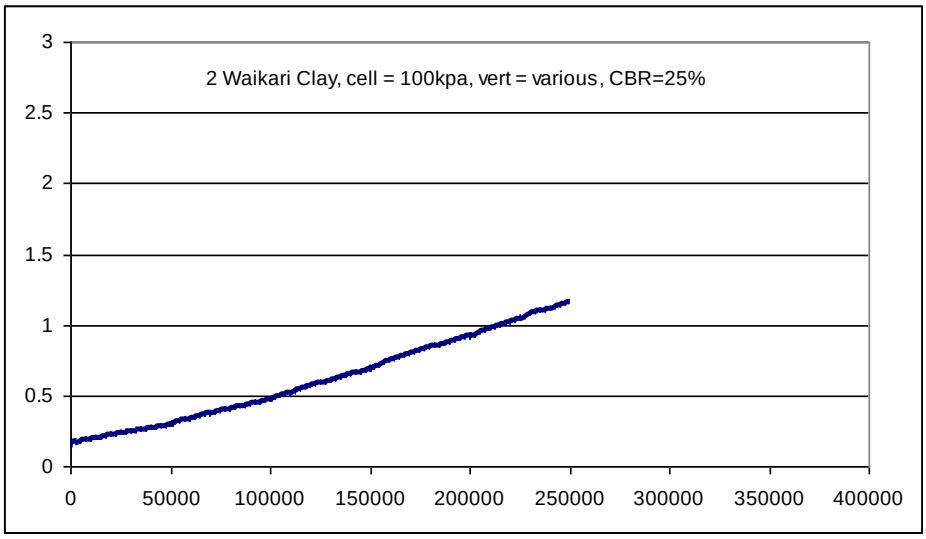
2 Waikari Clay, cell = 100kpa, vert = various, CBR=25%
3
2.5
2
1.5
1
0.5
0
0
50000
100000
150000
200000
250000
300000
350000
400000

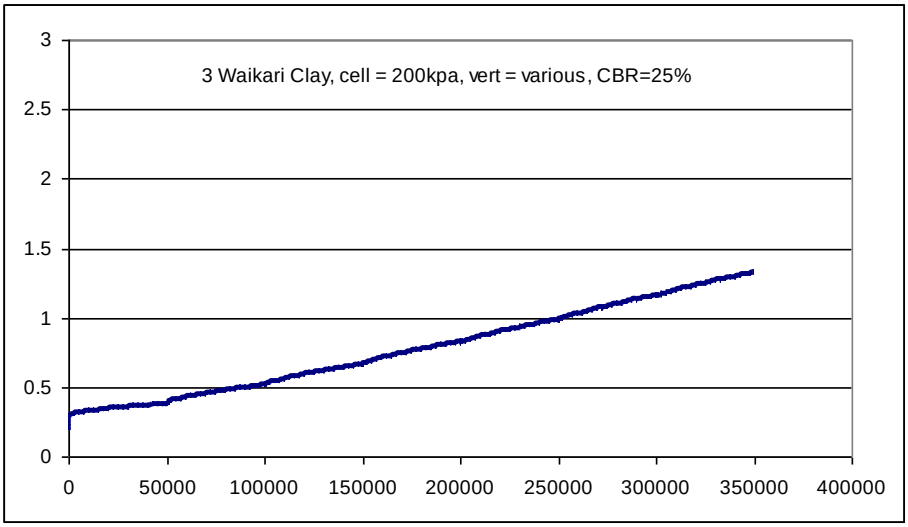
3 Waikari Clay, cell = 200kpa, vert = various, CBR=25%
3
2.5
2
1.5
1
0.5
0
0
50000
100000
150000
200000
250000
300000
350000
400000

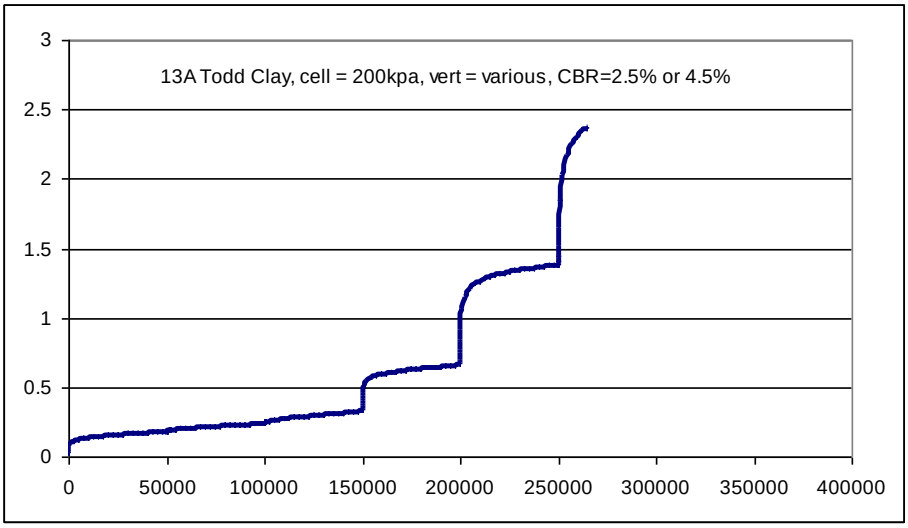
13A Todd Clay, cell = 200kpa, vert = various, CBR=2.5% or 4.5%
3
2.5
2
1.5
1
0.5
0
0
50000
100000
150000
200000
250000
300000
350000
400000

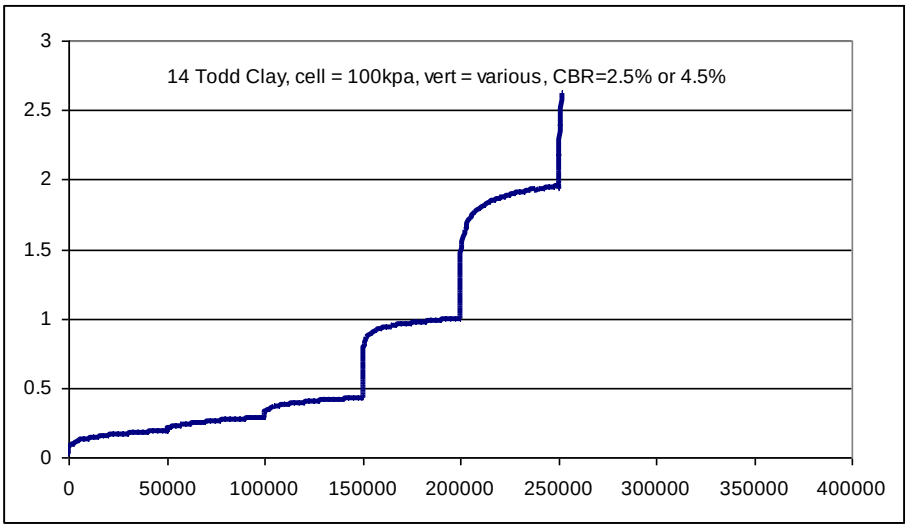
14 Todd Clay, cell = 100kpa, vert = various, CBR=2.5% or 4.5%
3
2.5
2
1.5
1
0.5
0
0
50000
100000
150000
200000
250000
300000
350000
400000

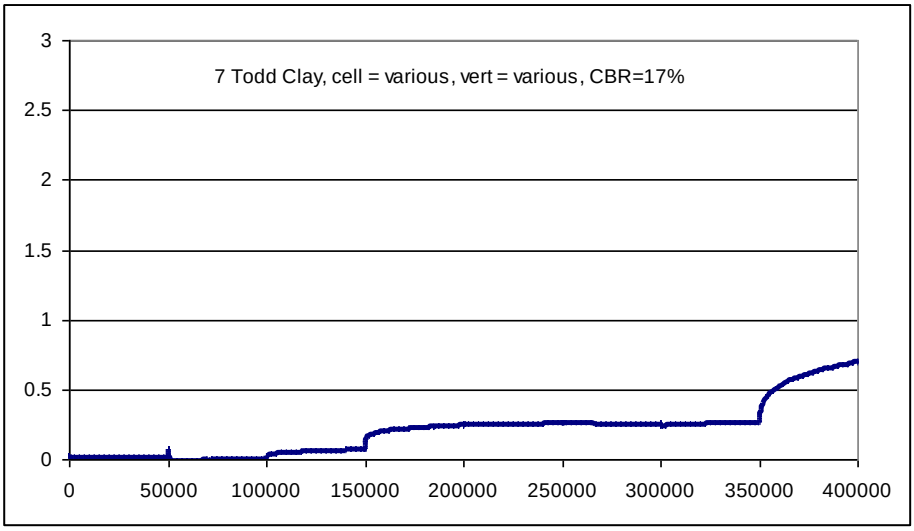
7 Todd Clay, cell = various, vert = various, CBR=17%
3
2.5
2
1.5
1
0.5
0
0
50000
100000
150000
200000
250000
300000
350000
400000

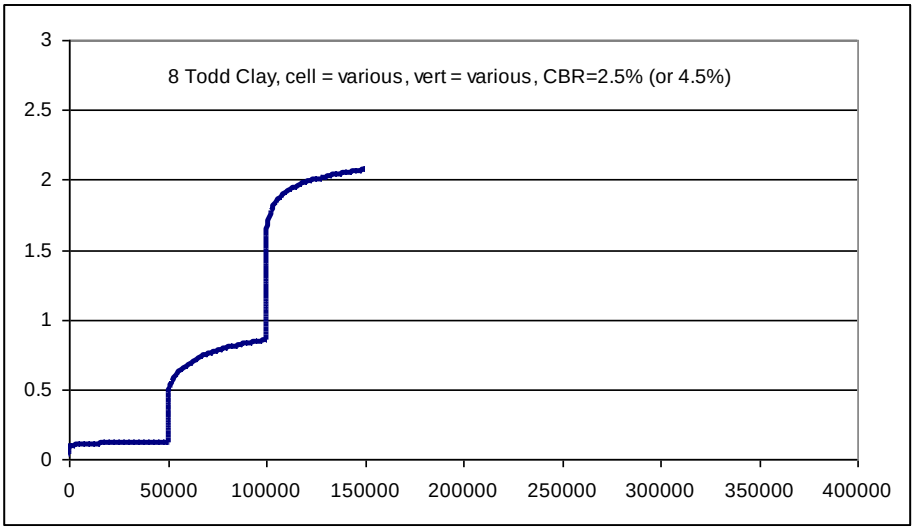
8 Todd Clay, cell = various, vert = various, CBR=2.5% (or 4.5%)
3
2.5
2
1.5
1
0.5
0
0
50000
100000
150000
200000
250000
300000
350000
400000

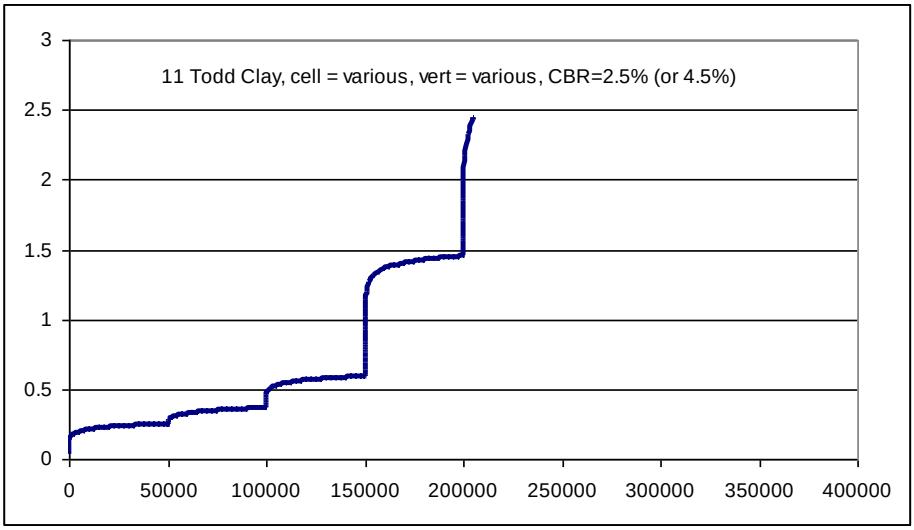
11 Todd Clay, cell = various, vert = various, CBR=2.5% (or 4.5%)
3
2.5
2
1.5
1
0.5
0
0
50000
100000
150000
200000
250000
300000
350000
400000

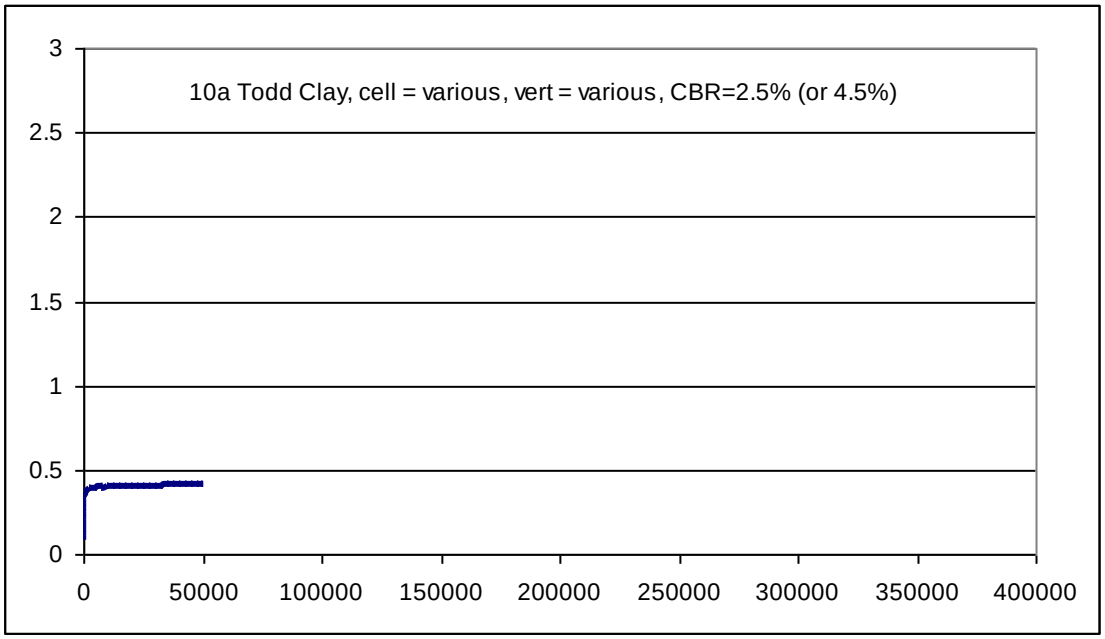
10a Todd Clay, cell = various, vert = various, CBR=2.5% (or 4.5%)
3
2.5
2
1.5
1
0.5
0
0
50000
100000
150000
200000
250000
300000
350000
400000

Appendix B: Repeated load triaxial testing and rut depth modelling technical note

Repeated load triaxial testing and rut depth modelling for pavement materials (granular, modified, local, recycled, waste, stabilised subgrade)

Dr Greg Arnold, PaveSpec Ltd (email: greg.arnold@pavespec.co.nz web: www.rltt.co.nz (please check web for latest contact details and laboratory location)

What is repeated load triaxial (RLT) testing?

The RLT apparatus applies repetitive loading on cylindrical materials for a range of specified stress conditions, the output is deformation (shortening of the cylindrical sample) versus number of load cycles (usually 50,000) for a particular set of stress conditions. Multi-stage RLT tests are used to obtain deformation curves for a range of stress conditions to develop models for predicting rutting.

Resilient modulus information can also be obtained for pavement design in CIRCLY and finite element models.

Figure B1 RLT apparatus and setup

Figure B2 Typical output from permanent strain RLT testing

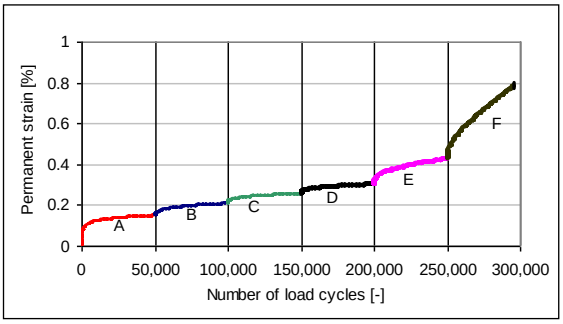

Analysis of RLT testing results – rut depth modelling

The method developed by Dr Arnold in his Doctorate studies at the University of Nottingham, UK is used to interpret the results to predict the rut depth in a pavement. First step is to develop a mathematical relationship between stress (both vertical and horizontal) with permanent strain rate (slope of each deformation curves (figure B2), eg % deformation per 1 million load cycles).

Figure B3 Fitting the permanent strain rate model to RLT testing results

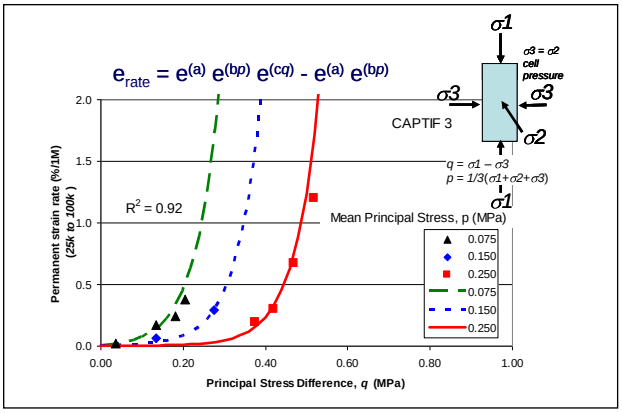

Figure B4 Rut depth prediction from RLT testing for CAPTIF (accelerated pavement test) trial

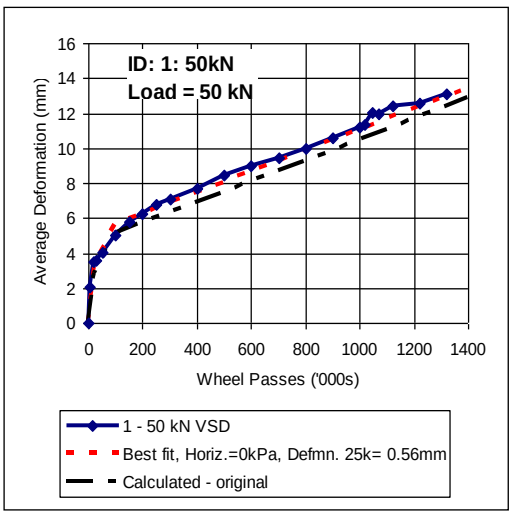

Next step is to use a finite element model (to model the non-linear elastic behaviour of a pavement material and to avoid discontinuities as occurs in CIRCLY which results in high tensile stresses) to compute the stresses (both vertical and horizontal underneath a standard axle load (8.2 tonne dual tyred axle or higher if designing for ports etc). Stresses are exported into a spreadsheet to calculate the deformation rate at depth increments in the pavement from the permanent strain model (figure B3). Results showed very good predictions of rutting that occurred at CAPTIF (figure 4) (Arnold 2004).

Applications for RLT testing and rut depth modelling

Preventing early failure

Recent research has shown that even if your aggregate complies with M4 that they do not perform equally. The aggregate may fail by shear (figure B5) within six months after the pavement has been constructed especially if it gets wet. The RLT testing can quickly identify aggregates where there may be a risk of this occurring as often the sample fails before the completion of all the stress stages (figure B2).

Figure B5 Shear failure in aggregate layer

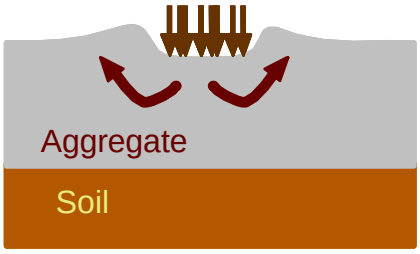

Modified/stabilised materials for high trafficked roads

Small quantities of cement, lime or other additive are classified as a modified aggregate in the *New Zealand supplement to the Austroads pavement design guide*. Modified aggregates are recommended in the New Zealand supplement for use for high trafficked state highways as an economical alternative to structural asphalt. Using the RLT testing will identify the most appropriate amount of additive and using rut depth modelling can predict the amount of extra life that can be obtained through modification compared with the source aggregate.

Modified/stabilised marginal local materials as a lower cost to TNZ M4 (and may perform better!)

RLT testing and rut depth modelling allow any material that does not comply with a current specification to be assessed as suitable or not for the chosen application in the pavement.

This allows a local material non-compliant with the specifications to be modified by say adding cement to be approved for use. The NZTA is in the process of developing an RLT testing method and associated analysis to approve use of other materials on state highways.

Local materials for local roads

Footpaths, tennis courts, cul-de-sacs, low trafficked local roads do not need to use TNZ M/4 basecourse aggregate meant for state highways. In fact M4 is difficult to lay and compact for these small local jobs. RLT testing and rut depth prediction for the required application can allow say a local but dirty aggregate to be assessed as suitable for low trafficked situations and footpaths.

Waste and recycled materials

Waste or recycled materials like glass and reclaimed asphalt mixed with aggregate or otherwise can be tested in the RLT apparatus with rut depth modelling to determine appropriate applications as pavement base material.

PaveSpec Ltd

Dr Greg Arnold is the Director of PaveSpec Ltd which along with offering specialist pavement advice and design is a company that has just recently purchased a state of the art repeated load triaxial apparatus for testing pavement materials.

Appendix C: Recommended additions to the New Zealand supplement to the 2004 Austroads pavement design guide

This appendix sets out suggested changes to the *NZ supplement to the 2004 Austroads pavement design guide.* The heading numbers relate to the same chapters and sections in the Austroads guide.

Chapter 6 Pavement materials

6.1 General

(Add)

Designers are encouraged to use new design strain criteria for use with CIRCLY have been developed for New Zealand granular and cemented materials. Section 6.2.2 details strain criteria to use for unbound and modified granular materials while section 6.4.2 details tensile strain criteria for cemented granular materials. These new design criteria are material specific and require repeated load triaxial (RLT) test data as per NZTA T/15 and/or flexural tensile strength from beam breakage tests or derived from indirect tensile strength tests. Presumptive values are given but should be used cautiously with the design being refined by using test data on actual materials used in the project.

In the absence of CIRCLY and new design criterion then figure 8.4 in the Austroads (2004) guide should be replaced with figures 6.1a and 6.1b for designing thin-surfaced granular pavements. These new design charts were developed from rut depth modelling carried out by Arnold and Werkmeister in 2010.

Figure 6.1a Recommended pavement thickness design chart for average quality aggregate combining Austroads (2004) and rut depth predictions

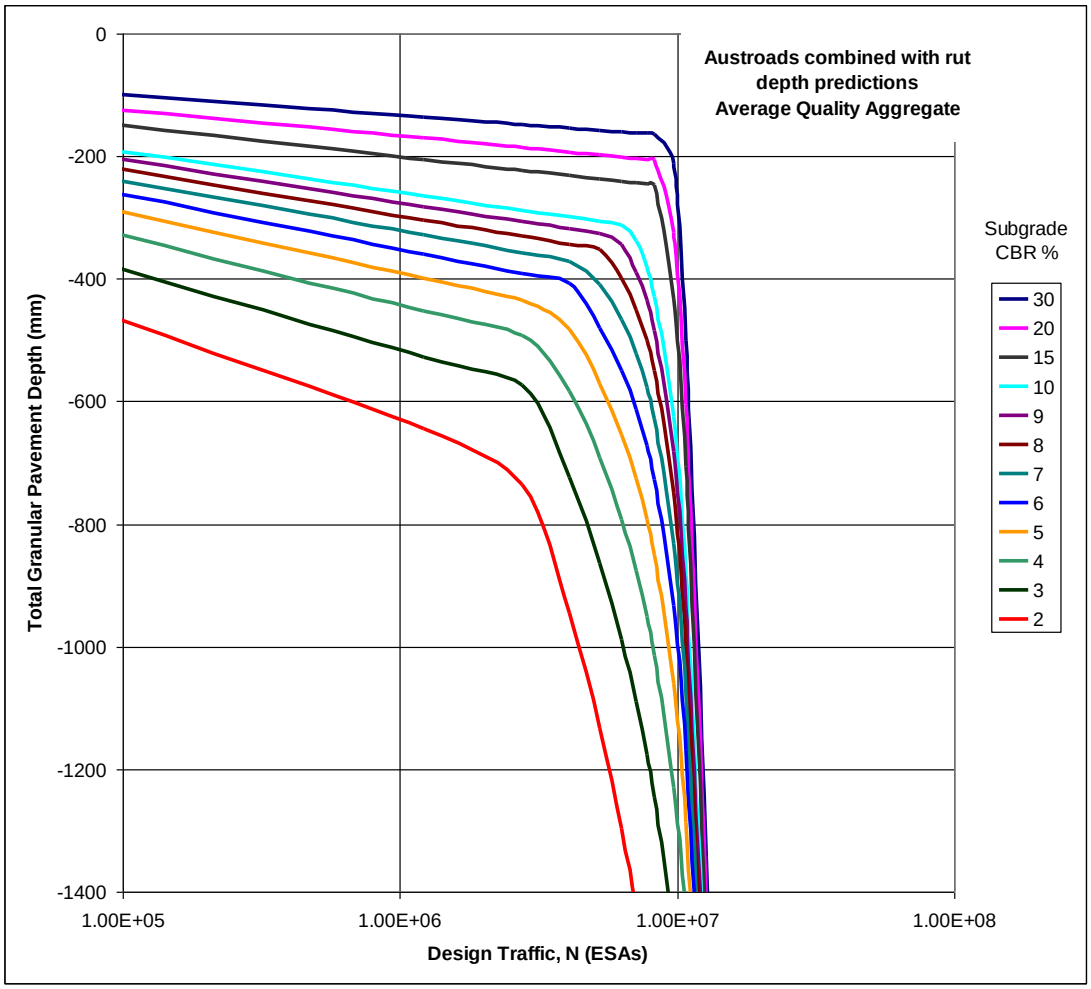

Figure 6.1b – Pavement thickness design chart for average quality aggregate derived from Austroads (2004) design guide and from rut depth modelling plotted on a linear scale

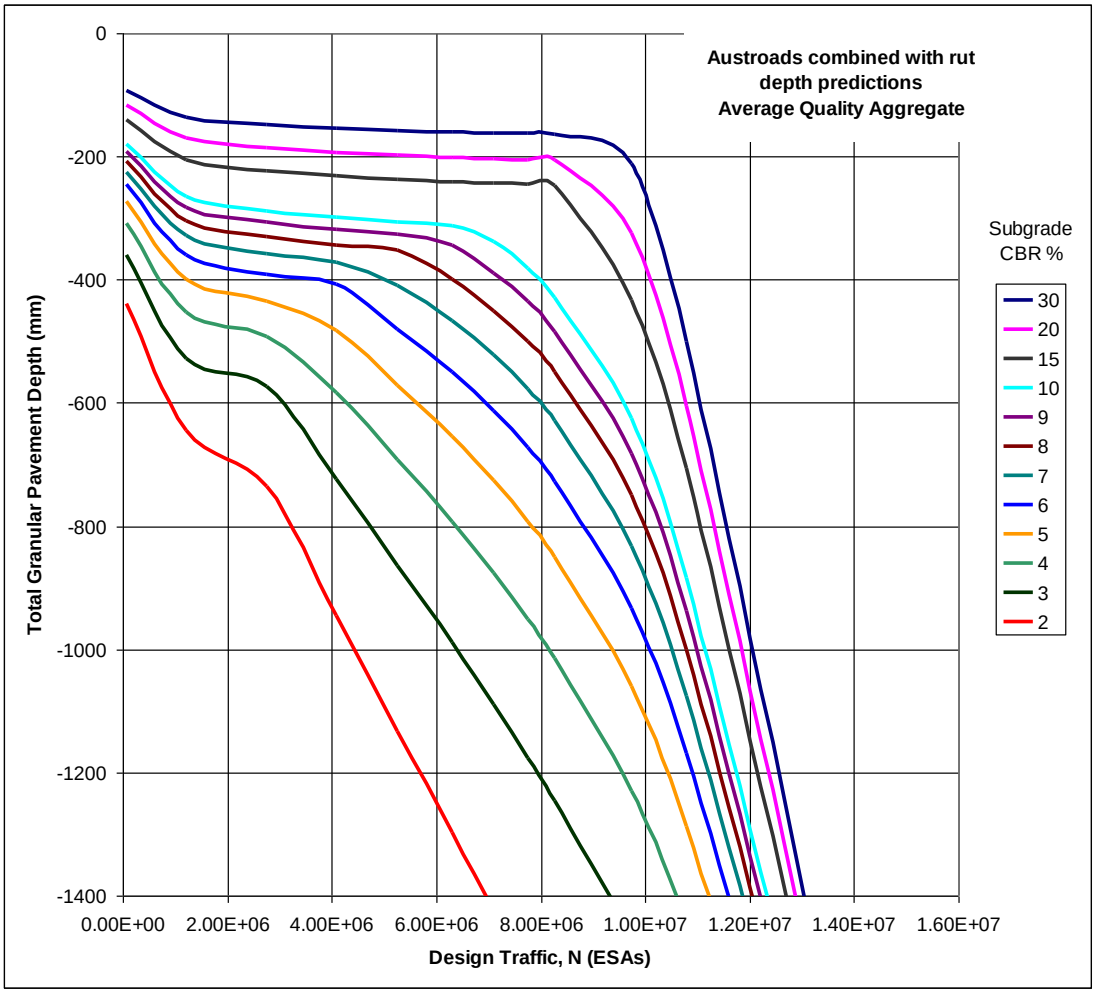

6.2 Unbound granular materials

6.2.1 Introduction

6.2.2 Basecourse and subbase design strain criteria for CIRCLY pavement design

For basecourse aggregate covered with a thin surface of less than 50mm then the vertical compressive strain at the bottom but within the basecourse layer is limited by equation 6.1. For cases where the cover is greater than 50mm then the basecourse will be treated as a subbase for design as per equation 6.2.

$$N_{BC} = M*[(a.f.k_{BC}/\text{resilient strain bottom of BC})\text{^}exp_{BC}] \quad \text{(Equation 6.1)}$$

where:

N_{BC} =life of basecourse in equivalent standard axles (ESAs)

a = constant to adjust strain at bottom of basecourse to a maximum strain in the basecourse

a = 1/(BC depth (mm) x 0.00905) – derived from equation 5.1

f = 2.0 - adjustment factor determined from validation to ensure calculated life from stain criterion is equal to life calculated from rut depth modelling

k_{BC} = constant found from RLT testing (NZTA T/15 and appendix D, presumptive values shown in table 6.1)

exp_{BC} = constant found from RLT testing (NZTA T/15 and appendix D, presumptive values shown in table 6.1)

resilient strain bottom of BC = resilient strain at the bottom of the basecourse layer as calculated using CIRCLY.

M= pavement depth multiplier due to reduced rutting in subgrade (table 6.2)

The life of the sub-base aggregate layer is found from equation 6.2:

$$N_{SB} = M*[(f.k_{SB}/resilient\ strain\ top\ of\ SB)\text{^}exp_{SB}] \quad \text{(Equation 6.2)}$$

Where:

N_{SB} =life of sub-base or basecourse if covered by more than 50mm of bound material in ESAs;

f = 2.0 – adjustment factor determined from validation to ensure calculated life from stain criterion is equal to life calculated from rut depth modelling

k_{SB} = constant found from RLT testing (NZTA T/15 and appendix D, presumptive values shown in table 6.1)

exp_{SB} = constant found from RLT testing (NZTA T/15 and appendix D, presumptive values shown in table 6.1)

resilient strain top of SB = resilient strain at the top of the subbase layer.

M= pavement depth multiplier due to reduced rutting in subgrade (table 6.1)

Table 6.1 Aggregate life multiplier from pavement depth resulting in reduced rutting in the subgrade

Subgrade CBR%	Pavement depth (mm) when aggregate life influences (D)	Aggregate life multiplier M (ie multiply computed life by M) – up to a maximum of M=1.8.
2	1000	M = Total pavement depth/D
3	854	
4	750	
5	670	
6	604	
7	548	
8	500	
9	458	
10	420	
11	385	
12	354	
13	325	
14	298	
15	273	

It is recommended that designers conduct their own RLT tests to obtain the constants in the design strain criterions for subbase and basecourse aggregates, while the range of values found unbound aggregates from the Pavespec Ltd database of RLT tests are shown in table 6.2. The use of modified and cemented granular materials will require independent RLT tests to determine appropriate constants for the design stain criterion as detailed in Appendix D and NZTA T/15. Further, the constants in table 6.2 were derived from dry tests in the RLT apparatus. A separate design is needed if the case for saturation of the granular layers is considered using equation constants derived from saturated RLT tests.

Table 6.2 Constants and exponent values for CIRCLY design strain criterions

$N = (f.a.k/micro\text{-}strain)^{exp}$ f=2.0 (see Eqn. 6.1 and 6.2)		Sub-base linear Extrapolation to 3.3% (NB: K for Circly = b*2 – see appendix A)			Basecourse linear Extrapolation to 3.3% (NB: K for Circly = b*2 – see appendix A)	
Strain criterion		b	exp		b	exp
Upper (best)		80,000	3.4		700,000	2.4
Middle		66,000	3.4		400,000	2.4
Lower (poor)		55,000	3.4		250,000	2.4

(see below for details how to obtain these constants from RLT tests)

6.3 Modified granular materials

(Add)

A design procedure for these materials has now been developed for use in CIRCLY using design strain criterion for basecourse and/or sub-base granular materials as per equations 6.1 and 6.2 above, except material specific equation constants will be derived from RLT tests on modified granular materials. Due to increase deformation resistance with modified materials then this should result in an increase in pavement life when compared with unbound granular materials, particularly in a saturated condition. Nevertheless, the extra life from modified materials maybe restricted by 'its' fatigue life as determined by equation 6.3 in section 6.4.2 'Cemented materials'. The fatigue life of modified materials must be considered in design if any improvements in life beyond an unbound granular material are being considered.

Appendix D: Method to determine vertical compressive strain criterion from repeated load triaxial test data

Step 1:

Determine the average slope (%/1M) as per table D1 as measured in the RLT test and resulting load cycles to achieve a permanent strain limit (3.3%).

Table D1 Calculation of average permanent strain slope from 6-stage RLT test

RLT test stage (table 2)	[2]Permanent strain (%) (see figure 1)	[1]Permanent strain slope (%/1M) (slopes) A	Number of load cycles (N) to achieve a permanent strain of 3.3% $N = 3.3/A * 10^6$
Stage A	P_{25k}	$=(P_{50k}-P_{25k})/0.025M$	$= 3.3 / [(P_{50k}-P_{25k})/0.025M]$
	P_{50k}		
Stage B	P_{75k}	$=(P_{100k}-P_{75k})/0.025M$	$= 3.3 / [(P_{100k}-P_{75k})/0.025M]$
	P_{100k}		
Stage C	P_{125k}	$=(P_{150k}-P_{125k})/0.025M$	$= 3.3 / [(P_{150k}-P_{125k})/0.025M]$
	P_{150k}		
Stage D	P_{175k}	$=(P_{200k}-P_{175k})/0.025M$	$= 3.3 / [(P_{200k}-P_{175k})/0.025M]$
	P_{200k}		
Stage E	P_{225k}	$=(P_{250k}-P_{225k})/0.025M$	$= 3.3 / [(P_{250k}-P_{225k})/0.025M]$
	P_{250k}		
Stage F	P_{275k}	$=(P_{300k}-P_{275k})/0.025M$	$= 3.3 / [(P_{300k}-P_{275k})/0.025M]$
	P_{300k}		
Average		$= P_{avg} = (\sum Slopes)/6$	

Note: 1: If any of the loading stages do not complete the full amount of loading cycles because the deformation limit of 1.0% was achieved then table 5 calculations will not strictly apply. In this situation the average tangential permanent strain slope achieved is used in replace of the value from 25,000 to 50,000 load cycles.

2: Permanent strain values for any given load cycle are the average of the previous 10 readings in the RLT test to account for any noise in the data.

Figure D1 Permanent strain points for determination of permanent strain slopes

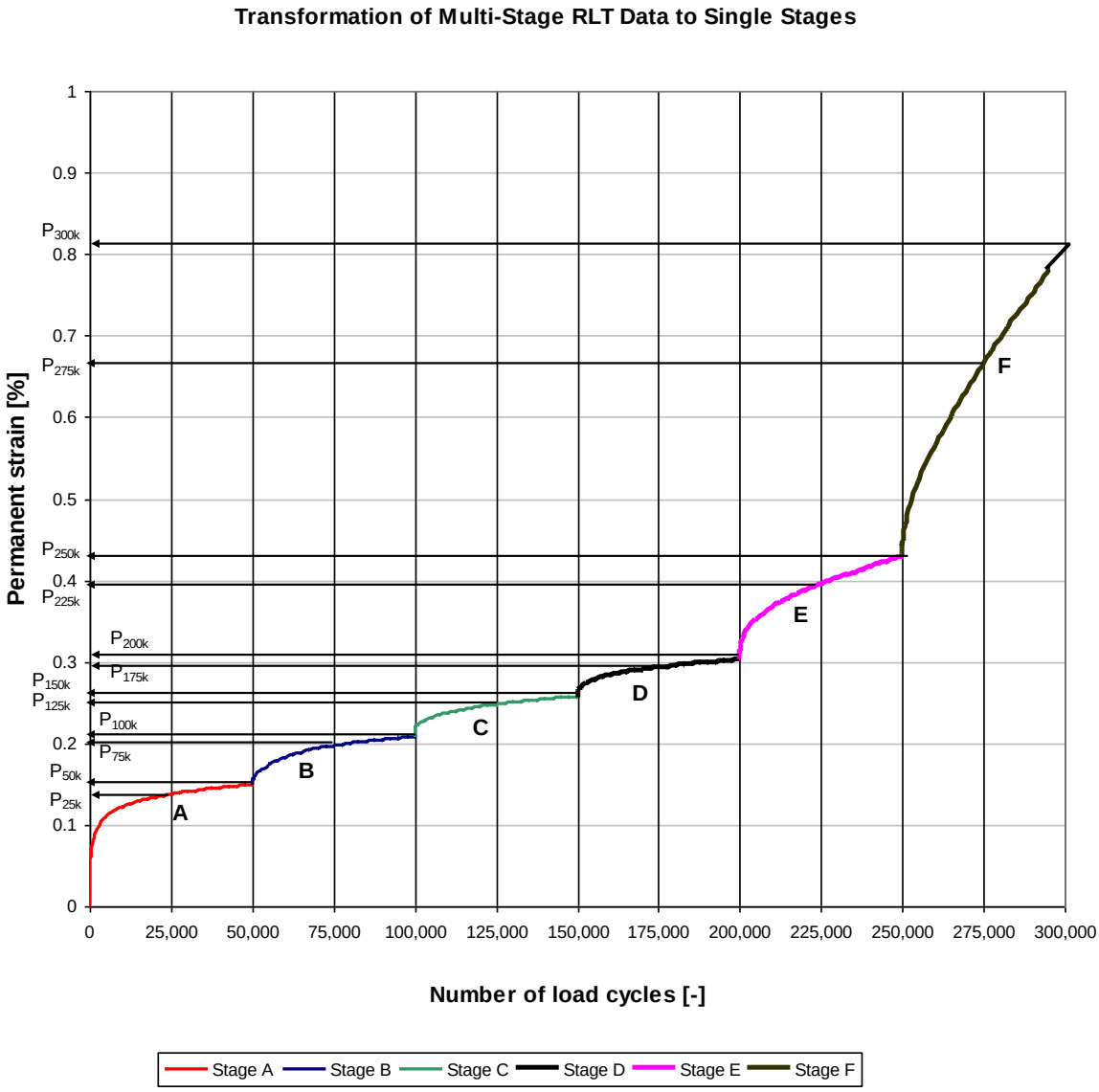

Step 2:

Determine the relationship between life (N, table D1) and resilient elastic strain as recorded in the RLT test. Then plot log (N) versus log (micro-strain) and determine line of best fit for slope and intercept constants (*a* and *b*) as shown in figure D1.

Table D2 Calculation of average permanent strain slope from 6-stage RLT test

			Log10 both sides and calculate slope (a) and intercept (b) (see figure 1) – Log(ε) = a.log(N) + b	
RLT test stage (table 2)	Vertical resilient strain	Number of load cycles (N) to achieve a permanent strain of 3.3% N = 3.3/A * 10^6	Log (ε)	Log (N)
Stage A	ε_A	= 3.3 / [(P_{50k}-P_{25k})/0.025M]		
Stage B	ε_B	= 3.3 / [(P_{100k}-P_{75k})/0.025M]		
Stage C	ε_C	= 3.3 / [(P_{150k}-P_{125k})/0.025M]		
Stage D	ε_D	= 3.3 / [(P_{200k}-P_{175k})/0.025M]		
Stage E	ε_E	= 3.3 / [(P_{250k}-P_{225k})/0.025M]		
Stage F	ε_F	= 3.3 / [(P_{300k}-P_{275k})/0.025M]		

Figure D2 Example plot of log(N) versus log(strain) for calculating line of best fit for slope and intercept constants (a and b)

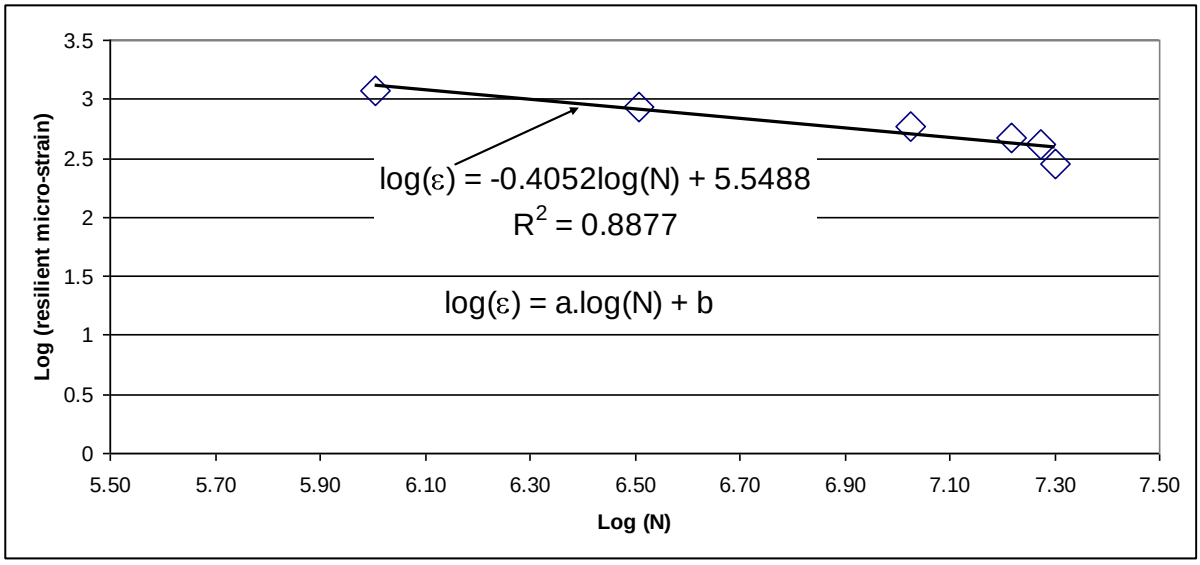

Step 3:

From line of best fit for slope and intercept constants (*a* and *b*) as shown in figure D2 in step 2 determine power law exponent and constant for strain criterion uses in CIRCLY (equation D1):

$$N = (K/\text{micro-strain})^{exp} \qquad \text{Equation D1}$$

Where,

N	=	Fatigue life in equivalent standard axles (ESAs)
K	=	$[10^{b}]$. f
b	=	Intercept constant, *b* in log(N) vs log(strain) relationship (figure D1)
f	=	2.0 - adjustment factor determined from validation to ensure calculated life from stain criterion is equal to life calculated from rut depth modelling
exp	=	(1/a)*(-1)
a	=	Slope constant, *a* in log(N) vs log(strain) relationship (figure D2)
micro-strain	=	Vertical compressive resilient strain at the top of the subbase aggregate layer or at a depth of 80mm from the surface in the basecourse layer.